Regulatory Factor of Three-dimensional Microvessel Network *in Vitro*

March 2009

Akinori Ueda

Abstract

Microvessel network formation is critical in regeneration medicine and tissue engineering, because these networks are essential for the formation and maintenance of organ functions. Regenerated three-dimensional (3-D) tissue cannot maintain its physiological function in the absence of a 3-D microvessel network because diffusion alone could not supply sufficient nutrients and O2 to the tissue. Extensive 3-D microvessel networks of significant depth are, therefore, required to include in the regenerated tissues. In this study, we focused for the shear stress arise from blood flow, distribution of growth factors, and hypoxic conditions, as the control factors for in vitro 3-D network formation. We structured the in vitro model of 3-D network using bovine endothelial cells (ECs), experimented to examine the effect of these factors on network formations. Shear stress has an effect on functions of ECs, which covers vessel wall, including proliferation and migration. Firstly, we created the experimental setup in which ECs are loaded shear stress and observed over time, then showed that the albumin uptake into ECs decreased and change of glycocalyx on surface of ECs are involved in the phenomenon. To assess the effect of shear stress on micro-vessel formation, we used an in vitro 3D model in which ECs were induced by a basic fibroblast growth factor (bFGF) to invade a collagen gel. The observation using time-lapse microscopy indicated that shear stress promoted the growth of 3D network formation in vitro thorough enhancement of ECs migration. Next we used models, in which ECs were seeded on two patterned environments, and observed the 3-D structure of the networks using confocal scanning microscopy. This study showed that growth factor distribution affects the morphology of the EC network. We finally focused on the effect of hypoxia on network formation, and found that hypoxia induces 3-D networks with depth and breadth, even in the absence of external growth factors. These results indicated that 3-D network formation could be controlled by changing environment surrounding ECs *in vitro*, and would be contribute for the realization of 3-D organ regeneration as significant knowledge for linking gene and cell level factors with tissue engineered approach.

Abstract (Japanese)

[訳題] 生体外 3 次元毛細血管様ネットワーク形成の制御因子

血管の形成は，すべての組織の形成・機能維持に不可欠であり，再生医学の展開においても重要な課題である．3 次元的な臓器においては，酸素や栄養分の輸送が拡散のみでは十分に行われないため，組織内に 3 次元的な血管ネットワークが組み込まれることが望まれる．本研究では生体外 3 次元ネットワークの制御因子として，血流に起因するせん断応力や増殖因子の分布，低酸素状態に着目し，これらの因子の血管ネットワーク形成に及ぼす影響を調べることを目的としてウシの血管内皮細胞を用いた生体外モデルを使用して実験を行った．血管内腔を覆う内皮細胞にはせん断応力が作用しており，この血行力学的応力が内皮細胞の増殖，遊走など各種機能に影響を与えていることが分かっている．本研究では先ず，せん断応力負荷の環境下にある内皮細胞を経時的に観察可能な実験系を作製，内皮細胞へのアルブミンの取り込み能が高せん断応力下で抑制されること，並びに内皮細胞表層に存在する糖衣の変化が影響していることを示した．続いて内皮細胞をコラーゲンゲルの上に播種し，増殖因子 bFGF を添加する生体外血管ネットワークモデルを作製した．せん断応力負荷実験系に血管ネットワークの生体外モデルを組み込み，タイムラプス顕微鏡観察による観察を行ったところ，せん断応力によって内皮細胞の遊走能が亢進され，3 次元ネットワークの形成が促進されることを明らかになった．次に静置培養下で増殖因子の分布の異なる 2 種類のネットワークモデルを作製し，共焦点顕微鏡を用いてそれぞれのモデルにおけるネットワークの 3 次元的形態を解析した．その結果，増殖因子の深さ方向の分布が，ゲル内でのネットワークの広がり方に影響を与えることが示された．さらに内皮細胞に低酸素を負荷する実験系を用いて，低酸素状態が内皮細胞の 3 次元的なネットワーク形成能にどのような影響を与えるのかを調べた．低酸素を負荷された内皮細胞は，増殖因子を添加しなくてもコラーゲンゲル内に深さと広がりを伴った，3 次元的なネットワークを形成した．これらの結果は，生体外において内皮細胞の周辺環境を適宜変化させることにより，3 次元ネットワーク形成が制御可能であることを示しており，組織工学的アプローチと遺伝子・細胞レベルの要素研究を繋ぐ重要な知見として 3 次元的な臓器の再生に資すると考えられる．

Contents

List of abbreviations and symbols

2-D	two-dimensional
3-D	three-dimensinal
b	flow channel width
DMEM	Dulbecco's modified Eagle's medium
ECM	extracellular matrix
ECs	endothelial cells
EGF	epidermal growth factor
ELISA	enzyme-linked immunosorbent assay
FBS	fetal bovine serum
FGF	fibroblast growth factor
h	flow channel height
HEPES	2-[4-(2-hydroxyethyl)-1-piperazinyl] ethanesulfonic acid
ICAM	intercellular adhesion molecule
IL	interleukin
LDL	low-density lipoprotein
μ	viscosity
P	Blood pressure
PBS	phosphate buffered saline
Q	flow rate
r	vessel diameter
SMCs	smooth muscle cells
τ	shear stress
TEM	transmission electron microscopy
TGF	transforming growth factor
TNF	tumor necrosis factor
u	blood flow
VEGF	vascular endothelial growth factor

Chapter I

General Introduction

1-1. The Structure of Vessels

Vessels are fundamental structure, which are distributed to any part of the body of living organism. The vessels consist of endothelial cells (ECs) on the luminal surfaces and the surrounding parietal cells. Arteries start from heart as aorta and repeated branch to elastic artery, muscular artery, small artery, and then are distributed every tissue and organ as microvessels. After that, they are circulated to heart through venous system.

The wall of large blood vessel consists of 3 layers, tunica intima, tunica media and tunica adventitia (Fig. 1-1). Monolayer of ECs covers internal side of tunica intima and contacts with blood flow directly. There is basal layer between ECs monolayer and surrounding external layers. Tunica media consists of smooth muscle cells (SMCs) and extracellular matrix (ECM), such as collagen and elastin. Tunica adventia means outside of external elastic lamina and mainly consists of ECMs. Internal elastic lamina and external elastic lamina divide these 3 layers.

Microvessels consist of ECs and pericytes. Pericytes are different from SMCs and are wrapped in basal layer with ECs. Then, ECs have direct contact with pericytes.

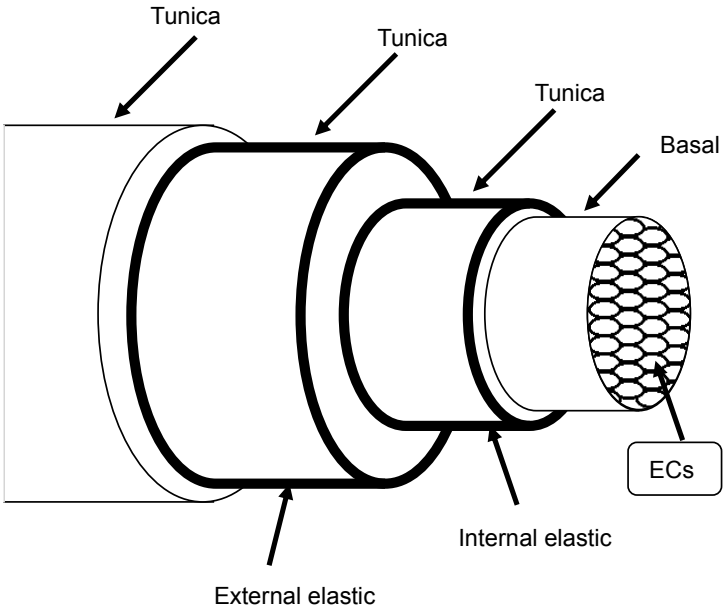

Fig. 1-1 The structure of vessels. The wall of large blood vessel consists of 3 layers, tunica intima, tunica media and tunica adventitia. Monolayer of ECs covers internal side of tunica intima and contacts with blood flow directly.

1-2. The Function of ECs

Although ECs were once regarded as lining between vessel lumen and organ, many important functions of ECs are beginning to understand as a result of the progress of ECs study (Ando, 1996).

ECs permeate only a selected intravascular substance to outside of a vessel. ECs regulate permeation of low-molecular weight substance due to change the cellular intervals. For high-molecular weight substance, ECs uptake the substance using phagocytic vesicle and transport that to subendothelium (trans-cytosis).

ECs arrest hemorrhage by blood clotting when the vessel cause bleeding, while ECs have antithronbotic property when the vessel is under normal conditions. ECs combine the contradictory properties and use both properties as the situation demands.

For the control of vessel tonus, the factor which is directly linked to the regulation of blood circulation, ECs play the role to release the factor which makes SMCs relax or constrict. ECs interact with other vascular cells via adhesion molecules, ECM, or cytokines and are deeply engaged in bood clotting, tissue inflammation and immune reaction.

ECs play starring role in remodeling of blood vessels which accompany ontogenetic generation, growth or environmental change. ECs also secret growth factors which are necessary for formation of vascular tissue.

1-3. Shear Stress and ECs

1-3-1. Shear Stress in Vessels

Vessel wall is subjected to hemodynamically stress such as shear stress arise from blood flow, normal stress arise from blood pressure, and transmural stress (Fig. 1-2). Shear stress has an effect on only endothelium, which covers vessel wall, and deforms ECs in the direction of blood flow. The stress arise from blood pressure is affects not only ECs but also SMCs, fibroblast cells and so on.

Shear stress is noticed because the remodeling of blood vessel and the arteriosclerosis depends on not blood pressure but blood flow changes.

The estimate value of shear stress is 1-2 Pa in human aorta under physiological condition and 0.1–0.6 Pa in vein (Kamiya *et al*., 1984). Because actual vessels represent complicated shapes, *in vivo* shear stress, which is subjected vessel wall, differs in different area according to blood flow speed. In curves and bifurcations of vessels, blood flow separates from vessel wall or becomes sluggish, then indicate unsteady and characteristic blood flow distribution.

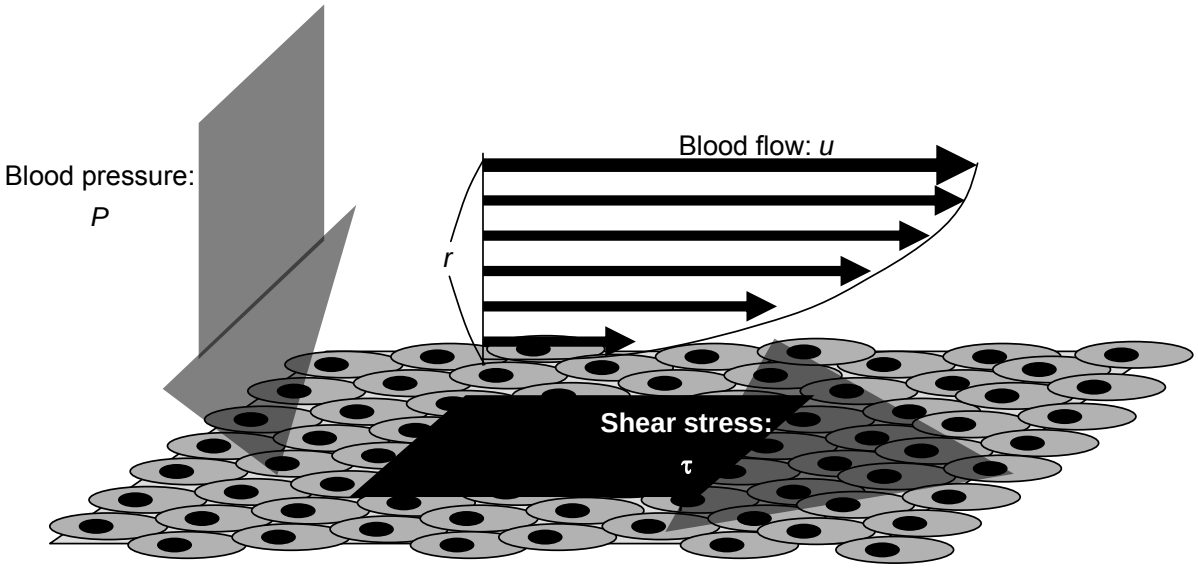

Normal stress
P = Blood pressure

Shear stress

$$\tau = \mu \frac{du}{dr}$$

Fig. 1-2 Hemodynamic stress for vessel wall.

1-3-2. The Influence of Shear Stress on ECs

Shear stress affects ECs morphology and many functions.

ECs represent cobblestone appearance under static culture condition, while they elongate and are oriented in the flow direction under shear stress subjected condition. This phenomenon depends on shear stress value and shear loaded time. Dewey *et al*. subjected 0.8 Pa for 48 h (Dewey *et al*., 1984), Eskin *et al*. subjected 3.4 Pa for 6.5 h (Eskin *et al*., 1984), and Levesque *et al*. 8.5 Pa for 1-4 h, and then they observed changes of ECs morphology and alignment (Levesque *et al*., 1985). Remuzzi *et al*. showed that the morphology change caused by shear stress (0.8 Pa for 72h) restituted 72 h after stopped loading (Remuzzi *et al*., 1984). ECs under blood flow constant condition *in vivo* shape oval and the long axis arrange to flow direction, whereas those under the area where blood flow changes or becomes sluggsh shape circular and have no directionality. These morphological changes are thought as adjustment reaction to shear stress stimulation.

The vessel diameter changes with blood flow alteration, which is called “flow-diameter relationship”. The change of vessel shape according to vessel flow has been known since a long time ago, Schretzenmayr already described in 1933 (Schretzenmayr, 1933). From subsequent studies, flow-diameter relationship is thought as adjustment reaction which keeps wall shear stress constant (Rodbard, 1975; Kamiya *et al*., 1980). Because shear stress affects only ECs, this relationship is regarded as dependent reaction of ECs.

Shear stress also affects protein transportation into ECs. Sprague *et al*. showed that ECs uptake of LDL (low density lipoprotein) increased by shear stress of 3.0 Pa for 24 h, while shear stress of 0.1 Pa for 24 h had no effect (Sprague *et al*., 1987). Kudo *et al*. showed that albumin uptake under shear stress of 1.0 Pa for 48 h was higher than that of no-shear stress condition, whereas the uptake under high shear stress (6.0 Pa) was lower (Kudo *et al*., 1998).

1-4. Glycocalyx

1-4-1. Glycocalyx Shape

The endothelial cell surface is characterized by various extracellular domains of membrane-bound molecules, the glycocalyx (Pries *et al*., 2000), which can sence the shear force of flowing blood (Gonzalez-Castillo *et al*., 2003; Mochizuki *et al*., 2003). Luft visualized the endothelial glycocalyx layer in vitro by using ruthenium red staining in an electron microscopic study, and found that the glycocalyx layer is about 20 nm thick (Luft, 1966). Subsequent *in vitro* electron microscopic observations of the molecules revealed that the glycocalyx thickness is less than 100 nm (Sims *et al*., 1991). *In vivo* studies (Pries *et al*., 1994; Pries *et al*., 1997) have revealed thicker glycocalyx layers, ranging from 0.5 mm to over 1.0 mm. This difference in thickness is due to the preparation and staining techniques, which cause the collapse of the glycocalyx structures (Luft, 1966; Pries *et al*., 2000; Van Damme *et al*., 1994; Van den Berg *et al*., 2003).

1-4-2. Function of Glycocalyx

The glycocalyx surface forms a complex three-dimensional array of soluble plasma components, including many proteins and solubilized glycosaminoglycans (GAG). Thus, the glycocalyx layer restricts the flow of plasma and denies access of red blood cells and macromolecules to the vascular wall (Constantinescu *et al*, 2003; Pries *et al*., 2000, Van den Berg *et al*., 2003). Therefore, the glycocalyx layer is important to the interaction between blood and endothelium. Its properties, such as capillary barrier function and interaction with plasma components, have been studied (Pries *et al*., 2000). The glycocalyx consists of protein, glycolipid, and proteoglycans, including exposed charged groups, and also contains membrane-bound molecules, such as selectins and integrins (Risau, 1995; Siegel *et al*., 1997), involved in immune reactions and inflammatory processes (Ley, 1996; Platts *et al*., 2003; Springer, 1995).

The intracellular uptake of macromolecules is possibly regulated by glycocalyx properties, such as surface charge and morphological barriers. The glycocalyx surface has a negative charge, because the glycocalyx has some acidic mucopolysaccharide sidechains (GAG), which contain many carboxyl and sulfate groups. Most plasma proteins, such as albumin, in the glycocalyx surface have a negative charge. Thus, the glycocalyx layer repulses the anionic proteins electrostatically. Previous studies show increased permeability when glycocalyx or albumin is neutralized (Swanson *et al*., 1994; Van Haaren *et al*., 2003).

1-4-3. Glycocalyx and Shear Stress

The thickness of the glycocalyx layer might be associated with shear stress. Haldenby *et al*. report that the glycocalyx thickness depends on the local region of the vessel, and thus might be associated with shear stress because shear stress differs according to the type of blood vessel (Haldenby *et al*., 1994). In addition, Wang et al. reported that the glycocalyx layer was thin in low shear regions such as sidewalls of the bifurcation, and thick in high shear regions such as a divider of the bifurcation (Wang *et al*., 1991).

1-5. Microvessel Network Formation

1-5-1. Angiogenesis and Vasculogenesis

There are 2 types of new microvessel formation of fetal period; vasculogenesis and angiogenesis (Fig. 1-3). The process of vasuculogenesis is as follows: undifferentiated endothelial progenitor cells (EPCs) arrive at vessel formation region, then proliferate and differentiate in that place and form new blood vessels. These existing ECs then formed vessel networks after sprout, proliferate and migrate; this process is angiogenesis. Fetal vessel formation, in this way, starts with vasculogenesis and continue with vasculogenesis and angiogenesis, then network formation is

completed.

Vasculogenesis was previously thought to be a phenomenon which is observed only in fetal period and then angiogenesis regarded as an only physiological and pathological vessel formation process in adult body. Asahara *et al*., however, indicated that EPCs exist in blood circulation and are involved in vessel formation (Asahara *et al.*, 1997). Microvessel formation in adult body, in fact, contains both angiogenesis and vasculogenesis.

The first step of angiogenesis is departure of mural cells which are around the ECs. In the site of mural cells departure, ECs are affected by angiogenesis inducible factor such as vascular endothelial growth factor (VEGF) and fibroblast growth factor (FGF), and secret various proteases, then digest basal membrane and ECM. ECs migrate and proliferate repeatedly in the space which is created by the digestion, and then form new microvessels. After that, pericytes surround and enclose the immature microvessels composed by ECs only, then ECs migration and proliferation are stopped, new basement membrane is created and mature microvessels are formed.

In vasculogenesis, EPCs are produced in bone marrow and then circulating blood flow. These EPCs are stimulated by angiogenesis inducible factor and get to the place of new vessel formation, then differentiate EC and join microvessel formation (Isner *et al*., 1999). The subsequent process is similar to angiogenesis.

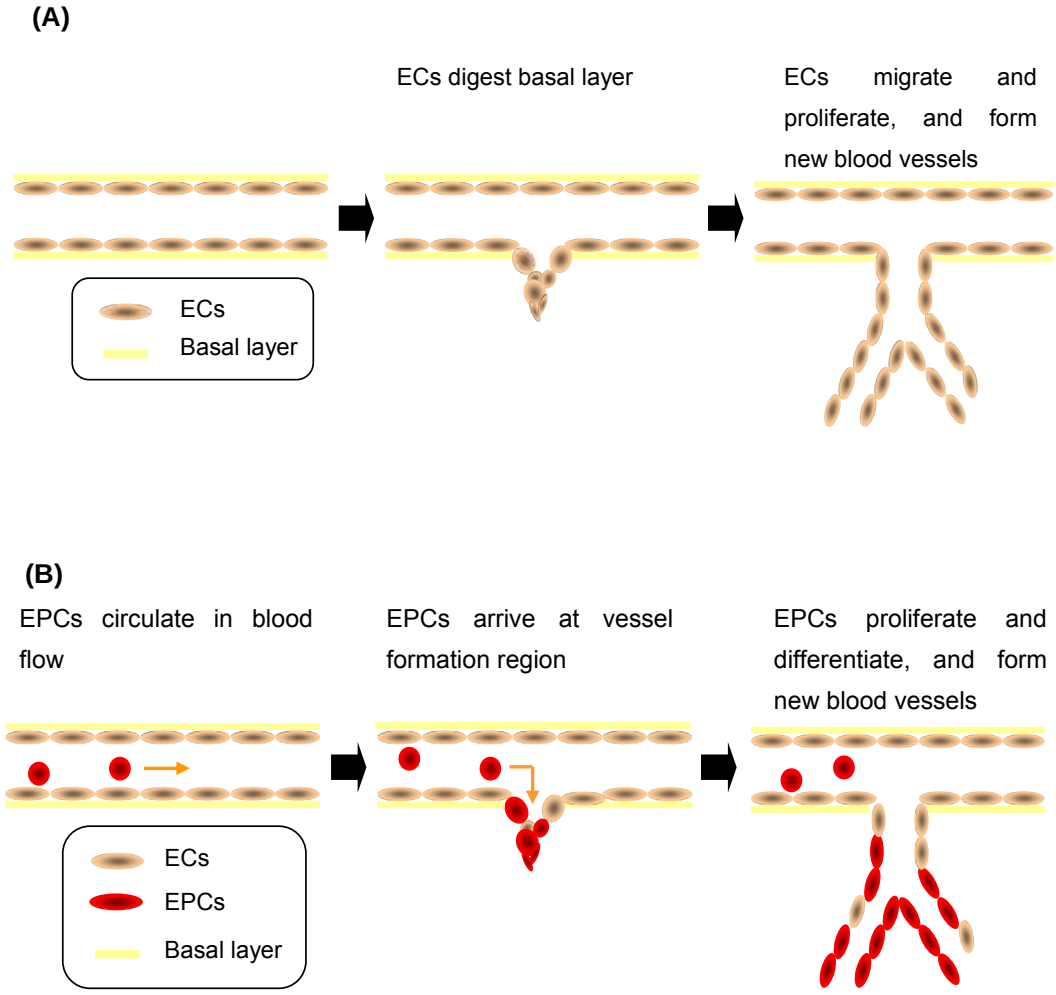

Fig. 1-3 Mechanism of new microvessel formation. There are 2 types of new microvessel formation of fetal period; angiogenesis (A) and vasculogenesis (B).

1-5-2. Regulation Factor of New Microvessel Formation

The formation of new microvessels is regulated by balance of promotion factors and inhibitory factors (Sato, 1996). The microvessel formation takes place when the promotion factors exceed the inhibitory factors.

VEGF, FGF, and epidermal growth factor (EGF) are widely known as promotion factor. The degree of participation to vessel formation of these factors is, however, still unclear.

VEGF is reported to involve the microvessel formation in many lesion such as, cancer, diabetic retinopathy, myocardial infraction, and chronic rheumatism. VEGF promotes ECs proliferation, migration and lumen formation, then increases microvessel formation and vascular permeability. Secretion of plasminogen activator (PA) and expression matrix metalloproteinase (MMP) and receptor of PA are also increased by VEGF, then basement membrane is digested.

FGF comprise the growth factor family consisted of ~20 members. ECs predominantly express FGF receptor-1 (FGFR1), and acidic FGF (aFGF) and basic FGF (bFGF), both can bind to FGFR1, transfer signals to ECs. The important factors in FGF family for network formation are aFGF and bFGF. FGF activate ECs proliferation, migration, proteinase secretion and lumen formation.

EGF family is consisted by EGF, transforming growth factor-α (TGF-α), heparin binding EGF like growth factor (HB-EGF) and so on. All EGF family binds to EGF receptor and only EGF and TGF-α are reported to have an effect on new microvessel formation. TGF-α widely exists *in vivo* and is secreted by tumor cell, then is thought to be an important factor of microvessel formation.

Inhibitory factor include interleukin 1 (IL-1) and tumor necrosis factor-α (TNF-α) are also known as regulating factor of microvessel formation. IL-1 is secreted by various cells including ECs and inhibits ECs proliferation. TNF-α affects antagonistically in vivo microvessel formation; this factor promotes microvessel formation in low concentration, whereas inhibits that in high

concentration.

Since angiogenesis is one of the physiological responses to a low-O_2 environment, hypoxia is one of the major factors controlling network formation (Vincent *et al*., 2002). In addition, solid tumors are commonly hypoxic (Fukushima *et al*., 2001), and O_2 concentration is an important determinant of tumor growth. Angiogenesis-promoting factors, such as growth factors and their receptors, are induced by hypoxic conditions *in vivo* (Hoper *et al*., 1995), and hypoxia also induces angiogenic factors *in vitro* (Yamagishi *et al*., 1999). Hypoxia induces expression of VEGF (Fukushima *et al*., 2001; Ikeda *et al*., 1995; Ladoux *et al*., 1993; Shweiki *et al*., 1992; Shweiki *et al*., 1995; Tuder *et al*., 1995), and HIF-1α (hypoxia inducible factor) is associated with angiogenesis and expression of bFGF and PDGF (Bos *et al*., 2005). Hypoxic conditions also caused an increase in levels of mRNA for the VEGF receptors KDR/Flk and Flt (Tuder *et al*., 1995), and aortic cells cultured under hypoxic conditions expressed increased amounts of Flk-1 and FGFR1, and that they were more responsive to VEGF and bFGF than were those exposed to room air (Akimoto *et al*., 2002; Akimoto *et al*., 2003). Furthermore, the VEGF receptor KDR was up-regulated in human umbilical vein endothelial cells in response to hypoxia (Waltenberger *et al*., 1996).

1-5-3. Microvessel Formation in a Lesion

Although the new microvessel formation is required in ontogenetic growth, the formation hardly observed in adult tissue. Pathological angiogenesis is, however, occurred in a lesion, such as cancer, arteriosclerosis, and diabetic retinopathy. The microvessel formation is closely linked to progress of these diseases (Carmeliet *et al*., 2000; Kanayasu-Toyoda *et al*., 1996).

Diabetic retinopathy is typical example of pathologic condition which is caused by newly-formed network itself. Diabetes cause interference of retinal microvasculature result from prolonged hyperglycemia, then microvessl formation are induced to overcome ischemia of retina.

These microvessels are fragile and trigger bleed, then result in blindness.

Cancer is the example of the pathologic condition which is caused by abnormal proliferation of cancer cells result from new microvessel formation. Growth factors which are secreted by tumor cells induces new vessel formation. The new vessels supply nutrient to the tumor cells, then cause abnormal proliferation.

New microvessel formation is also involved in arteriosclerosis. Increased vessels in intima of arteriolosclerosis are thought to play important role in bleeding and edema generation in the intima.

In contrast, new vessel formation is required for recovery from disease according to the condition such as ischemia. When narrowing of coronary artery cause, the other coronary artery makes collateral vessels. This phenomenon is the result of which ischemic cardiocyte secretes angiogenesis promotion factor to improve blood flow. This ability, however, decrease with age.

1-5-4. Needs for Microvessel Network Formation in Tissue Engineering

Control of microvessel network formation is key issue in tissue engineering (regenerative medicine) because vessels are essential for the formation and maintenance of organ functions. While two-dimensional (2-D) tissue, such as skin and retina, has been applied in clinical tissue engineering, three-dimensional (3-D) tissue has not regenerated. Regenerated 3-D tissue cannot maintain its physiological function in the absence of a 3-D microvessel network because diffusion alone can not supply sufficient nutrients and O_2 to the tissue. In the absence of vascularization, diffusion limits tissues to a thickness of less than ~100 μm (Shimizu *et al*., 2002)); therefore, extensive 3-D microvessel networks of significant depth are required to supply O_2 and nutrients to cells comprising regenerated 3-D tissues.

1-5-5. Microvessel Formation Studies Using *in Vitro* Models

In vitro models of network formation have been used to study the mechanism of microvessel network formation in detail (Vailhé *et al.*, 2001). *In vitro* models are divided into 2 categories; 2-D models and 3-D models.

Matrigel model is widely known 2-D model (Fig. 1-4 (A)). Matrigel is the component of basement membrane which is extracted from EHC mouse sarcoma. The main ingredients of Matrigel are laminin, type IV collagen, heparan sulfate proteoglycan and enactin / nidogen. In addition, Matrigel normally contains growth factors such as TGF-β and FGF. ECs, which are seeded onto Matrigel, form 2-D capillary-like network on the gel (Deroanne *et al*., 2001). Collagen sandwich model is also used commonly as 2-D model (Fig. 1-4 (B)). In this model, ECs are seeded between 2 layers of collagen gel, then form 2-D networks (Deroanne *et al*., 2001). 2-D models are widely used because they could be made and analyzed easily.

In contrast, there are 3-D models in which ECs, seeded on a collagen gel, invade into the gel and form networks. Montesano *et al*. indicated that ECs on a collagen gel invaded into the gel and formed 3-D capillary-like networks by adding growth factors (Montesano *et al*., 1985; Montesano *et al*., 1986; Pepper *et al*., 1995). These models mimic the *in vivo* network formation processes, such as sprouting, proliferation and migration (Fig. 1-4 (C)). 3-D models are similar to *in vivo* environment compared to 2-D models. Spheroid model is also one of the 3-D models. In this model, spheroid (circular aggregation of ECs) is seeded in a collagen gel and added growth factors, then ECs form capillary-like networks (Korff *et al*., 1999; Vernon *et al*., 1999).

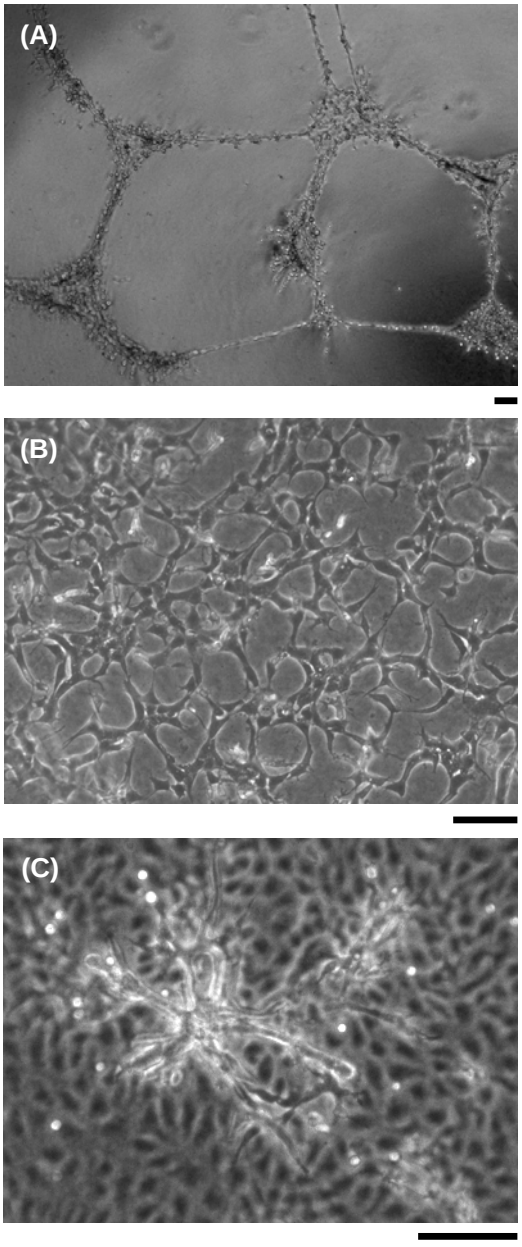

Fig. 1-4 *In vitro* models for microvessel mormation studies. (A) Matrigel model and (B) collagen sandwich model. (C) 3-D capillary-like network model. Bar indicates 100 μm.

1-6. Objectives and Outlines of This Thesis

This thesis deals with ECs microvessel formation. The control of new microvessel formation is a matter of importance for cure of disease or tissue engineering as described above. Previous studies have found many angiogenesis / vasculogenesis promotion or inhibition factors, but little is known about the effect of these factors on microvessel network formation itself.

In vivo studies showed that shear stress affects the ECs properties and plays a important role for vessel remodeling, but the purely effect of shear stress on network formation was hardly known. Because we think shear stress is one of the most important key factors for the control of microvessel formation, we tried to reveal the relation between shear stress and network formation. Firstly, we created the experimental setup in which ECs are loaded shear stress and examined the effect of shear stress on surface structure and function of ECs, albumin uptake into ECs (Chapter II). Using this setup, we could load arbitrary volume of shear stress and could observe EC under the shear-loaded condition using microscopy. We subsequently remodeled the shear loading setup, and then investigated the effect of shear stress on 3-D network formation (Chapter III).

Not only inducing network formation, we also need to control the network morphology to apply to tissue engineering. Because 3-D tissue needs an internal vessel network, control of 3-D networks is needed to introduce microvessels deep into tissue. The concentration profile of extracellular growth factor is an important factor in controlling 3-D microvessel networks. Recent findings indicated that the morphology of such networks is influenced by the extracellular growth factor distribution *in vivo*. To form 3-D networks that extend deep into tissue, this study focused on the effect of the concentration gradient of growth factor on the morphology of the network. (Chapter IV).

Hypoxia is thought to be one of the major factors of network formation, because angiogenesis is one of physiological responses to a low-O_2 environment. Previous studies revealed that

angiogenesis inducible factors, such as growth factors and receptors, are induced by hypoxic condition. Although *in vitro* studies also showed that hypoxia induces angiogenic factors, there are hardly studies about the effect of hypoxia on network formation. Because hypoxia has huge potential on microvessel formation, revealing the effect of hypoxia on network formation leads to the control of microvessel formation. We therefore focus on the effect of hypoxia on network formation (Chapter V).

These studies described above are finally summarized and concluded (Chapter VI). In the final chapter, we also discuss about the significance of this thesis and the vista for the future.

References

Akimoto T, Hammerman MR. Fibroblast growth factor 2 promotes microvessel formation from mouse embryonic aorta. Am J Physiol Cell Physiol. 2003; 284: C371-C377.

Akimoto T, Liapis H, Hammerman MR. Microvessel formation from mouse embryonic aortic explants is oxygen and VEGF dependent. Am J Physiol Regul Integr Comp Physiol. 2002; 283: R487-R495

Ando J. Shear stress and endothelial cells. Medical Review. 1996. (in Japanese)

Asahara T, Murohara T, Sullivan A, Silver M, van der Zee R, Li T, Witzenbichler B, Schatteman G, Isner JM. Isolation of putative progenitor endothelial cells for angiogenesis. Science. 1997; 275: 964-967.

Bos R, van Diest PJ, de Jong JS, van der Groep P, van der Valk P, van der Wall E. Hypoxia-inducible factor-1alpha is associated with angiogenesis, and expression of bFGF, PDGF-BB, and EGFR in invasive breast cancer. Histopathology. 2005; 46: 31-36.

Carmeliet P, Jain RK. Angiogenesis in cancer and other diseases. Nature. 2000; 407: 249-257.

Constantinescu AA, Vink H, Spaan JA. Endothelial cell glycocalyx modulates immobilization of leukocytes at the endothelial surface. Arterioscler Thromb Vasc Biol. 2003; 23: 1541-1547.

Deroanne CF, Lapiere CM, Nusgens BV. In vitro tubulogenesis of endothelial cells by relaxation of the coupling extracellular matrix-cytoskeleton. Cardiovasc Res. 2001; 49: 647-658.

Dewey CF Jr, Bussolari SR, Gimbrone MA Jr, Davies PF. The dynamic response of vascular endothelial cells to fluid shear stress. J Biomech Eng. 1981; 103: 177-185.

Eskin SG, Ives CL, McIntire LV, Navarro LT. Response of cultured endothelial cells to steady flow. Microvasc Res. 1984; 28: 87-94.

Fukumura D, Xu L, Chen Y, Gohongi T, Seed B, Jain RK. Hypoxia and acidosis independently

up-regulate vascular endothelial growth factor transcription in brain tumors in vivo. Cancer Res. 2001; 61: 6020-6024.

Gonzalez-Castillo C, Rubio R, Zenteno-Savin T. Coronary flow-induced inotropism is modulated by binding of dextrans to the endothelial luminal surface. Am J Physiol Heart Circ Physiol. 2003; 284: H1348-H1357.

Haldenby KA, Chappell DC, Winlove CP, Parker KH, Firth JA. Focal and regional variations in the composition of the glycocalyx of large vessel endothelium. J. Vasc. Res. 1994; 31: 2-9.

Hoper J, Jahn H. Influence of environmental oxygen concentration on growth and vascular density of the area vasculosa in chick embryos. Int J Microcirc Clin Exp. 1995; 15: 186-92.

Ikeda E, Achen MG, Breier G, Risau W. Hypoxia-induced transcriptional activation and increased mRNA stability of vascular endothelial growth factor in C6 glioma cells. J Biol Chem. 1995; 270: 19761-19766.

Isner JM, Asahara T. Angiogenesis and vasculogenesis as therapeutic strategies for postnatal neovascularization. J Clin Invest. 1999; 103: 1231-1236.

Kamiya A, Togawa T. Adaptive regulation of wall shear stress optimizing vascular tree function. Bull Math Biol. 1984; 46: 127-137.

Kamiya A, Togawa T. Adaptive regulation of wall shear stress to flow change in the canine carotid artery. Am J Physiol Heart Circ Physiol. 1980; 239: H14-H21.

Kanayasu-Toyoda T, Morita I, Murota S. Endothelial cell function and angiogenesis. Nippon Yakurigaku Zasshi. 1996; 107: 99-107. (in Japanese)

Korff T, Augustin HG. Tensional forces in fibrillar extracellular matrices control directional capillary sprouting. J Cell Sci. 1999; 112: 3249-3258.

Kudo S, Ikezawa K, Matsumura S, Ikeda M, Oka K, Tanishita K. Effect of wall shear stress on macromolecule uptake into cultured endothelial cells. Trans. JSME. 1998; 64B: 367-374.

Ladoux A, Frelin C. Hypoxia is a strong inducer of vascular endothelial growth factor mRNA expression in the heart. Biochem Biophys Res Commun. 1993; 195: 1005-1010.

Levesque MJ, Nerem RM. The elongation and orientation of cultured endothelial cells in response to shear stress. J Biomech Eng. 1985; 107: 341-347.

Ley K. Molecular mechanisms of leukocyte recruitment in the inflammatory process. Cardiovasc Res. 1996; 32: 733-742.

Luft JH. Fine structure of capillary and endocapillary layer as revealed by ruthenium red. Microcirc Symp Fed Proc. 1966; 25: 1773-2783.

Mochizuki S, Vink H, Hiramatsu O, Kajita T, Shigeto F, Spaan JA, Kajiya F. Role of hyaluronic acid glycosaminoglycans in shear-induced endothelium-derived nitric oxide release. Am J Physiol Heart Circ Physiol. 2003; 285: H722-726.

Montesano R, Orci L. Tumor-promoting phorbol esters induce angiogenesis in vitro. Cell. 1985; 42: 469-477.

Montesano R, Vassalli JD, Baird A, Guillemin R, Orci L. Basic fibroblast growth factor induces angiogenesis in vitro. Proc Natl Acad Sci USA. 1986; 83: 7297-7301.

Pepper MS, Ferrara N, Orci L, Montesano R. Leukemia inhibitory factor (LIF) inhibits angiogenesis in vitro. J Cell Sci. 1995; 108: 73-83.

Platts SH, Linden J, Duling BR. Rapid modification of the glycocalyx caused by ischemia-reperfusion is inhibited by adenosine A2A receptor activation. Am J Physiol Heart Circ Physiol. 2003; 284: H2360-2367.

Pries AR, Secomb TW, Gaehtgens P. Microvascular blood flow resistance: role of endothelial surface layer. Am J Physiol Heart Circ Physiol. 1997; 273: H2272-2279.

Pries AR, Secomb TW, Gathtgens P. The endothelial surface layer. Pflügers Arch-Eur J Physiol. 2000; 440: 653-666.

Pries AR, Secomb TW, Gessner T, Sperandio MB, Gross JF, Gaehtgens P. Resistance to blood flow in microvessels in vivo. 1994; Circ Res 75: 904-915.

Remuzzi A, Dewey CF Jr, Davies PF, Gimbrone MA Jr. Orientation of endothelial cells in shear fields in vitro. Biorheology. 1984; 21: 617-630.

Risau W. Differentiation of endothelium. FASEB J. 1995; 9: 926-933.

Rodbard S. Vascular caliber. Cardiology. 1975; 60: 4-49.

Sato Y. Regulators of angiogenesis. Nippon Yakurigaku Zasshi. 1996; 107: 109-117. (in Japanese)

Schretzenmayr A. Uber kreislaufregulatorische Vorgange an den grossen Arterien bei der Muskelarbeit. Pflugers Arch Ges Physiol. 1933; 232: 743–748.

Shimizu T, Yamato M, Isoi Y, Akutsu T, Setomaru T, Abe K, Kikuchi A, Umezu M, Okano T. Fabrication of pulsatile cardiac tissue grafts using a novel 3-dimensional cell sheet manipulation technique and temperature-responsive cell culture surfaces. Circ Res. 2002; 90: e40.

Shweiki D, Itin A, Soffer D, Keshet E. Vascular endothelial growth factor induced by hypoxia may mediate hypoxia-initiated angiogenesis. Nature. 1992; 359: 843-845.

Shweiki D, Neeman M, Itin A, Keshet E. Induction of vascular endothelial growth factor expression by hypoxia and by glucose deficiency in multicell spheroids: implications for tumor angiogenesis. Proc Natl Acad Sci U S A. 1995; 92: 768-772.

Siegel G., Malmsten M. The role of the endothelium in inflammation and tumor metastasis. Int J Microcirc Clin Exp. 1997; 17: 257-272.

Sims DE, Westfall JA, Kiopes AL, Horne MM. Preservation of tracheal mucus by nonaqueous fixative. Biotech Histochem. 1991; 66: 173-180.

Sprague EA, Steinbach BL, Nerem RM, Schwartz CJ. Influence of a laminar steady-state

fluid-imposed wall shear stress on the binding, internalization, and degradation of low-density lipoproteins by cultured arterial endothelium. Circulation. 1987; 76: 648-656.

Springer TA. Traffic signals on endothelium for lymphocyte recirculation and leukocyte emigration. Annu Rev Physiol. 1995; 57: 827-872.

Swanson JA, Kern DF. Characterization of pulmonary endothelial charge barrier. Am J Physiol Heart Circ Physiol. 1994; 266: H1300-1303.

Tuder RM, Flook BE, Voelkel NF. Increased gene expression for VEGF and the VEGF receptors KDR/Flk and Flt in lungs exposed to acute or to chronic hypoxia. Modulation of gene expression by nitric oxide. J Clin Invest. 1995; 95: 1798-1807.

Vailhé B, Vittet D, Feige JJ. In vitro models of vasculogenesis and angiogenesis. Lab Invest. 2001; 81: 439-452.

Van Damme MPI, Tiglias J, Nemat N, Preston BN. Determination of the charge content at the surface of cells using a colloid titration technique. Anal Biochem. 1994; 223: 62-70.

Van den Berg BM, Vink H, Spaan JA. The endothelial glycocalyx protects against myocardial edema. Circ Res. 2003; 92: 592-594.

Van Haaren PM, VanBavel E, Vink H, Spaan JA. Localization of the permeability barrier to solutes in isolated arteries by confocal microscopy. Am J Physiol Heart Circ Physiol 2003; 285: H2848-H2856.

Vernon RB, Sage EH. A novel, quantitative model for study of endothelial cell migration and sprout formation within three-dimensional collagen matrices. Microvasc Res. 1999; 57: 118-133.

Vincent KA, Feron O, Kelly RA. Harnessing the response to tissue hypoxia: HIF-1 alpha and therapeutic angiogenesis. Trends Cardiovasc Med. 2002; 12: 362-367.

Waltenberger J, Mayr U, Pentz S, Hombach V. Functional upregulation of the vascular endothelial

growth factor receptor KDR by hypoxia. Circulation. 1996; 94: 1647-54.

Wang S, Okano M, Yoshida Y. Ultrastructure of endothelial cells and lipid deposition on the flow dividers of brachiocephalic and left subclavian arterial bifurcations of the rabbit aorta. Doumyakukouka. 1991; 19: 1089-1100. (in Japanese)

Yamagishi S, Kawakami T, Fujimori H, Yonekura H, Tanaka N, Yamamoto Y, Urayama H, Watanabe Y, Yamamoto H. Insulin stimulates the growth and tube formation of human microvascular endothelial cells through autocrine vascular endothelial growth factor. Microvasc Res. 1999; 57: 329-339.

Chapter II

Effect of Glycocalyx on Shear-dependent Albumin Uptake in Endothelial Cells

2-1. Introduction

Atherosclerotic legions appear in regions of low shear stress in relatively large arteries, such as the carotid bifurcation and the coronary artery (Caro *et al*., 1971). Atherosclerosis is initiated by the uptake of low density lipoprotein (LDL) (Schwenke *et al*., 1989), which is highly associated with hemodynamic stress. Some studies demonstrate that the transport of macromolecules such as albumin across the cell membrane is strongly affected by the shear stress on endothelial cells (Packham *et al*., 1967, Somer *et al*., 1972). Kudo *et al*. measured the effect of shear stress on albumin uptake into endothelial cells *in vitro*, and reported an increased uptake at lower shear stress and a decreased uptake at higher shear stress(Kudo *et al*., 1998; Kudo *et al*., 2000). However, the mechanism of this biphasic response of uptake remains unclear.

The endothelial cell surface is characterized by various extracellular domains of membrane-bound molecules, the glycocalyx (Pries *et al*., 2000), which can sence the shear force of flowing blood (Gonzalez-Castillo *et al*., 2003, Mochizuki *et al*., 2003). Luft visualized the endothelial glycocalyx layer *in vitro* by using ruthenium red staining in an electron microscopic study, and found that the glycocalyx layer is about 20 nm thick (Luft *et al*., 1966). Subsequent *in vitro* electron microscopic observations of the molecules revealed that the glycocalyx thickness is less than 100 nm (Sims *et al*., 1991). *In vivo* studies (Pries *et al*., 1997; Pries *et al*., 1994) have revealed thicker glycocalyx layers, ranging from 0.5 μm to over 1.0 μm. This difference in

thickness is due to the preparation and staining techniques, which cause the collapse of the glycocalyx structures (Luft *et al*., 1966; Pries *et al*., 2000; Van Haaren *et al*., 2003; Vink *et al*., 2000).

The glycocalyx surface forms a complex three-dimensional array of soluble plasma components, including many proteins and solubilized glycosaminoglycans (GAG). Thus, the glycocalyx layer restricts the flow of plasma and denies access of red blood cells and macromolecules to the vascular wall (Constantinescu *et al*., 2003; Pries *et al*., 2000; Van den Berg *et al*., 2003). Therefore, the glycocalyx layer is important to the interaction between blood and endothelium. Its properties, such as capillary barrier function and interaction with plasma components, have been studied (Pries *et al*., 2000). The glycocalyx consists of protein, glycolipid, and proteoglycans, including exposed charged groups, and also contains membrane-bound molecules, such as selectins and integrins (Risau, 1995; Siegel *et al*., 1997), involved in immune reactions and inflammatory processes (Ley, 1996; Platts *et al*., 2003; Springer, 1995).

The intracellular uptake of macromolecules is possibly regulated by glycocalyx properties, such as surface charge and morphological barriers. The glycocalyx surface has a negative charge, because the glycocalyx has some acidic mucopolysaccharide sidechains (GAG), which contain many carboxyl and sulfate groups. Most plasma proteins, such as albumin, in the glycocalyx surface have a negative charge. Thus, the glycocalyx layer repulses the anionic proteins electrostatically. Previous studies show increased permeability when glycocalyx or albumin is neutralized (Swanson *et al*., 1994; Van Haaren *et al*., 2003).

The thickness of the glycocalyx layer might be associated with shear stress. Haldenby et al. report that the glycocalyx thickness depends on the local region of the vessel, and thus might be associated with shear stress because shear stress differs according to the type of blood vessel (Haldenby *et al*., 1994). In addition, Wang et al. reported that the glycocalyx layer was thin in low

shear regions such as sidewalls of the bifurcation, and thick in high shear regions such as a divider of the bifurcation (Wang *et al*., 1991).

Here, we studied the effect of glycocalyx on the shear-dependent uptake of macromolecules into endothelial cells. We measured the albumin uptake into cultured endothelial cells with imposed shear stress stimulus, and visualized the morphology of the glycocalyx layer, such as thickness. To determine the effect of surface charge of the glycocalyx layer on the uptake, we measured the albumin uptake for a neutralized glycocalyx layer.

2-2. Materials and Methods

2-2-1. Cell Culture

Cultured bovine aorta endothelial cells (BAECs; lot. 32010, Cell Systems, U.S.A.) were used in all experiments. Specimens for the albumin uptake measurements were prepared as follows. BAECs were seeded in 25-cm^2 culture flasks (3014, Falcon, U.S.A.) and cultured in Dulbecco's modified Eagle's medium (DMEM; 31600-34, GIBCO, U.S.A.) containing 10% fetal bovine serum (FBS; lot. 9K2087, JRH Biosciences, U.S.A.), 1% antibiotic-antimycotic (GIBCO BRL 15240-062, LIFE TECH, U.S.A.) and 15 mM HEPES (346-D1373, DOJINDO, Japan). The culture flasks were maintained at pH 7.3 and 37°C in a CO_2 incubator. BAECs of passages 5-9 were used for the uptake measurements. Specimens for observation of the glycocalyx layer by using electron microscopy were prepared as follows. BAECs were seeded on a glass dish (3910-035, IWAKI, Japan) or plastic-bottom dish (Falcon, U.S.A.) coated with 2% collagen type Ⅳ (CELLMATRIX-4-20, Nitta Gelatin, Japan), and then used for observation when they reached confluency in 7-10 days. A glass-bottom dish was used because when BAECs are observed at high magnification, the bottom of the dish must be thin with respect to the working distance. A plastic-bottom dish was used when BAECs are observed by using an electron microscope.

2-2-2. Shear Stress Loading

The culture medium described above was used as perfusate. A rectangular flow chamber (0.02 cm high, 2.0 cm wide, 1.20 cm long) was placed over the dish containing BAECs and then placed in the flow circuit (Fig. 2-1). The perfusate was circulated through the flow circuit by a roller pump (MP-3N, EYELA, Japan), thus exposing the BAECs to laminar flow (the pulsatile component was about ± 5%). Total priming volume was 50 ml. The wall shear stress in the rectangular flow chamber, and thus the shear stress applied to the endothelial cells, was calculated as

$$\tau=6\mu Q/h^2 \cdot b \qquad (1)$$

where τ is wall shear stress (Pa), μ is the viscosity (8.5×10^{-4} Pa・s, measured by a rotational viscometer at 37°C), Q is flow rate (cm^3/s), h is the flow channel height (0.02 cm), and b is the flow channel width (2.0 cm). Table 1 lists the flow rate and calculated wall shear stress, which ranged between 0.5-3.0 Pa.

The BAECs were exposed to the shear stress for 48 hours. The perfusate was kept at 37°C by using a water bath and was gassed with a mixture of 5% CO_2-95% air to maintain a pH 7.3 throughout the experiment.

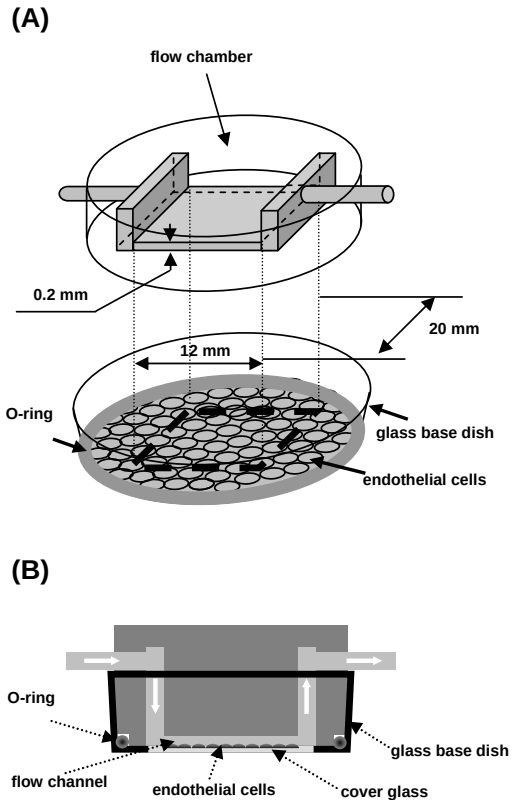

Fig. 2-1 Apparatus for loading shear stress. (A) Flow chamber installed inside a glass-base dish. (B) Cross-section of assembled flow chamber showing endothelial cells (on cover glass) exposed to shear stress by a flow of perfusate.

2-2-3. Preparation of Fluorescent Albumin

The albumin uptake into the cells was determined by measuring the fluorescence of tetramethylrhodamin isothiocyanate conjugated albumin (TRITC-albumin; A-847, Molecular Probes, U.S.A.). To remove free TRITC dye, TRITC-albumin was centrifuged at 4°C 8 times with an ultrafilter (CENTREX UFB-C30, IWAKI, Japan). The resulting TRITC-albumin was mixed with serum bovine albumin (B-4287, Sigma, U.S.A.) and dissolved in DMEM to reach a final concentration of 4.0 mg/ml (albumin concentration of 10% FBS).

2-2-4. Albumin Uptake

Fig. 2-2 summarizes the procedure for uptake measurements. After the shear stress had been applied to the cells for 48 hours, the flow chamber was switched to another flow circuit to determine the uptake of TRITC-albumin by perfusing TRITC-albumin for 1 hour under the same shear stress. The flow chamber was then removed from the flow circuit and rinsed with fresh medium without TRITC-albumin for 5 minutes.

The albumin uptake was measured by using confocal laser scanning microscopy (MRC 600 system, BIO-RAD Microscience, U.S.A.) that involved an inverted microscope (TMD 300, Nikon) with an objective lens [63× (NA 1.4) Plan-apo, Nikon, Japan]. The fluorescence of TRITC excited by the 488-nm spectral line of a 25-mW argon ion laser was detected at a wavelength longer than 515 nm. The scan rate was 512 lines/sec, and each individual image was an average of three successive images. The fluorescence images and the phase contrast images were acquired simultaneously as follows. The flow chamber was mounted on the stage of the invert microscope, and the fluorescent and the phase contrast images were acquired at 5 random locations in the specimen. Each set of image data consisted of 11 serial tomographic images in a vertical direction (height direction of the cell) at intervals of 1 μm. Simultaneously, the albumin uptake into the same

cells (same lot and generation of cells) was measured without shear stress stimulus as control data.

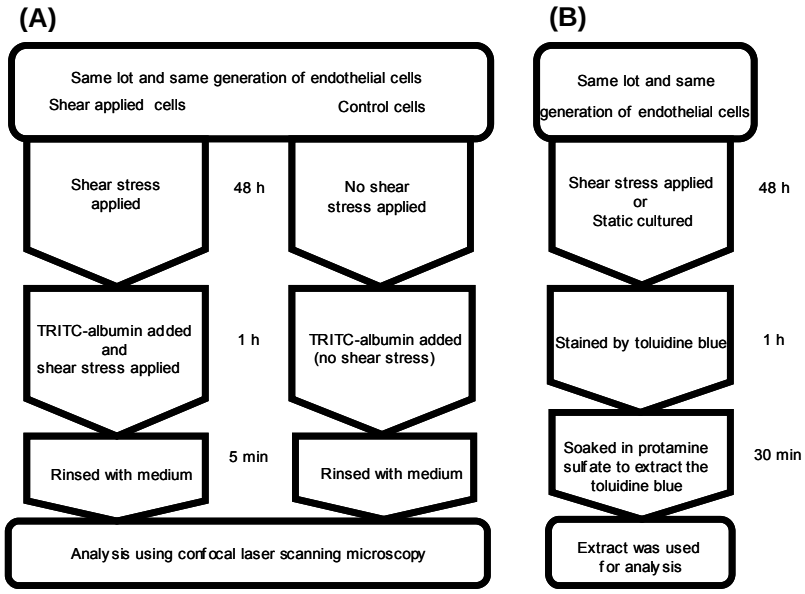

Fig. 2-2 Procedure for albumin uptake measurements. (A) Procedure to measure albumin uptake into endothelial cells with and without applied shear stress and (B) procedure to measure cell surface charge.

2-2-5. Image Analysis

The acquired fluorescence images were analyzed by using an image analysis software (NIH Image). The fluorescence intensity of TRITC-albumin was determined by using an integrated image from the 11 tomographic images (see preceding section). The edges of BAECs were determined using phase contrast images, and then applied to the corresponding fluorescence image. The average fluorescent intensity for each individual cell was determined. Finally, the normalized uptake was calculated as the ratio of average intensity of an individual cell under shear stress conditions to that under static conditions.

2-2-6. Measurement of the Thickness of Stained Glycocalyx-layer Structures by TEM

After shear stress loading, the structure of the glycocalyx layer was observed by using transmission electron microscopy (TEM). After the loading, the BAECs on the plastic dish were washed in PBS (+) (05913, Nissui, Japan) and 0.2 M sodium cacodylate buffer (29810, TAAB, U.K.), and then prefixed by 3.6% glutaraldehyde (EM Grade, 35330, TAAB, U.K.) including 1500 ppm ruthenium red and 0.2 M sodium cacodylate buffer for 24 hours at room temperature. The BAECs were then rinsed with 0.2 M sodium cacodylate buffer with sucrose, and were postfixed by 1.0% osmium tetroxide including 1000 ppm ruthenium red and 0.2 M sodium cacodylate buffer for 3 hours at room temperature. The BAECs were dehydrated by using acetone and then embedded in Epon. The Epon samples were sectioned into ultrathin specimens (about 80 nm thick), which were then observed using TEM. Acquired images were analyzed by using an image analyzing software (NIH Image) on a computer (Macintosh G4, Apple computers) to determine the thickness of the glycocalyx layer. The thickness of the stained glycocalyx layer was estimated based on TEM images to determine the brightness along the line normal to the glycocalyx layer direction. In this

estimation, we defined the edge of the stained glycocalyx layer as the position of middle brightness along the line as illustrated in Fig. 2-3. The thickness of the stained structure was measured at 30 points for each individual cell.

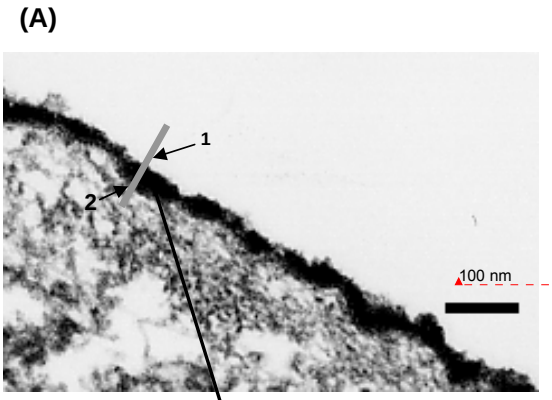

書式変更
書式変更
削除: plotprofile
書式変更
書式変更
書式変更
書式変更
書式変更
書式変更
書式変更
書式変更
書式変更

Fig. 2-3 Determination of the thickness of the glycocalyx layer. Edge of glycocalyx layer was defined by the position of middle brightness along the line shown in (A), and the thickness was determined by the distance between the points of middle brightness as shown in (B). The brightness is expressed by 256 gradations.

2-2-7. Measurement of Cell Surface Charge

After the shear stress loading, the charge of the glycocalyx layer was determined by measuring the amount of toluidine blue (Sigma, U.S.A.) on the glycocalyx layer. Toluidine blue was used because it was cationic ions, which combine with the negative charge on the glycocalyx layer, thus the charge on the cell surface is directly related to the amount of toluidine blue in the layer (Thethi *et al*., 1997).

After loading, the BAECs were washed in PBS (+) and 0.25 M sucrose (31365-1201, Junsei Chemical, Japan), and then stained by a mixture of 0.25 M sucrose and 0.001% toluidine blue for an hour at 4°C. The BAECs were washed in 0.25 M sucrose 5 times, and then soaked for 30 minutes at 4°C in 0.1 mg/ml protamine sulfate (Type X, P-4020, Sigma, U.S.A.) to extract the toluidine blue, which combined with the glycocalyx. The toluidine blue was displaced by the protamine sulfate because protamine sulfate has higher affinity for carboxyl groups and sulfate groups in the glycocalyx than the toluidine blue.

To measure the amount of charge on the cells, we used Van Damme's method (Van Damme *et al*, 1994) and the amount of toluidine blue on the glycocalyx was estimated based on the absorption rate, which depends of the concentration of toluidine blue. First, the extract was transferred to quartz glass cuvettes to measure the absorbance of the extract by using a double beam spectrophotometer (U-3400, Hitachi, Japan) at an extinction wavelength of 640 nm. Next, the average absorbance for each individual cell was determined (average by measuring the fluorescence of the same sample 10 times).

2-2-8. Neutralization of Glycocalyx Charge

The glycocalyx was neutralized by adding protamine sulfate (Type X, P-4020, Sigma, U.S.A.) to the perfusate to a final concentration of 0.001 mg/ml. Protamine sulfate was used as a charge

neutralizer because its isoelectric point (pI) is 10-12 (Swanson *et al*., 1994).

After the shear stress was applied for 48 hours, the BAECs were exposed to the perfusate with protamine sulfate for 30 minutes to neutralize the glycocalyx. The flow circuit was then rinsed with fresh DMEM without protamine sulfate. Then, the BAECs were exposed to the perfusate with TRITC-albumin, and finally the fluorescence intensity of TRITC was measured to determine the amount of albumin uptake.

2-2-9. Statistical Analysis

Data are presented as mean ± S.D. The number of replicated experiments performed is n. Student's t test was used to test for differences, which were considered significant at an error level of $P < 0.05$.

2-3. Results

2-3-1. Effect of Shear Stress on Albumin Uptake

Fig. 2-4 shows the fluorescent and phase contrast images of endothelial cells under applied shear stress up to 3.0 Pa for 48 hours. Each fluorescent image is the integration of 11 serial tomographic images of endothelial cells. The phase contrast images reveal the morphology changes of endothelial cells due to the applied shear stress. The polygonal shape of the cells under static conditions (no applied shear stress) became elongated in the flow direction, similar to previously reported results (Davis, 1995; Davis *et al*., 1993; Fukushima *et al*., 2001; Nerem *et al*., 1992).

Fig. 2-4 reveals the dependency of the albumin uptake on the applied shear stress. The distribution of fluorescent spots in individual cells at a shear stress of 1.0 Pa appeared to be denser

than under static conditions, revealing enhanced albumin uptake by the applied shear stress. In contrast, the distribution of fluorescent spots at a shear stress of 3.0 Pa was clearly sparser compared to that under static conditions. Thus, the albumin uptake was restricted when the shear stress exceeded 2.0 Pa.

To quantify the albumin uptake into the cells, we measured the brightness intensity of the fluorescent images of Fig. 2-4 by using NIH image analysis. Fig. 2-5 shows the average brightness intensity of each image in Fig. 2-4. The relative light intensity (y-axis) is an indicator of the ratio of the albumin uptake with applied shear stress to that without shear stress. The albumin uptake (i.e., relative light intensity) increased by 16% at a shear stress of 1.0 Pa between shear stress conditions and static conditions, a statistically significant difference ($P < 0.05$). In contrast, at a shear stress of 3.0 Pa the uptake decreased to 27% between shear stress conditions and static conditions, a statistically significant difference ($P < 0.001$) .

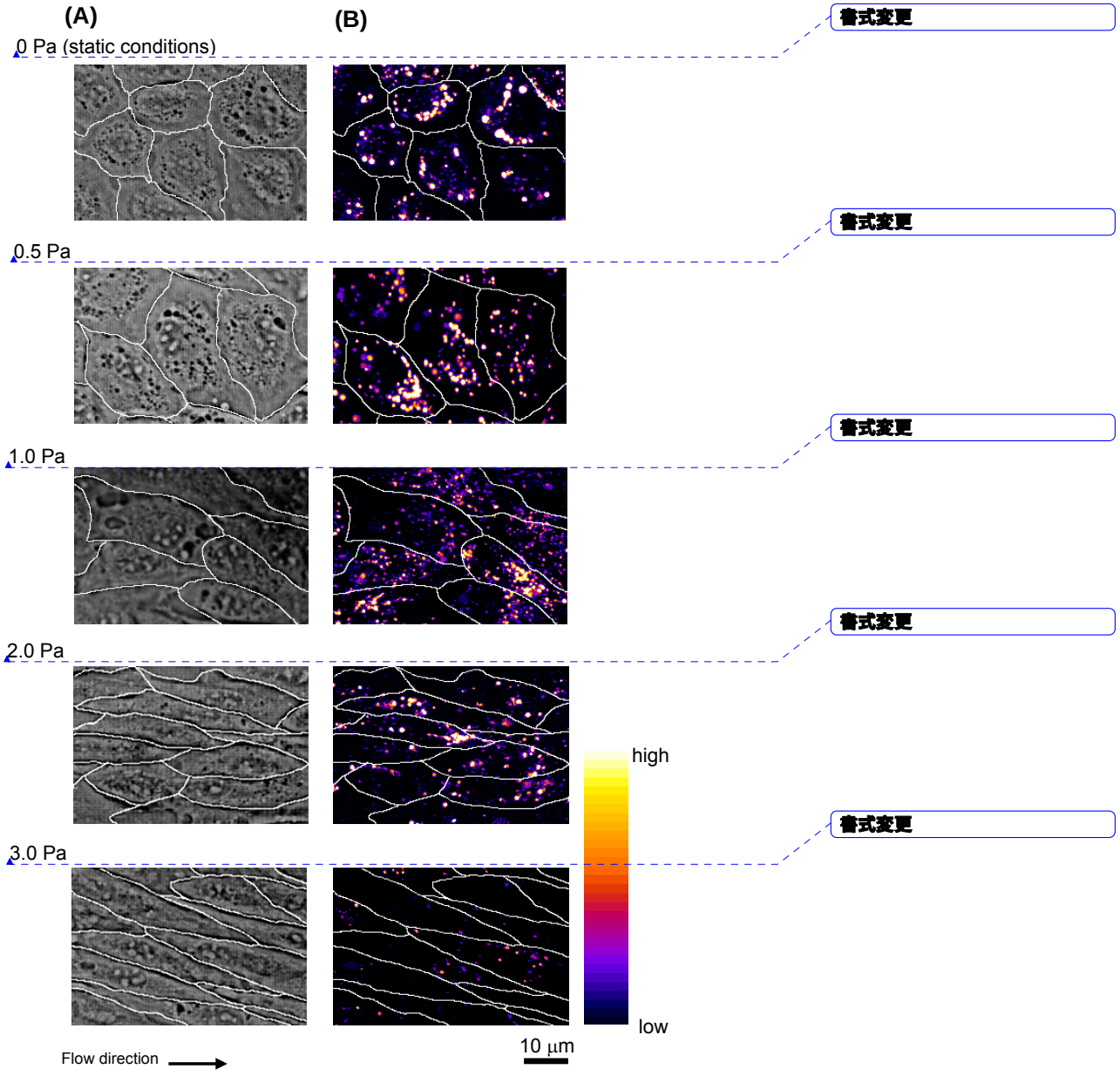

Fig. 2-4 Images of endothelial cells under applied shear stress. Phase contrast (A) and confocal images (B) of albumin uptake into endothelial cells with and without applied shear stress.

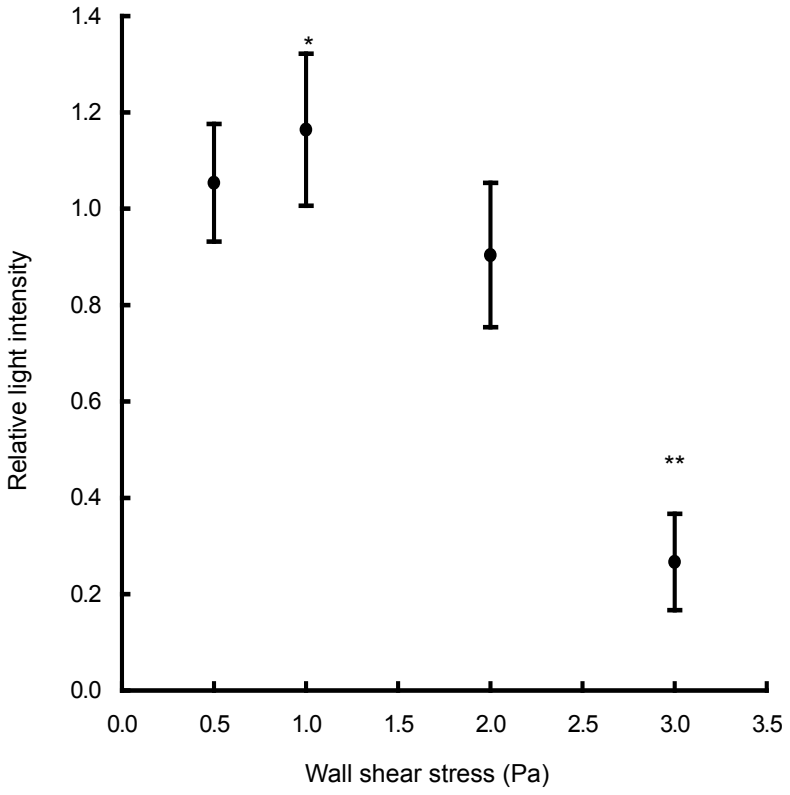

Fig. 2-5 Effect of shear stress on albumin uptake. The relative light intensity (y-axis) was used as an indicator of the normalized albumin uptake (ratio of the uptake with applied shear stress to that without shear stress). 5 fluorescent images per dish were taken randomly and the average fluorescent intensity for an individual cell was determined. Data are mean ± S.D., n = 6. Significant differences were evident between static conditions and applied shear stress of 1.0 Pa (* $P < 0.05$) and 3.0 Pa (** $P < 0.001$).

2-3-2. Effect of Shear Stress on Morphology of the Glycocalyx Layer

Fig. 2-6 (A) shows a TEM image of a cross-section of a representative endothelial cell under static conditions. The glycocalyx layer stained by ruthenium red appears on the surface edge of the endothelial cell. The brightness in the TEM image corresponds to the atomic weight of the detected substance, namely, the brighter the area, the higher the atomic weight. Therefore, the glycocalyx layer labeled with ruthenium red is dimmer. The image reveals that endothelial cells were uniformly covered by the glycocalyx layer. Fig. 2-6 (B) is a magnified view of the gap junction site between endothelial cells as indicated by a white arrow. The thickness of the glycocalyx layer slightly varies along the surface edge of each cell.

Fig. 2-7 shows TEM images of the glycocalyx layer under various levels of applied shear stress. Although the glycocalyx layer showed a slightly uneven surface, the overall nature of the glycocalyx layer geometries illustrate the influence of applied shear stress. The glycocalyx layer under an applied shear stress up to 1.0 Pa was similar to that under static conditions. However, the glycocalyx layer under an applied shear stress above 2.0 Pa was 26% thicker than that under static conditions. The glycocalyx layer under an applied shear stress of 3.0 Pa was significantly thicker, 74%. Fig. 2-8 shows the estimated layer thickness. The glycocalyx thickness is relatively constant for shear stress up to 2.0 Pa, but 74% thicker at a shear stress of 3.0 Pa compared to that under static conditions ($P < 0.05$).

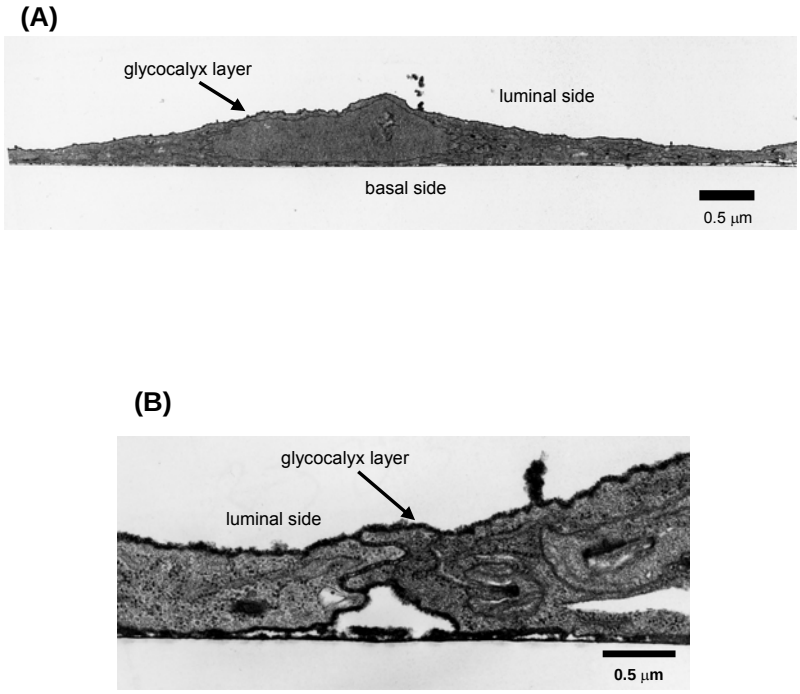

Fig. 2-6 TEM image of glycocalyx. (A) TEM image of the cross-section of a representative endothelial cell covered with glycocalyx under static conditions. (B) TEM image of the gap junction (white arrow) between representative endothelial cells covered with glycocalyx under static conditions.

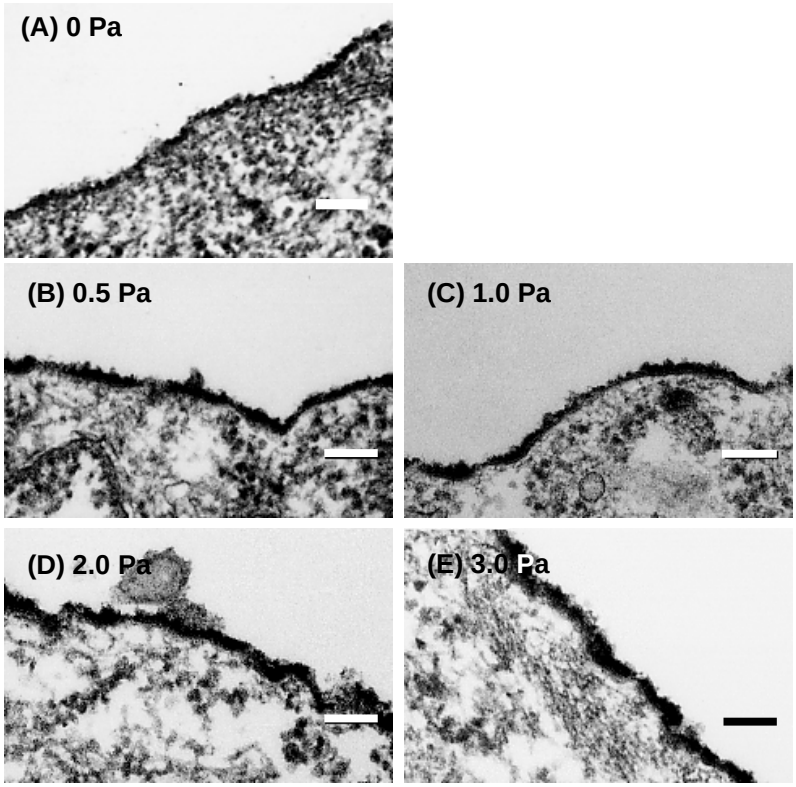

Fig. 2-7 Glycocalyx layer under various levels of applied shear stress. TEM images of glycocalyx layers (A) without shear stress (static conditions), and with shear stress of (B) 0.5 Pa, (C) 1.0 Pa, (D) 2.0 Pa, and (E) 3.0 Pa. Bar scale: 100 nm.

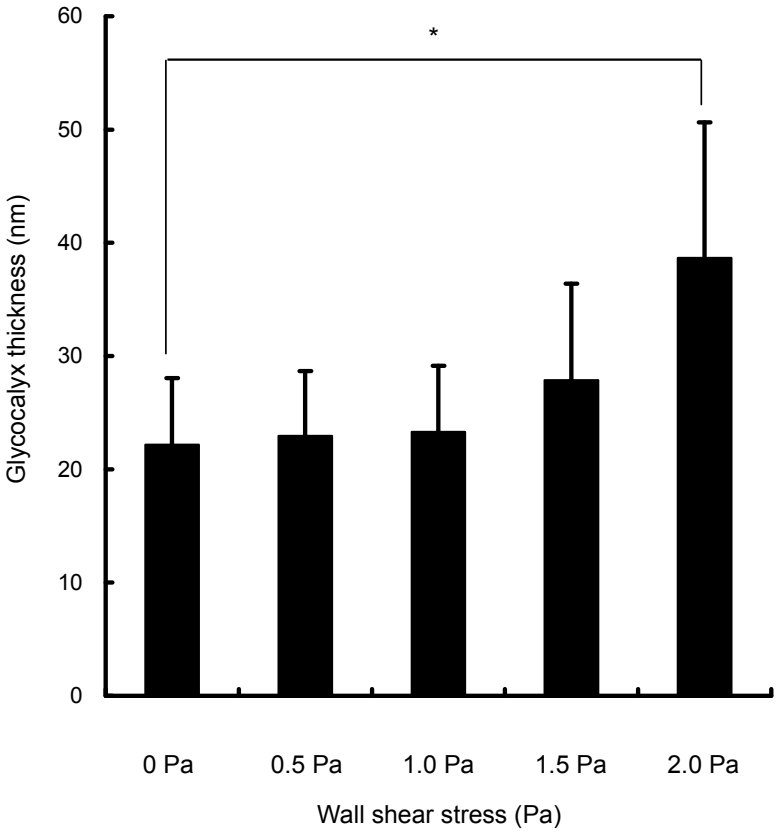

Fig. 2-8 Effect of applied shear stress on glycocalyx thickness. Data are mean ± S.D., n = 5. Significant difference was evident between the static conditions and applied shear stress conditions only at 3.0 Pa (*P < 0.05).

2-3-3. Effect of Shear Stress on Endothelial Surface Charge

Fig. 2-9 shows the effect of applied shear stress on the endothelial surface charge determined from the amount of toluidine blue. The relative absorbance (y-axis) is an indicator of the surface charge of each individual cell, and is defined as the measured absorbance divided by the number of cells (Thethi *et al*., 1997). Similar to results for the glycocalyx thickness (see preceding section), the charge level (i.e., relative absorbance) remained relatively constant for shear stress up to 2.0 Pa, and was 84% higher at a shear stress of 3.0 Pa compared to that under static conditions ($P < 0.05$).

2-3-4. Effect of Neutralized Surface Charge on Shear-dependent Albumin Uptake

Fig. 2-10 shows the effect of applied shear stress on albumin uptake with the charge of the glycocalyx neutralized by protamine sulfate. Again, same as in Fig. 2-5, the relative light intensity (y-axis) is used as an indicator of the normalized albumin uptake. The black and white symbols indicate the albumin uptake with and without neutralized charge, respectively. The albumin uptake without neutralized charge was the same as in Fig. 2-5. The albumin uptake with the neutralized charge increased with applied shear stress, except for a shear stress of 2.0 Pa, and increased by 75% at 3.0 Pa compared with that without a neutralized charge.

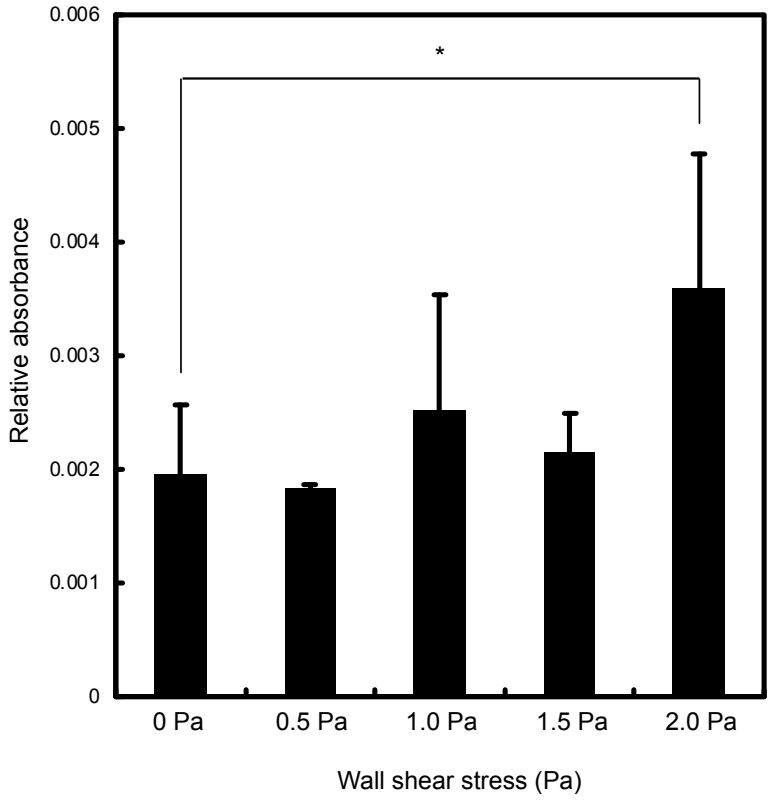

Fig. 2-9 Effect of shear stress on surface charge. Relative absorbance (y-axis) was used as an indicator of the surface charge of an individual cell, and was defined as the measured absorbance divided by the number of cells. Data are mean ± S.D., n = 4. Significant difference was evident between static conditions and applied shear stress conditions only at 3.0 Pa (*P < 0.05).

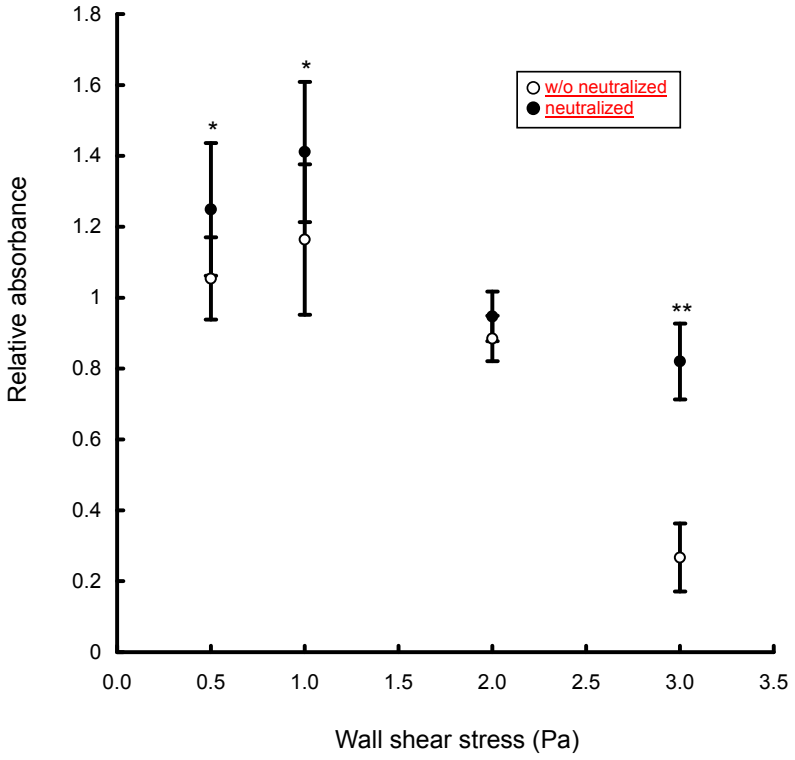

Fig. 2-10 Effect of shear stress on albumin uptake with and without the charge of glycocalyx being neutralized. Data are mean ± S.D., n = 6 (w/o neutralized charge) and 3 (neutralized charge). Significant differences were evident between conditions not neutralized and neutralized conditions at 0.5, 1.0 Pa (*P < 0.05), and 3.0 Pa (**P < 0.001). The relative intensity was defined as the ratio of albumin uptake with shear stress to that without shear stress.

2-4. Discussion

2-4-1. Shear Dependence of Albumin Uptake

This study identifies the dual response of albumin uptake to applied shear stress (Fig. 2-4). Kudo *et al*. also mentioned the dual response of albumin uptake to applied shear stress (Kudo *et al*., 1998). In their study, the albumin uptake increased by 30% at lower shear stress (1.0 Pa) compared with that under static conditions, and decreased by 76% at higher shear stress (6.0 Pa). Our results are similar, the only difference being in the experimental procedure. In the study by Kudo *et al*., albumin was transported into the cells under static conditions for 1 hour after shear stress was applied for 48 hours. They assumed that the cells have memories of previous experiences of imposed shear stress stimulus. In our study, the albumin was transported into the cells after shear stress was applied for 48 hours, but the shear stress was still applied to the cells during the uptake process for 1 hour. Our results therefore confirmed the reproducibility of the dual response of albumin uptake to shear stress stimulus and we provide additional information on the role of the glycocalyx in albumin transfer.

This dual response of albumin uptake is consistent with the lower-shear hypothesis proposed by Caro *et al*., who postulated that increased transport of LDL under low shear stress initiates the formation of atherosclerotic lesions (Caro *et al*., 1971). The shear dependence of macromolecule uptake in the vessel wall has been reported (Davis *et al*., 1984; Sprague *et al*., 1987; Wang *et al*., 1991; Waters, 1996).

2-4-2. Change in Stained Glycocalyx Structures

In our *in vitro* experiment, the glycocalyx layer labeled with ruthenium red appeared “fluffy” (Figs. 2-6 and 2-7) and covered the entire endothelial surface membrane at a thickness ranging from 20 to 40 nm.

The glycocalyx thickness tended to increase at a high shear stress of 3.0 Pa, but remained relatively constant at a shear stress up to 2.0 Pa, indicating that the glycocalyx is sensitive to shear stress above 3.0 Pa. This is consistent with results reported by Wang et al., in which the glycocalyx-layer thickness at rabbit aortic bifurcation was thicker at high shear stress regions (Wang *et al*., 1991). Our results are also consistent with those by Baldwin *et al*., in which the glycocalyx-layer thickness of rabbit aortic endothelium was 20 nm (Baldwin *et al*., 1984), and those by Rostgaard *et al*., in which the glycocalyx-layer thickness of rat capillary of intestinal villus was 50 nm (Rostgaard *et al*., 1997).

Arisaka *et al*. reported that the application of shear stress to endothelial cells of thoracic aortas of pigs for 24 hours increased both the glycosaminoglycan (GAG) and protein synthesis (Arisaka *et al*., 1995). Because proteoglycan consists of GAG and core protein, the increased thickness of the glycocalyx layer in our study is associated with the enlarged proteoglycan.

2-4-3. Change in Surface Charge

At a shear stress of 3.0 Pa, the glycocalyx thickness increased by 74% compared with that under static conditions (Fig. 2-8), and the surface charge level increased by 84% (Fig. 2-9). The similarity in these increases indicates that the shear dependency of glycocalyx thickness is associated with that of the charge levels. We measured the charge of glycocalyx layer by using Van Damme's method (Van Damme *et al*., 1994) and toluidine blue, which stained the glycocalyx and was transported into the intracellular space. The transport of toluidine blue hinders the identification of the charge distribution in glycocalyx. Such detrimental transport was avoided by doing the staining of glycocalyx at 4°C, because a low temperature restricts the metabolic and diffusion activities in cells.

2-4-4. Effect of Neutralized Charge on Albumin Uptake

In this study, protamine sulfate was used as an anionic neutralizer. Cytotoxic aspects of protamine sulfate had to be considered. We confirmed the viability of endothelial cells stained by protamine sulfate by doing a dye exclusion test with 1.0% trypan blue. Another problem of using protamine sulfate is that it might induce albumin permeability across the membrane. Swanson *et al*. showed that native albumin permeability across pulmonary endothelial cells increased with the addition of protamine sulfate, whereas cationic albumin permeability did not (Swanson *et al*., 1994). Their findings indicate that protamine sulfate does not destroy cellular functions, but binds to the anionic charges on the endothelium.

2-5. Conclusive summary

The albumin uptake into endothelial cells at a shear stress of 1.0 Pa increased by 16% and that at 3.0 Pa decreased by 27%, compared to the uptake in cells under static conditions (no shear stress). The shear-dependence of albumin uptake is highly associated with glycocalyx. At a shear stress of 3.0 Pa, the thickness of stained glycocalyx-layer structures increased by 70% and the glycocalyx charge increased by 80%, compared to that under static conditions. The albumin uptake at a shear stress of 3.0 Pa for a neutralized (no charge) glycocalyx layer was almost twice that of cells with a charged layer. The findings in our study reveal that glycocalyx influences the albumin uptake in endothelial cells at higher shear stress (3.0 Pa).

References

Arisaka T, Mitsumata M, Kawasumi M, Tohjima T, Hirose S, Yoshida Y. Effects of shear stress on glycosaminoglycan synthesis in vascular endothelial cells. Ann. N. Y. Acad. Sci. 1995; 748: 543-54.

Baldwin AL, Winlove CP. Effects of perfusate composition on binding of ruthenium red and gold colloid to glycocalyx of rabbit aortic endothelium. J. Histochem. Cytochem. 1984; 32: 259-66.

Caro CG, Fitz-Gerald JM, Schroter RC. Atheroma and arterial wall shear observation, correlation and proposal of a shear dependent mass transfer mechanism for atherogenesis. Proc Roy Soc Lond B. 1971; 177: 109-59.

Constantinescu AA, Vink H, Spaan JA. Endothelial cell glycocalyx modulates immobilization of leukocytes at the endothelial surface. Arterioscler Thromb Vasc Biol. 2003; 23: 1541-1547.

Davies PF, Dewey Jr. CF, Bussolari SR, Gordon EJ, Gimbrone Jr. MA. Influence of hemodynamic forces on various endothelium function. J Clin Invest. 1984; 73: 1121-1129.

Davis PF, Tripathi SC. Mechanical stress mechanisms and the cell: an endothelial paradigm. Circulation Res. 1993; 72: 239-245.

Davis PF. Flow-mediated endothelial mechano-transduction. Physiological Reviews. 1995; 75: 519-560.

Fukushima S, Nagatsu A, Kaibara M, Oka K, Tanishita K. Measurement of surface topography of endothelial cell and wall shear stress distribution on the cell. JSME Int J C. 2001; 44: 972-981.

Gonzalez-Castillo C, Rubio R, Zenteno-Savin T. Coronary flow-induced inotropism is modulated by binding of dextrans to the endothelial luminal surface. Am J Physiol Heart Circ Physiol.

2003; 284: H1348-H1357.

Haldenby KA, Chappell DC, Winlove CP, Parker KH, Firth JA. Focal and regional variations in the composition of the glycocalyx of large vessel endothelium. J. Vasc. Res. 1994; 31: 2-9.

Kudo S, Ikezawa K, Matsumura S, Ikeda M, Oka K, Tanishita K. Effect of wall shear stress on macromolecule uptake into cultured endothelial cells. Trans. JSME. 1998; 64B: 367-374.

Kudo S, Morigaki R, Saito J, Ikeda M, Oka K, Tanishita K. Shear-stress effect on mitochondrial membrane potential and albumin uptake in cultured endothelial cells. Biochem Biophys Res Commun. 2000; 270: 616-621.

Ley K. Molecular mechanisms of leukocyte recruitment in the inflammatory process. Cardiovasc Res. 1996; 32: 733-42.

Luft JH. Fine structure of capillary and endocapillary layer as revealed by ruthenium red. Microcirc Symp Fed Proc. 1966; 25: 1773-2783.

Mochizuki S, Vink H, Hiramatsu O, Kajita T, Shigeto F, Spaan JA, Kajiya F. Role of hyaluronic acid glycosaminoglycans in shear-induced endothelium-derived nitric oxide release. Am J Physiol Heart Circ Physiol. 2003; 285: H722-726.

Nerem RM. Vascular fluid mechanics, the arterial wall, and atherosclerosis. Trans ASME J Biomech Eng. 1992; 114:274-282.

Packham MA, Roswell HC, Jorgensen L, Mustard JF. Localized protein accumulation in the wall of the aorta. Exptl Molec Pathol. 1967; 7: 214-32.

Platts SH, Linden J, Duling BR. Rapid modification of the glycocalyx caused by ischemia-reperfusion is inhibited by adenosine A2A receptor activation. Am J Physiol Heart Circ Physiol. 2003; 284: H2360-2367.

Pries AR, Secomb TW, Gaehtgens P. Microvascular blood flow resistance: role of endothelial surface layer. Am J Physiol Heart Circ Physiol. 1997; 273: H2272-9.

Pries AR, Secomb TW, Gathtgens P. The endothelial surface layer. Pflugers Arch-Eur J Physiol. 2000; 440: 653-666.

Pries AR, Secomb TW, Gessner T, Sperandio MB, Gross JF, Gaehtgens P. Resistance to blood flow in microvessels in vivo. Circ Res. 1994; 75: 904-915.

Risau W. Differentiation of endothelium. FASEB J. 1995; 9: 926-33.

Rostgaard J, Qvortrup K. Electron Microscopic Demonstrations of filamentous molecular sieve plugs in capillary fenestrate. Microvas Res. 1997; 53: 1-13.

Schwenke DC, Carew TE. Initiation of atherosclerotic lesions in cholesterol-fed rabbits. I. Focal increases in arterial LDL concentration precede development of fatty streak lesions. Arteriosclerosis. 1989; 9: 895-907.

Siegel G., Malmsten M. The role of the endothelium in inflammation and tumor metastasis. Int J Microcirc Clin Exp. 1997; 17: 257-72.

Sims DE, Westfall JA, Kiopes AL, Horne MM. Preservation of tracheal mucus by nonaqueous fixative. Biotech Histochem. 1991; 66: 173-180.

Somer JB, Schwartz J. Focal 3H-cholesterol uptake in the pig aorta. 2. Distribution of 3H-cholesterol across the aortic wall in areas of high and low uptake in vivo. Arteriosclerosis. 1972; 16: 377-388.

Sprague EA, Steinbach BL, Nerem RM, Schwartz CJ. Influence of a laminar steady-state fluid-imposed wall shear stress on the binding, internalization, and degradation of low-density lipoproteins by cultured arterial endothelium. Circulation. 1987; 76: 648-656.

Springer TA. Traffic signals on endothelium for lymphocyte recirculation and leukocyte emigration. Annu Rev Physiol. 1995; 57: 827-872.

Swanson JA, Kern DF. Characterization of pulmonary endothelial charge barrier. Am J Physiol Heart Circ Physiol. 1994; 266: H1300-H1303.

Thethi K, Jurasz P, MacDonald AJ, Befus AD, Man SFP, Duszyk M. Determination of cell surface charge by photomeric titration. J Biochem Biophy Methods. 1997; 34: 137-145.

Van Damme MPI, Tiglias J, Nemat N, Preston BN. Determination of the charge content at the surface of cells using a colloid titration technique. Anal Biochem. 1994; 223: 62-70.

Van den Berg BM, Vink H, Spaan JA. The endothelial glycocalyx protects against myocardial edema. Circ Res. 2003; 92: 592-594.

Van Haaren PM, VanBavel E, Vink H, Spaan JA. Localization of the permeability barrier to solutes in isolated arteries by confocal microscopy. Am J Physiol Heart Circ Physiol. 2003; 285: H2848-H2856.

Vink H, Duling BR. Capillary endothelial surface layer selectively reduces plasma solute distribution volume. Am J Physiol Heart Circ Physiol. 2000; 278: H285-H289.

Wang S, Okano M, Yoshida Y. Ultrastructure of endothelial cells and lipid deposition on the flow dividers of brachiocephalic and left subclavian arterial bifurcations of the rabbit aorta. Doumyakukouka. 1991; 19: 1089-1100.

Waters CM. Flow-induced modulation of the permeability of endothelial cells cultured on microcarrier beads. J Cell Physiol. 1996; 168: 403-411.

Chapter III

Effect of Shear Stress on Microvessel Network Formation of Endothelial Cells with *in Vitro* Three-dimensional Model

3-1. Introduction

Angiogenesis is the formation of new microvessels (capillaries) by endothelial cells (ECs) migrating and proliferating from the pre-existing vessel. This process is essential for numerous physiological events such as embryonic development, ovulation, and wound healing (Gerwins *et al*., 2000). Angiogenesis is also beneficial for tissue recovery by reperfusion of ischemic tissue, but is maladaptive for arteriosclerosis, diabetes, and tumor growth (Carmeliet *et al*., 2000).

Angiogenesis consists of a growth phase and a stabilization phase of microvessel formation (Vailhé *et al*., 2001). The growth phase involves four steps: [1] dissolution of the basement membrane of the existing vessel and its surrounding extracellular matrix, [2] migration and proliferation of endothelial cells in the created space, [3] lumen formation within the endothelial sprout, and [4] formation of loops by anastomoses of sprouts. The stabilization phase involves three steps: [1] arrest of endothelial cell proliferation, [2] reconstruction of a basement membrane around the neovessels, and [3] coverage of the immature capillary with pericytes.

Tumor development has definite need for angiogenesis, and several angiogenic molecules have been identified, including fibroblast growth factor (FGF) and vascular endothelial growth factor (VEGF) families (Folkman *et al*., 1992). In particular, basic fibroblast growth factor (bFGF) is necessary for vascular remodeling, and this cytokine is critical for new vessel formation (Montesano *et al*., 1986; Yang *et al*., 1998).

With three-dimensional (3-D) models, *in vitro* experiments have significantly advanced the understanding of angiogenesis. These models are based on the ability of stimulated ECs to invade substrates in a 3-D manner. When confluent cells cultured on gels are activated by cytokines such as bFGF (Montesano *et al*., 1986) and VEGF (Pepper *et al*., 1995) or by phorbol esters (Montesano *et al*., 1985), they invade the underlying gel and form capillary-like structures. Compared with 2D models (*e.g.,* Matrigel model), 3-D models more accurately represent an *in vivo* environment. In 3-D models, depending on the culture media composition, ECs are induced to sprout, proliferate, migrate, or differentiate in a 3-D manner (Vailhé *et al*., 2001).

Function and morphology of vascular systems are regulated by hemodynamic stress (Skalak, 1996). Numerous studies report that wall shear stress affects vascular remodeling. For example, Kamiya and Togawa reported that wall shear stress due to blood flow induces adaptive changes in blood vessels lumen *in vivo* (Kamiya *et al*., 1980). They suggested that the vessel is regulated to maintain a constant wall shear stress at its physiological level. Many *in vitro* studies using cultured ECs reported that application of fluid shear stress affects various cell functions and morphology (Ando *et al*., 1994; Fisher *et al*., 2001; Fukushima *et al*., 2001; Tanishita *et al*., 1999). Thus, wall shear stress is a major factor influencing the adaptive vessel regulation for physiological as well as pathophysiological processes.

Shear stress also plays a role as a significant stimulus for angiogenesis. *In vivo* studies, Ichioka *et al*. indicate that wound-healing angiogenesis is enhanced by the adaptive response of microvasculature to shear stress (Ichioka *et al*., 1997), and Nasu *et al*. show that increased blood flow causes tumor vascular enlargement (Nasu *et al*., 1999). Recent *in vitro* experiments, Gloe *et al*. identify that shear stress induces capillary-like structure formation (Gloe *et al*., 2002), and Cullen *et al*. find that shear stress is a physiologically relevant stimulus for EC migration and angiogenesis (Cullen *et al*., 2002).

However, *in vivo* studies on vascular remodeling need experimental manipulations such as A-V shunt and vasodilator administration to alter hemodynamic conditions. The two *in vitro* studies by Gloe *et al*. and Cullen *et al*. deal with capillary-like networks in 2D and primarily regard the networks as an evaluative criterion for physical and chemical stimulus (Gloe *et al*., 2002; Cullen *et al*., 2002). To clarify the details of the physiological and pathophysiological processes of angiogenesis under shear stress stimulus, 3-D networks of capillary-like structure must be reconstructed. We successfully reconstructed the 3-D network formation under shear stress stimulus. To assess the effect of shear stress on microvessel formation, we used an *in vitro* 3-D model in which ECs were induced by a basic fibroblast growth factor (bFGF) to invade a collagen gel. Bovine pulmonary microvascular ECs (BPMECs) were seeded onto collagen gels with bFGF and then placed in a parallel-plate flow chamber. A laminar shear stress of 0.3 Pa was applied to the surfaces of the ECs for 48 hours. The total length of the networks was measured and used as an index of network formation. The density and the number of bifurcations and endpoints of the networks were measured to evaluate the morphology of the network. The migration velocity and direction of the ECs on the surface of collagen gel were measured to evaluate the influence of shear stress on the cells of the confluent monolayer of the 3-D model. We considered the effect that shear stress applied to the ECs on the surface of collagen gel had on the network formation in the gel. Our results reveal that shear stress induces network formation, enhances EC migration velocity, and affects both the direction of EC migrate and the morphology of the network.

3-2. Materials and Methods

3-2-1. Cell Culture

Cultured BPMECs were purchased from Cell Systems (lot. 32030, USA) and were used in all

experiments. BPMECs had been used *in vitro* experiments as capillary ECs (Garcia *et al*., 2001; Tomii *et al*., 2002), the property and culture methods of these cells have been established. These cells were cultured in Dulbecco's modified Eagle's medium (DMEM; 31600-34, GIBCO, USA) supplemented with 10% fetal bovine serum (FBS; lot. 9K2087, JRH Biosciences, USA), 1% antibiotic-antimycotic (15240-062, GIBCO, USA), and 15 mM HEPES (346-D1373, DOJINDO, Japan). The BPMECs were seeded in 60-mm culture dishes (430166, Corning, USA.) and cultivated under standard conditions (37°C, 5% CO_2). BPMECs were passaged using of trypsin-EDTA (25300-054, GIBCO, USA). In our experiments, we used BPMECs passaged between 5 and 9 times.

3-2-2. *In vitro* Network Formation Assay

Collagen gels were prepared as follows: 8 volumes of type I collagen solution (3.0 mg/ml; Cellmatrix Type I-A, Nitta Gelatin, Japan) were mixed with 1 volume of 5× DMEM and 1 volume of 0.1 N NaOH (192-02175, Wako Pure Chemicals Industries, Japan) on ice. The mixture was then poured into a glass-base dish (3911-035, IWAKI, Japan) and allowed to gel at 37°C for 30 minutes.

BPMECs were seeded onto 1.53-mm-thick collagen gels at 4×10^5 cells per 35-mm culture dish. The cells reached confluence 72 hours after seeding, and 30 ng/ml bFGF (Recombinant Human Fibroblast Growth Factor-basic; 100-18B, Pepro Tech, UK) was added to the culture medium to promote network formation (Montesano *et al*., 1986; Pepper *et al*., 1995). The ECs were then incubated at 37°C in 5% CO_2. After the addition of bFGF, the ECs invaded the underlying gel and began forming the network. This 3-D network model was used in the experiments.

3-2-3. Application of Shear Stress

Collagen gels with 3-D networks were placed into a parallel-plate flow chamber made of

polycarbonate (Fig. 3-1), and the ECs grown on these collagen gels were subjected to well-defined laminar fluid shear stress by the flow of culture medium (DMEM). Flow of DMEM was provided by a sterile continuous-flow loop. Shear stress on ECs (τ, in Pa) was calculated by using the following formula:

$$\tau = 6 Q\mu / bh^2$$

where μ is fluid viscosity (8.5×10^{-4} Pa·s at 37°C), Q is flow rate (cm^3/s), h is the flow chamber height (0.2 mm), and b is the flow chamber width (20 mm). Because the main objective of this study was to show that the ability of microvasculature ECs to form new microvessel was modified under the conditions whether shear stress exists or not, the τ in the chamber was 0.30 ± 0.06 Pa to compare with previous *in vivo* study (Ichioka *et al*., 1997). The BPMECs were subjected to this τ for 48 hours. The flowing culture medium was kept at 37°C in a water bath and was gassed with 5% CO_2-95% air to maintain pH 7.5 throughout the experiment. Bubbles were removed by a bubble trap. The perfusate was circulated by a roller pump (MP-3N, EYELA, Japan) in the flow circuit. The total priming volume was 60 ml for the entire circuit. For control, the 3-D models were left at rest (static conditions, $\tau = 0$) under standard conditions (37°C, 5% CO_2) throughout the experiments.

3-2-4. Images of the Growth of 3-D Networks

To observe the 3-D networks, ECs were photographed using a phase contrast microscope (ECLIPSE TE300, Nikon, Japan) equipped with a CCD camera (CoolSNAP HQ, Roper Scientific, NJ). Phase-contrast images of the networks formed in collagen gels were recorded at 10-minute intervals for 48 hours with a microscope equipped with a time-lapse system (MetaMorph^{TM}-HDTL, Roper Scientific, NJ).

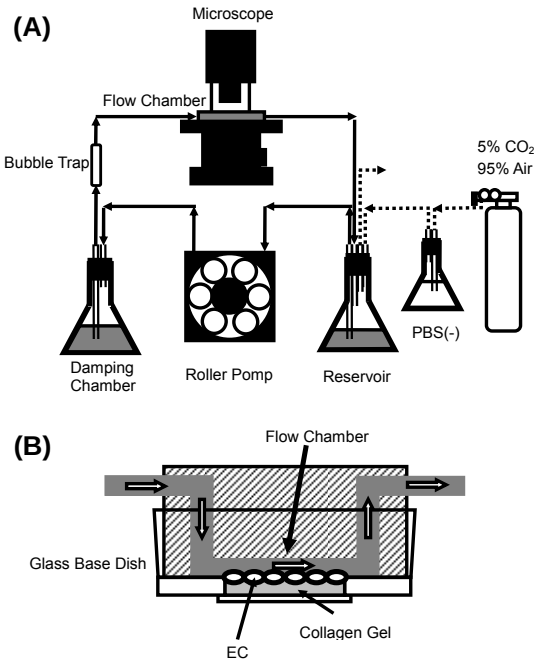

Fig. 3-1 Apparatus to apply shear stress to endothelial cells. (A) A flow chamber (dark shading) placed on the stage of a phase contrast microscope was connected to a continuous flow circuit of culture medium (DMEM; arrows) and gas (5% CO2-95% air; broken line). (B) ECs (ovals) in collagen gel (light shading) were subjected to shear stress by flow of DMEM (white arrows) for 48 hours. The height and width of the flow chamber were 0.2 mm and 20 mm, respectively.

3-2-5. Images of the Structure of 3-D Networks

The 3-D network models under static conditions were dyed with CellTracker Green BODIPY (C-2102, Molecular Probes, USA) to observe the 3-D structure of the network in detail. After 3-D networks were formed, the collagen gel sample was washed in serum-free culture medium. CellTracker at 25 mM concentration was added, and the network was incubated for 45 minutes at 37°C. After the sample was washed in serum-free culture medium, the images were recorded by using a laser scanning confocal microscope (MRC-600; BIO-RAD Laboratories, CA, USA) with a 20× objective lens. The emission of BODIPY excited at a wavelength of 488 nm with a 25-mW argon ion lasers was detected in the wavelength region longer than 515 nm. Images were recorded every 5 μm in depth, starting from the confluent layer.

3-2-6. Images of the Altitudinal Structure of the 3-D Networks

The structure of 3-D network models under static conditions was observed based on images obtained by using electron microscopy. The samples were prepared for electron microscopy as follows. The static-conditioned 3-D network model was fixed overnight with 2.5% glutaraldehyde in 0.1 M sodium cacodylate buffer (pH 7.4) (S-009, TAAB). The cells were washed in 0.1 M sodium cacodylate buffer, post-fixed in 1% osmium tetroxide in veronal acetate buffer for 2 hours, dehydrated in 70-100% ethanol for 30 minutes, and finally embedded in epon. Semi-thin sections (1 μm) and thin sections (800-1000 Å) were sliced perpendicular to the culture plane by using an LKB ultramicrotome. The thin sections were stained with uranyl acetate and lead citrate. The images were obtained by using an electron microscope (JEM-100S, JEOL).

3-2-7. Measurement of Network Morphology and EC Migration Using 2D Parameters

Although there were 3-D networks in the gel, we used 2D parameters because the formation of networks in a horizontal direction to the collagen surface was much larger than that in a perpendicular direction. The acquired phase images were analyzed by using a scion image analyzer (Scion Corporation, USA). When we measured the following parameters, we focused only on one network per dish. As ECs began forming the network all over the dish 24 hours after the addition of bFGF, there were more than 500 early networks in the dish and one network, near the center of the culture dish was randomly selected for analysis. The growth of the network was quantified by determining the total additive length of the network (Fig. 3-2 (A), (B)). The network density was calculated from the total additive length of the network divided by the area enclosing all the endpoints of the network (Fig. 3-2 (C)). The network length and its density with time were respectively normalized by the initial length and density (i.e., at 0 hours of applied shear stress). Coordinates of the network centroid were calculated as follows:

$$x = \Sigma x_i / n$$

$$y = \Sigma y_i / n$$

where x_i and y_i are the x- and y-coordinates of the i-th point along the network (Fig. 3-2 (B)).

Migration velocity and direction of ECs on the surface of collagen gel were calculated by tracking a single cell in the phase contrast images. Because these images were recorded at 10-minute intervals for 48 hours, it was easy to detect the successive movements of individual cells. We randomly chose some cells in the region near the network centroid (distance in the direction parallel to collagen surface between the network centroid and the cell was within 100 μm) and some cells far from the centroid (over 100 μm) and tracked each cell. The downstream direction of the flow was defined as 0°.

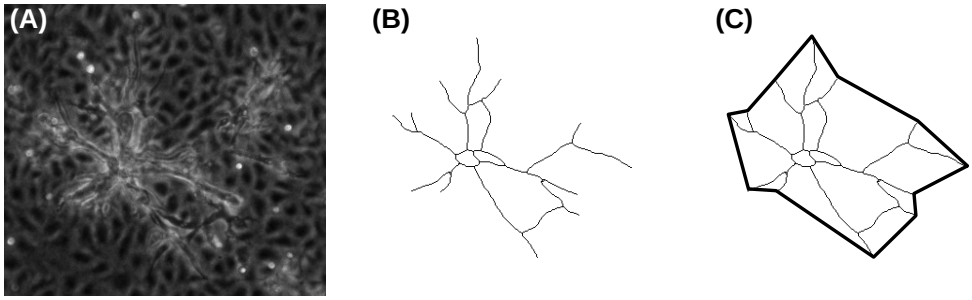

Fig. 3-2 Measurements of the network length, density, and centroid. (A) is a phase contrast image of network formation model under static conditions. (B) shows how the total length of the network was quantified from the phase contrast image. (C) shows how the area connecting the endpoints was quantified.

3-2-8. Statistical Analysis

Data are presented as mean ± S.D. The number of replicated experiments performed is n. Student's t test was used to test for differences, which were considered significant at an error level of $P < 0.05$. Using the F-test, the equality of variances of the direction of ECs migration on the gel was tested for all pairs of variables.

3-3. Results

3-3-1. Structure of the 3-D Network Formation Model

Growth factor bFGF enhanced the network formation in vitro

To assess the effect of shear stress on microvessel formation, we used an *in vitro* 3-D model in which ECs were induced to invade a collagen gel. BPMECs formed a confluent monolayer on the surface of the collagen gel 72 hours after seeding (Fig. 3-3 (A)), which we added 30 ng/ml bFGF. 24 hours after the addition of bFGF, the cells had invaded the underlying gel to begin forming the networks, which was slightly beneath the original monolayer. After 48 hours of incubation with bFGF, these cells organized into branching capillaries and formed an extensive network under the surface monolayer (Fig. 3-3 (B)), same as previous studies (Montesano *et al*., 1986; Pepper *et al*., 1995).

3-D network model reached a depth of 50 μm

To observe the 3-D structure of the network in detail, the ECs were dyed with CellTracker after 72 hours of incubation with bFGF and images were recorded every 5 μm in depth, starting from the confluent layer by using confocal laser scanning microscopy. These images were used to clarify the 3-D structure of the network with the help of image analysis software. The results clearly show

that cells invaded the collagen gel (Fig. 3-4), and reached a depth of up to 50 μm.

Images of thin sections perpendicular to the collagen surface obtained by using electron microscopy confirmed that the EC reconstructed the tubular structures, containing a clearly defined lumen consisting of multiple cells (Fig. 3-5).

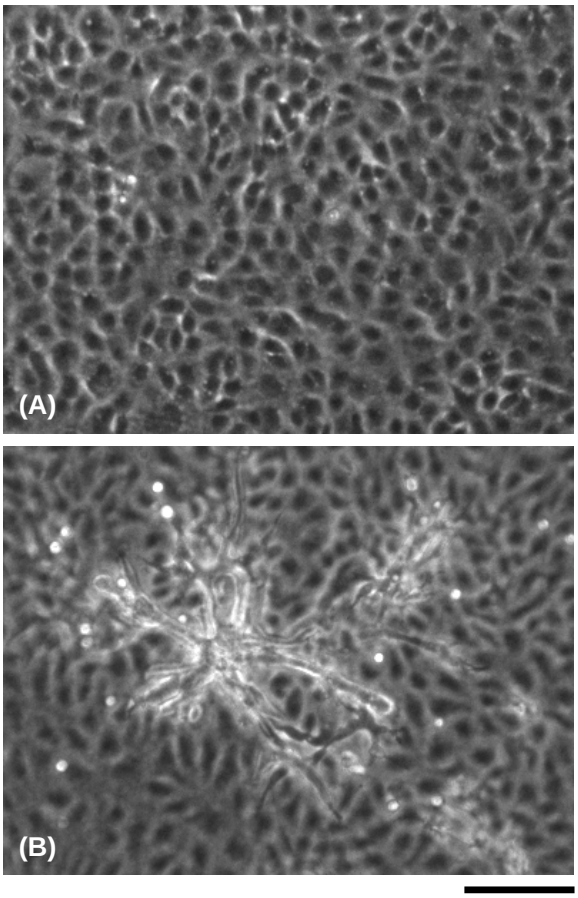

Fig. 3-3 *In vitro* model of 3-D network formation. ECs (A) grown to confluent on the surface of collagen gel and (B) incubated with bFGF (30 ng/ml) for 48 hours under static conditions. Bar scale: 100 μm.

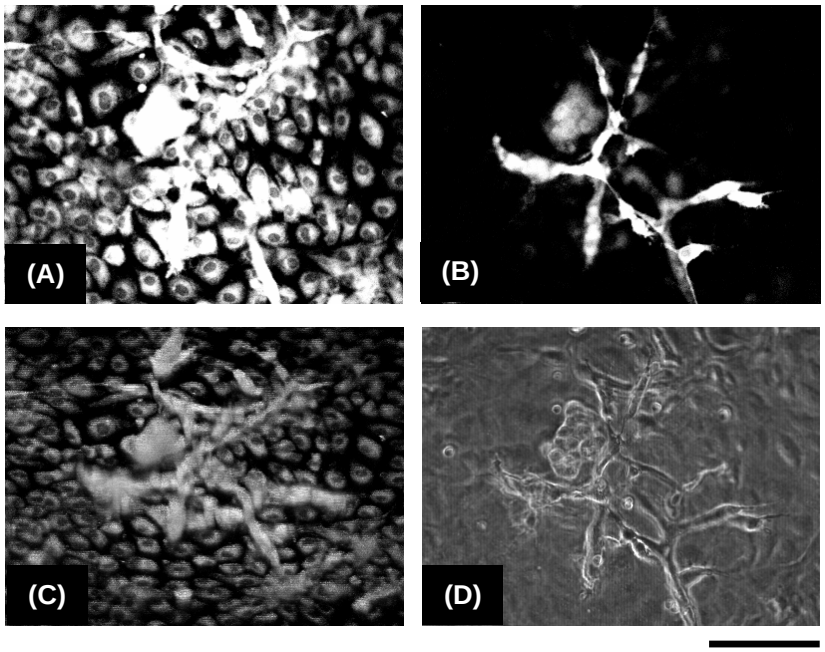

Fig. 3-4 Fluorescent image of 3-D network model under static conditions. Fluorescent image of (A) confluent monolayer and (B) structure 20 μm below the confluent monolayer. (C) Fluorescent image and (D) phase contrast image of the 3-D structure of the network. Bar scale: 100 μm.

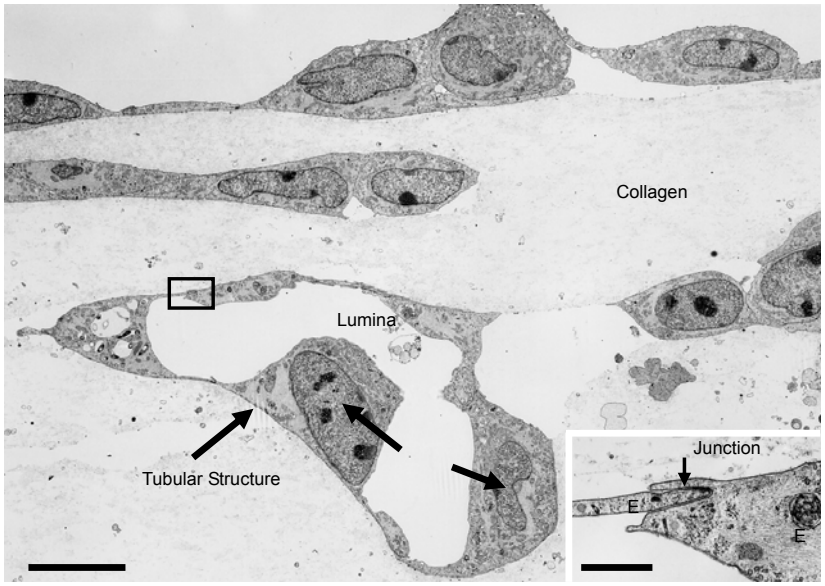

Fig. 3-5 Structure of 3-D network formation model under static conditions. Thin sections perpendicular to the culture plane of endothelial cells incubated with bFGF. Tubular structures composed of some cells enclosing lumina have formed inside the collagen gel. Bar scale: 10 μm. Close-up view of outlined area (Inset), showing the junction between two ECs. Bar scale: 1 μm.

3-3-2. Effect of Shear Stress on Microvessel Network Formation

Shear stress enhanced the growth of the microvessel network

To investigate the effect of shear stress on network formation, cells were incubated with bFGF for 24 hours and then subjected to laminar shear stress or left at static condition for 48 hours (Fig. 3-6). The total length of the network was measured as an index of network formation. Results show that after 9 hours (Fig. 3-7), applied shear stress did not significantly affect the network formation; the total length of the network under applied shear stress increased by a factor of 1.38 ± 0.14 compared with the initial length (i.e., at 0 hours of applied shear stress), similar to the increase under static conditions (1.42 ± 0.13). After approximately 10 hours, however, applied shear stress started to enhance the network formation (Fig. 3-7), compared with network formation under static conditions. After 24 hours, the enhancement was significant; the network length increased by a factor of 3.13 ± 0.46 under applied shear stress, compared with 2.17 ± 0.29 for static conditions ($P < 0.01$). After 48 hours, the enhancement reached a maximum; a factor of 6.17 ± 0.59 under applied shear stress, compared with 3.30 ± 0.41 for static conditions ($P < 0.01$), indicating that the total length under applied shear stress was 1.87 times longer than under static conditions. These results clearly show that the 3-D network formation was significantly enhanced by shear stress loading.

Effect of shear stress on network density and number of bifurcations and endpoints

The network density gradually decreased with time, and was independent of applied shear stress (Fig. 3-8).

The number of bifurcations and endpoints of a network are important geometrical parameters to evaluate the network growth process. The number of bifurcations of the networks increased with time, under either shear stress or static conditions, and there was no statistically significant

difference (Fig. 3-9 (A)). The number of endpoints increased at a similar rate both under shear stress and static conditions until approximately 10 hours, after which the number under shear stress conditions increased further, whereas those under static conditions did not. The maximum increase in the number of endpoints under shear stress conditions (at 42-45 hours) was more than 4 times higher than that under static conditions (Fig. 3-9 (B)).

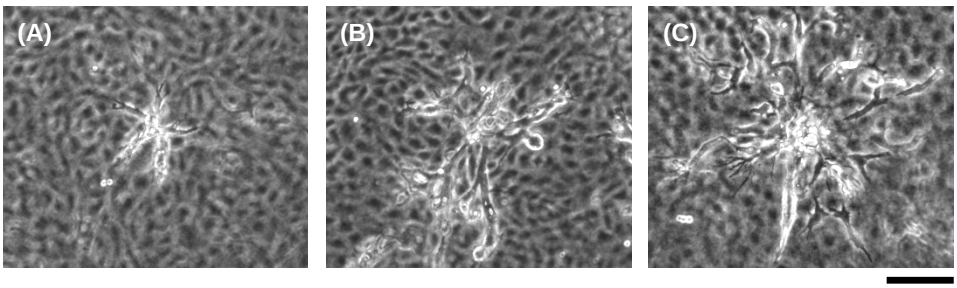

Fig. 3-6 Typical networks under shear stress and static condition. (A) shows the network at the start of experiment (0 h). (B) and (C) shows the network at the end of experiment (48 h). (B) shows the network under static condition and (C) shows the network under shear loaded condition. The direction of flow is left to right. The network under shear loaded condition expanded wider than that under static condition. Bar scale: 100 μm.

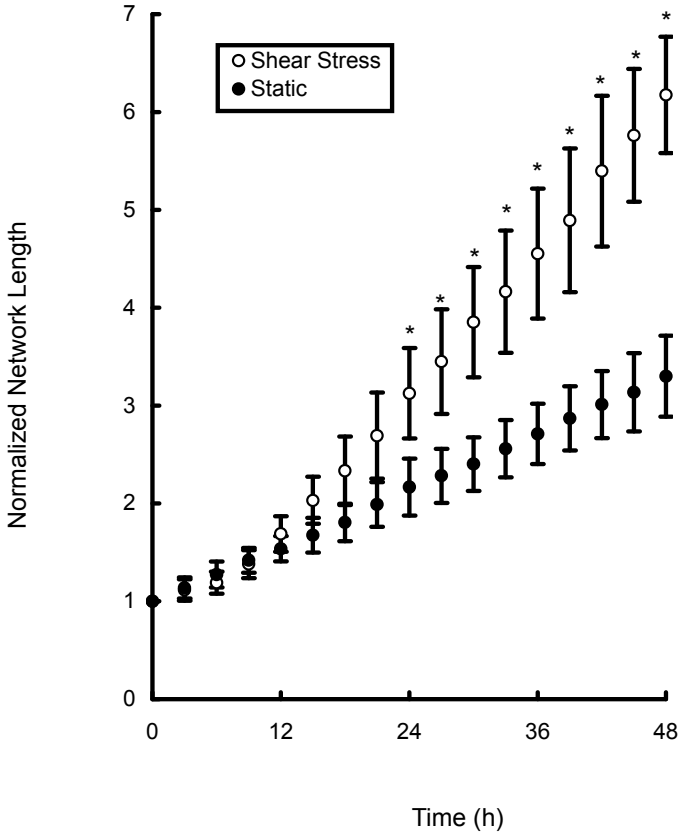

Fig. 3-7 Effect of shear stress on network length. Total length of the network under shear stress and static conditions were calculated every 3 hours. Total length was normalized by the initial total length (i.e., at 0 hours). Data are mean ± S.D., n=6, *P<0.01 vs static cultures.

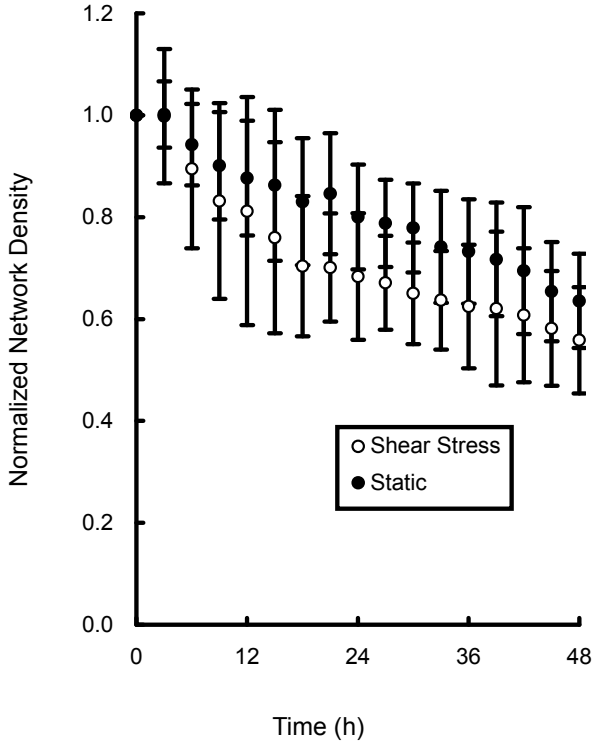

Fig. 3-8 Effect of shear stress on network density. Density of the network under shear stress and static conditions were calculated every 3 hours. Density was normalized by the initial density (i.e., at 0 hours). Data are mean ± S.D., n=6.

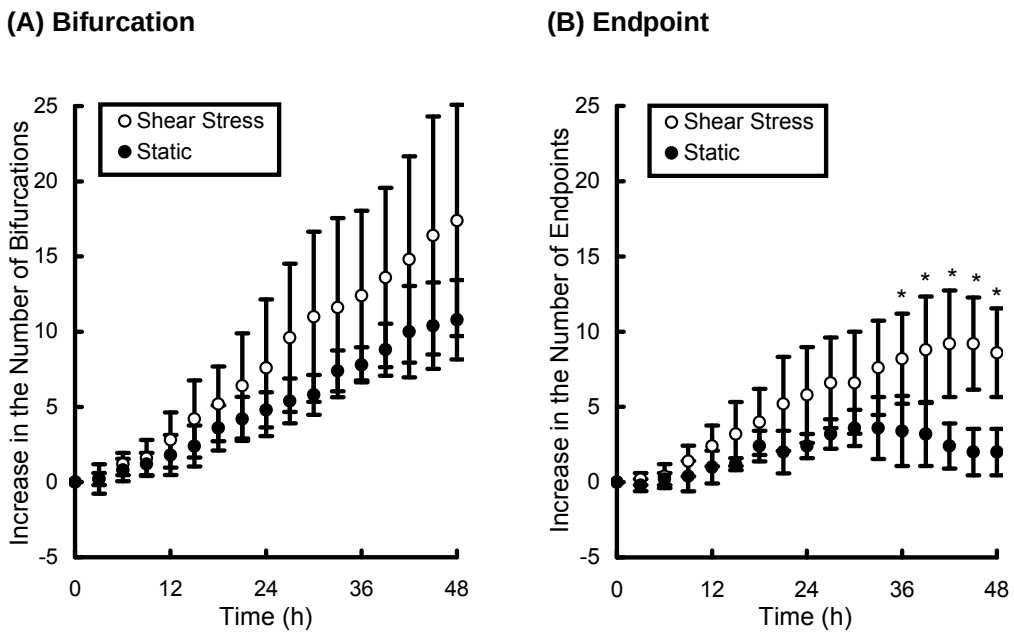

Fig. 3-9 The number of bifurcations and endpoints of a network. Effect of shear stress on (A) bifurcations and (B) endpoints of networks. Bifurcations and endpoints of network under shear stress and static conditions were calculated for every 3 hours. Data are mean ± S.D., n=5, *P<0.05 vs static cultures.

3-3-3. Effect of Shear Stress on the ECs of the Surface of Collagen Gel

Increase in migration velocity due to shear stress and bFGF

To estimate the influence of shear stress on the cells of the surface of the gel of this 3-D network formation model, we measured the migration velocity of the cells every hour up to 24 hours (Fig. 3-10). The migration velocity of cells under applied shear stress (24 h; 9.46 ± 4.29 μm/h; n=64) was significantly higher than that of cells under static conditions (6.40 ± 4.03 μm/h; n=77; $P<0.01$). Similarly, the migration velocity of cells treated with bFGF (24 h, 6.40 ± 4.03 μm/h; n=77) was significantly higher than that of cells without bFGF (4.03 ± 2.48 μm/h; n=29; $P<0.01$).

Effect of shear stress-induced EC migration velocity on network formation

To evaluate the effect of EC migration of the surface of the gel on the network formation, we measured the migration velocity at 20-24 hours (as a representative time) as a function of distance from the network centroid (Fig. 3-11). Under shear stress conditions, the migration velocity was lower near to the network centroid (< 100 μm). By contrast, under static conditions, the migration velocity was relatively constant throughout the network.

Effect of shear stress on the migration direction of ECs

To determine the effect of shear stress on the migration direction of ECs on the surface of the gel, we measured the angle of EC migration at 20-24 hours (as a representative time). The downstream direction of the flow was defined as 0°. The direction of shear-induced EC migration (Fig. 3-12 (A)) was approximately 0° in the region far from the network centroid (> 100 μm), but was random near the network centroid (< 100 μm). Using the F-test, we showed that the variances in the direction of ECs migration display a significant difference ($P<0.05$) between the region far from the network centroid and the region near the network centroid. In contrast, the direction of

cells under static conditions was random throughout the network (Fig. 3-12 (B)) and there is no significant difference in the variances of the migration direction.

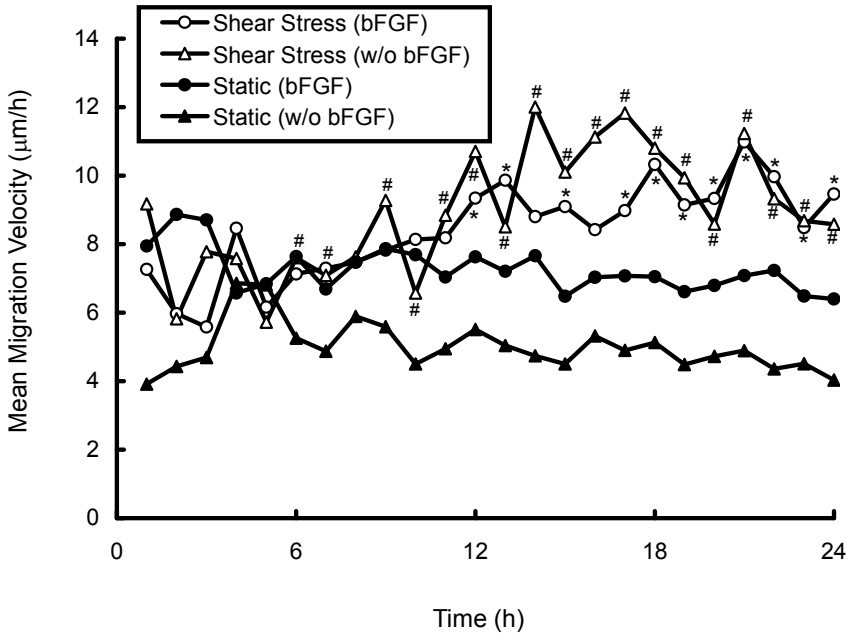

Fig. 3-10 Effect of shear stress and growth factor on migration velocity of ECs on the surface of collagen gel. Mean velocity of migration of ECs under shear stress and static conditions were calculated for each hour. Data are mean, n=64; Flow (bFGF), 25; Flow (w/o bFGF), 77; Static (bFGF), 29 (w/o bFGF), *P<0.05 Flow (bFGF) vs Static (bFGF), #P<0.05 Flow (w/o bFGF) vs Static (w/o bFGF).

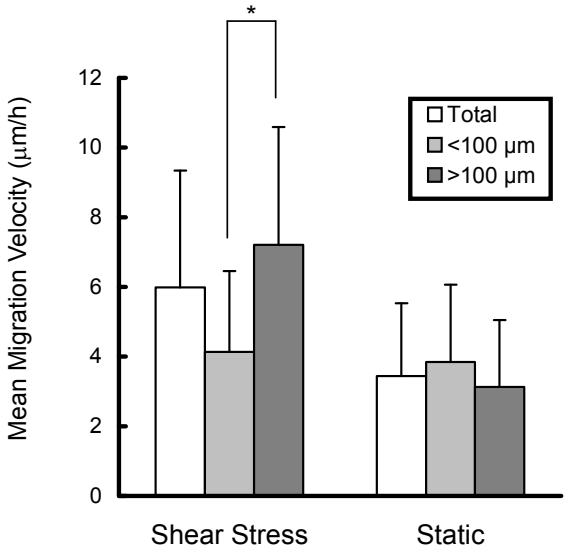

Fig. 3-11 Effect of Shear Stress on Migration Velocity of ECs on the Surface of Collagen Gel. ECs some of which were near the network (<100 μm) and some far from it (>100 μm) were tracked. Migration velocity of ECs under shear stress and static conditions were calculated at 20-24 hours (as a representative of time) of applied shear stress and static culture. Data are mean ± S.D., n=80-90, *P<0.01.

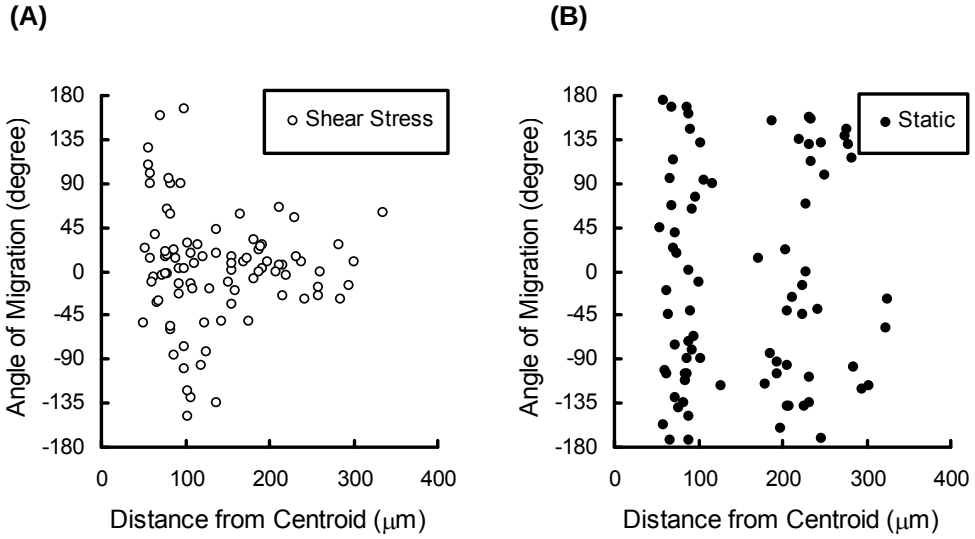

Fig. 3-12 Effect of shear stress on migration direction of ECs on the surface of collagen gel. ECs some of which were near the network (<100 μm) and some far from it (>100 μm) were tracked. (A) Angle of EC migration at 20-24 hours (as a representative of time) of applied shear stress and (B) that of under static condition. Downstream direction of the flow was defined as 0°. n = 80-90. (A) The direction of shear-induced EC migration was approximately 0° in the region far from the network centroid, while the direction was random near the network centroid. The variances in the direction of ECs migration display a significant difference (F test, P<0.05) between the region near the centroid and that far from the network centroid. (B) Under static conditions, the migration direction of ECs was random all over the place and there is no significant difference in the variances of the migration direction.

3-4. Discussion

3-4-1. Structure of the 3-D Network Formation Model

At a bFGF concentration of 30 ng/ml in the culture medium, 3-D formation of capillary-like structure by ECs in the collagen gel was successfully reconstructed. The presence of bFGF is essential for network formation (Montesano *et al.,* 1986, Pepper *et al.,* 1995). bFGF induces production of interstitial collagenase in the cultured ECs and augments the formation process of new capillaries (Slavin, 1995). In our model, the bFGF then induced new capillary-like structures to invade the underlying collagen gel (Fig. 3-3), and the newly formed structures organized themselves as distinct tubules resembling blood capillaries (Fig. 3-5).

ECs in the collagen gel constructed a lumen (Fig. 3-5). The lumen of the network consisted of a few cells, together with a gap junction. Most networks reached a depth of around 20 μm, with a maximum depth of about 50 μm from the root of the network to the tip. By using three different types of microscopy (phase contrast, confocal laser scanning, and electron) and a dye (CellTracker), we revealed the network formation process, including the destruction of capillary basement membranes, migration and formation into capillary structures.

3-4-2. Effect of Shear Stress on 3-D Network Formation

Correlation between blood flow and angiogenesis *in vivo* has been reported. For example, Ichioka *et al*. showed that the blood flow in vessels influenced angiogenesis (Ichioka *et al.,* 1997). They used vasodilator prazosin to modify the blood flow, and found that angiogenesis during wound healing in the rabbit ear chamber was positively influenced by elevated prazosin-induced shear stress. Nasu *et al*. observed growing tumor vessels *in vivo* to elucidate the relationship between blood flow and vascular enlargement, and showed that tumor angiogenesis depended more on local hemodynamics than on vascular growth factors (Nasu *et al.,* 1999). In an *in vitro* study,

Albuquerque *et al*. demonstrated that physiological shear stress enhances wound closure in cultured human umbilical vein and coronary artery ECs through the action of EC spreading and migration (Albuquerque *et al.,* 2000). In another *in vitro* study, Urbich *et al*. indicated that the shear stress-induced migration was independent of cell proliferation, but was dependent on the fibronectin receptor $\alpha_5\beta_1$ (Urbich *et al.,* 2002). Only few studies, however, have quantified the relationship between network formation and shear stress. Recent *in vitro* studies showed that flow induced the growth of the network formation of ECs in 2D (Cullen *et al.,* 2002; Gloe *et al.,* 2002). In our study, we successfully reconstructed a 3-D network formation model that mimics the conditions of an *in vivo* environment (Vailhe *et al.,*2001). The application of shear stress on the ECs resulted in an increased length of the entire network after approximately 10 hours (Fig. 3-7), the same time that active migration of cells on the collagen gel began (Fig. 3-10).

This refractory period, which required transmitting the effect of shear stress to EC features, was thought to be similar to previous studies. Franke *et al*. showed that the endothelial stress fibers could be induced by a 3 hours exposure of shear stress of 0.2 Pa (Franke *et al.,* 1984) and Ookawa *et al*. indicated that stress fiber-like structure was formed by a 3 hours exposure of shear stress of 2.0 Pa (Ookawa *et al.,* 1992). Wechezak *et al*. exposed shear stress of 0.93 Pa on ECs for 2 hours and observed that microfilament bundles and their associated focal contacts were concentrated in the proximal cell regions (Wechezak *et al.,* 1998). As just described, these changes in cytoskeleton and adherence protein need several hours and probably cause the refractory period of EC migration and network formation. For EC migration, Tanishita *et al*. also observed ECs under shear stress of 5 Pa in which migration velocity was 1-5 μm/h initially, accelerated slightly after 12 to 16 hours, finally reaching approximately 16 μm/h after 16 hours (Tanishita *et al.,* 1999). In our study, we observed that ECs required approximately 10 hours to transmit the effect of shear stress to not only EC migration but also network formation. Our study also revealed that the migration velocity and

direction of ECs on the confluent surface depended on the distance from the network centroid (Figs. 11 and 12). Thus, the nature of cellular migration strongly affects the network formation in the gel.

Numerous previous studies focused on relationships between shear stress and growth factors such as bFGF and VEGF. For example, Gloe *et al*. demonstrated that shear stress induced the release of bFGF from EC (Gloe *et al.,* 2002), and Malek *et al*. reported that laminar shear stress induced bFGF mRNA expression (Malek *et al.,* 1993). Milkiewicz *et al*. reported that higher capillary shear stress increases VEGF expression (Milkiewicz *et al.,* 2001), whereas Conklin *et al*. (Conklin *et al.,* 2002) reported that low shear stress increases VEGF expression in ECs. Furthermore, NO is associated with angiogenesis. For example, Smith *et al*. reported that eNOS enhances angiogenesis (Smith *et al.,* 2002), and Lee *et al*. showed that NO induces angiogenesis *in vivo* and *in vitro* by promoting EC migration and differentiation into capillaries (Lee *et al.,* 2000). Lee *et al*. also demonstrated that NO increased $\alpha_v\beta_3$ integrin expression in ECs (Lee *et al.,* 2000), a critical mediator of EC-matrix adhesion and migration. Although proteolysis is a key step in angiogenesis, matrix metalloproteinase does not increase after stimulation by shear stress (Rivilis *et al.,* 2002). Our results show that in the presence of bFGF the migration velocity of ECs without applied shear stress (static conditions) only slightly increased, whereas that of ECs under shear stress conditions significantly increased (Fig. 3-10).

Our results show that the network density was relatively unaffected by the shear stress (Fig. 3-8). To determine the effect of shear stress on the process of network formation, we measured the number of bifurcations and endpoints of the networks under shear stress and static conditions. Networks under static conditions showed slow elongation and bifurcation (Figs. 3-7 and 3-9 (A)), resulting in the fusion of some tips, and thus, the number of endpoints only slightly increased (Fig. 3-9 (B)). In contrast, under shear stress conditions, the endpoints of network branches were often extended, and the networks widely expanded with progressive elongation and bifurcation (Fig. 3-7

and 3-9 (A)), resulting in an increase in the number of bifurcations and endpoints (Fig. 3-9).

As observed above, this model well reproduced new microvessel formation *in vivo* and we could study about the effect of shear stress on that. There was however some points which cannot reproduce in this model. Capillary networks *in vivo* may have different outcomes because the matrix in this model, pure type I collagen gel, is not the typical matrix found *in vivo* and matrix composition may play an important roles in angiogenesis modulation (Iivanainen *et al.,* 2003; Madri *et al.,* 1983). The fact that expression of integrin may also be different from *in vivo* environment possibly affects tube formation and migration of ECs. As far as $\alpha_v\beta_3$ integrin, it plays critically important role in angiogenesis by bFGF both *in vitro* and *in vivo* environment (Brooks *et al.,* 1994; Friedlander *et al.,* 1995; Kuzuya *et al.,* 1999; Satake *et al.,*1998). Furthermore, endothelial progenitor cells (EPCs) also participate in new vessel formation *in vivo* (Asahara *et al.,* 1997) but we did not focus on EPCs in this study. We believe nonetheless that this experimental setup, combination of 3-D network formation model and shear loading application, is beneficial to show that the ability of microvasculature ECs to form new microvessels was modified under conditions whether shear stress exists or not.

In summary, shear stress promoted the growth of 3-D network formation *in vitro*. The enhancement became detectable 10 hours after the initiation of shear stress. After 48 hours, the growth rate (i.e. increase in network length) of a network under shear stress conditions was approximately 2 times faster than that of a network under static conditions. Furthermore, shear stress applied to ECs on the surface of collagen gel influenced the process of network formation in the gel. The endpoints of the network branches were extended, and the networks were significantly expanded due to repeated bifurcation and elongation.

References

Albuquerque ML, Waters CM, Savla U, Schnaper HW, Flozak AS. Shear stress enhances human endothelial cell wound closure in vitro. Am J Physiol Heart Circ Physiol 279: H293-H302, 2000.

Ando J, Tsuboi H, Korenaga R, Takada Y, Toyama-Sorimachi N, Miyasaka M, Kamiya A. Shear stress inhibits adhesion of cultured mouse endothelial cells to lymphocytes by downregulating VCAM-1 expression. Am J Physiol Cell Physiol 267: C679-C687, 1994.

Asahara T, Murohara T, Sullivan A, Silver M, van der Zee R, Li T, Witzenbichler B, Schatteman G, Isner JM. Isolation of putative progenitor endothelial cells for angiogenesis. Science 275: 964-967, 1997.

Brooks PC, Clark RA, Cheresh DA. Requirement of vascular integrin avb3 for angiogenesis. Science 264: 569-571, 1994.

Carmeliet P, Jain RK. Angiogenesis in cancer and other diseases. Nature 407: 249-257, 2000.

Conklin BS, Zhong DS, Zhao W, Lin PH, Chen C. Shear stress regulates occludin and VEGF expression in porcine arterial endothelial cells. J Surg Res 102: 13-21, 2002.

Cullen JP, Sayeed S, Sawai RS, Theodorakis NG, Cahill PA, Sitzmann JV, Redmond EM. Pulsatile flow-induced angiogenesis: role of Gi subunits. Arterioscler Thromb Vasc Biol 22: 1610-1616, 2002.

Fisher AB, Chien S, Barakat AI, Nerem RM. Endothelial cellular response to altered shear stress. Am J Physiol Lung Cell Mol Physiol 281: L529-L533, 2001.

Folkman J, Shing Y. Angiogenesis. J Biol Chem 267: 10931-10934, 1992.

Franke RP, Grafe M, Schnittler H, Seiffge D, Mittermayer C, Drenckhahn D. Induction of human vascular endothelial stress fibres by fluid shear stress. Nature 307: 648-649, 1984.

Friedlander M, Brooks PC, Shaffer RW, Kincaid CM, Varner JA, Cheresh DA. Definition of two angiogenic pathways by distinct av integrins. Science 270: 1500-1502, 1995.

Fukushima S, Nagatsu A, Kaibara M, Oka K, Tanishita K. Measurement of surface topography of endothelial cell and wall shear stress distribution on the cell. JSME Int J C-Mech Sy 44: 972-981, 2001.

Garcia JG, Liu F, Verin AD, Birukova A, Dechert MA, Gerthoffer WT, Bamberg JR, English D. Sphingosine 1-phosphate promotes endothelial cell barrier integrity by Edg-dependent cytoskeletal rearrangement. J Clin Invest 180: 689-701, 2001.

Gerwins P, Skoldenberg E, Claesson-Welsh L. Function of fibroblast growth factors and vascular endothelial growth factors and their receptors in angiogenesis. Crit Rev Oncol Hematol 34: 185-194, 2000.

Gloe T, Sohn HY, Meininger GA, Pohl U. Shear stress-induced release of basic fibroblast growth factor from endothelial cells is mediated by matrix interaction via integrin avb3. J Biol Chem 277: 23453-23458, 2002.

Ichioka S, Shibata M, Kosaki K, Sato Y, Harii K, Kamiya A. Effects of shear stress on wound-healing angiogenesis in the rabbit ear chamber. J Surg Res 72: 29-35, 1997.

Iivanainen E, Kahari VM, Heino J, Elenius K. Endothelial cell-matrix interactions. Microsc Res Tech 60: 13-22, 2003.

Kamiya A, Togawa T. Adaptive regulation of wall shear stress to flow change in the canine carotid artery. Am J Physiol Heart Circ Physiol 239: H14-H21, 1980.

Kuzuya M, Satake S Ramos MA, Kanda S, Koike T, Yoshino K, Ikeda S, Iguchi A. Induction of apoptotic cell death in vascular endothelial cells cultured in three-dimensional collagen lattice. Exp Cell Res 248: 498-508, 1999.

Lee PC, Kibbe MR, Schuchert MJ, Stolz DB, Watkins SC, Griffith BP, Billiar TR, Shears LL II.

Nitric oxide induces angiogenesis and upregulates avb3 integrin expression on endothelial cells. Microvasc Res 60: 269-280, 2000.

Madri JA, Williams SK. Capillary endothelial cell cultures: phenotypic modulation by matrix components. J Cell Biol 97: 153-165, 1983.

Malek AM, Gibbons GH, Dzau VJ, Izumo S. Fluid shear stress differentially modulates expression of genes encoding basic fibroblast growth factor and platelet-derived growth factor B chain in vascular endothelium. J Clin Invest 92: 2013-21, 1993.

Milkiewicz M, Brown MD, Egginton S, Hudlicka O. Association between shear stress, angiogenesis, and VEGF in skeletal muscles in vivo. Microcirculation 8: 229-241, 2001.

Montesano R, Orci L. Tumor-promoting phorbol esters induce angiogenesis in vitro. Cell. 42: 469-477, 1985.

Montesano R, Vassalli JD, Baird A, Guillemin R, Orci L. Basic fibroblast growth factor induces angiogenesis in vitro. Proc Natl Acad Sci USA 83: 7297-7301, 1986.

Nasu R, Kimura H, Akagi K, Murata T, Tanaka Y. Blood flow influences vascular growth during tumour angiogenesis. Br J Cancer 79: 780-786, 1999.

Ookawa K, Sato M, Ohshima N. Changes in the microstructure of cultured porcine aortic endothelial cells in the early stage after applying a fluid-imposed shear stress. J Biomech 25: 1321-1328, 1992.

Pepper MS, Ferrara N, Orci L, Montesano R. Leukemia inhibitory factor (LIF) inhibits angiogenesis in vitro. J Cell Sci 108: 73-83, 1995.

Rivilis I, Milkiewicz M, Boyd P, Goldstein J, Brown MD, Egginton S, Hansen FM, Hudlicka O, Haas TL. Differential involvement of MMP-2 and VEGF during muscle stretch- versus shear stress-induced angiogenesis. Am J Physiol Heart Circ Physiol 283: H1430-H1438, 2002.

Satake S, Kuzuya M, Ramos M A, Kanda S, Iguchi A. Angiogenic stimuli are essential for survival

of vascular endothelial cells in three-dimensional collagen lattice. Biochem Biophys Res Commun 244: 642-646, 1998.

Skalak TC, Price RJ. The role of mechanical stresses in microvascular remodeling. Microcirculation 3: 143-165, 1996.

Slavin J. Fibroblast growth factors: at the heart of angiogenesis. Cell Biol Int 19: 431-444, 1995.

Smith RS Jr, Lin KF, Agata J, Chao L, Chao J. Human endothelial nitric oxide synthase gene delivery promotes angiogenesis in a rat model of hindlimb ischemia. Arterioscler Thromb Vasc Biol 22: 1279-1285, 2002.

Tanishita K, Nagayama K, Fujii M, Kudou S. Empirical study on grouping behavior of individual endothelial cells under shear stress. JSME Int J C-Mech Sy 42: 715-720, 1999.

Tomii Y, Kamochi J, Yamazaki H, Sawa N, Tokunaga T, Ohnishi Y, Kijima H, Ueyama Y, Tamaoki N, Nakamura M. Human thrombospondin 2 inhibits proliferation of microvascular endothelial cells. Int J Oncol 20: 339-342, 2002.

Urbich C, Dernbach E, Reissner A, Vasa M, Zeiher AM, Dimmeler S. Shear stress-induced endothelial cell migration involves integrin signaling via the fibronectin receptor subunits a5 and b1. Arterioscler Thromb Vasc Biol 22: 69-75, 2002.

Vailhe B, Vittet D, Feige JJ. In vitro models of vasculogenesis and angiogenesis. Lab Invest. 81: 439-452, 2001.

Wechezak AR, Wight TN, Viggers RF, Sauvage LR. Endothelial adherence under shear stress is dependent upon microfilament reorganization. J Cell Physiol 139: 136-146, 1986.

Yang HT, Ogilvie RW, Terjung RL. Exercise training enhances basic fibroblast growth factor-induced collateral blood flow. Am J Physiol Heart Circ Physiol 274: H2053-H2061, 1998.

Chapter IV

Initial bFGF Distribution Affects the Depth of Three-dimensional Microvessel Networks *in Vitro*

4-1. Introduction

Angiogenesis is essential for numerous physiological and pathological events, such as embryonic growth and cancer progression, and has therefore been extensively studied. *In vitro* models of the formation of new microvessels (capillaries) by endothelial cells (ECs) have been used to clarify the mechanism of angiogenesis. Folkman and Haudenschilid were the first to successfully form a two-dimensional (2D) capillary-like structure *in vitro* (Folkman *et al*., 1980). Since then, 2D models have been used to study angiogenesis and to screen the activity of angiostatic molecules (Vailhé *et al*., 2001). Kubota *et al*. showed that ECs formed capillary-like structures on Matrigel, a laminin-rich matrix (Kubota *et al*., 1988). Capillary-like structure formation has also been induced in 2D cultures and modulated by various extracellular matrixes (ECM), such as fibronectin, collagen IV, and gelatin (Ingber *et al*., 2002).

Because vessels are essential for the formation and maintenance of organ function, the control of three-dimensional (3-D) microvessel formation is critical for regenerative medicine and tissue engineering. Necrosis of cells occurs in 3-D regenerated tissue because the transfer of nutrients and oxygen is not adequately maintained by diffusion alone. To maintain a sufficient nutrient and oxygen supply in the absence of vascularization, approximately 100 μm is the maximal thickness (Shimizu *et al*, 1986). The construction of 3-D tissue, therefore, needs a microvessel network deep in the tissues.

In vitro 3-D vessel networks induced by growth factors have been observed (Montesano *et al*, 1986; Pepper *et al*., 1995). Montesano *et al*. and Pepper *et al*. showed that growth factors such as vascular endothelial cell growth factor (VEGF) and basic fibroblast growth factor (bFGF) promote capillary-like network formation in collagen gel, and that the networks in the gel are formed in a 3-D manner and have lumen (Montesano *et al*, 1986; Pepper *et al*., 1995), but methods to control the formation of 3-D microvessel networks have yet to be developed.

The concentration profile of extracellular growth factor is important in controlling 3-D microvessel networks. Recent findings indicate that the morphology of such networks is influenced by the extracellular growth factor distribution *in vivo* (Ruhrberg *et al*., 2002; Gerhardt *et al*., 2003). Ruhrberg *et al*. showed that neural tubes that secrete VEGF normally establish a steep concentration gradient and attract the tips of filopodia, thereby controling the vascular branching pattern during embryogenesis (Ruhrberg *et al*., 2002). Gerhardt *et al*. showed that filopodia of network tip-cells detect the VEGF gradient generated by retinal astrocytes and that tip-cell migration depends on VEGF distribution, whereby continuous networks are formed (Gerhardt *et al*., 2003). The role of extracellular growth factor distribution in controlling the formation of 3-D microvessel networks must be clarified *in vitro*.

To introduce microvessels deep into tissue, it is necessary to control 3-D microvessel networks. This study focuses on the effects of the concentration gradient of growth factors used in seeding ECs on network morphology in the formation of deep 3-D networks. First, ECs were seeded on two patterned environments: collagen gel containing bFGF and incubated without bFGF medium (gel-bFGF model), and collagen gel containing no bFGF and incubated with bFGF medium (medium-bFGF model). The time course change of growth factor distribution in both models was measured using ELISA. The morphology of the formed network was observed in 3-D using confocal laser scanning microscopy. The effect of the concentration gradient on the network

formation process was also clarified by measuring the migration of ECs on the collagen gel. Results revealed that the initial growth factor distribution affects (a) both EC migration on the process of the network formation and the number of sprouting points, and (b) network morphology, as evidenced by the networks in the gel-bFGF model extending deeper into the collagen gel than those in the medium-bFGF model.

4-2. Materials and Methods

4-2-1. Cell Culture

Cultured bovine pulmonary microvascular ECs (BPMECs) were purchased from Cell Systems (lot. 32030, USA) and used in all experiments. The BPMECs were cultured in Dulbecco's modified Eagle's medium (DMEM; 31600-34, GIBCO, USA) supplemented with 10% fetal bovine serum (FBS; lot. 9K2087, JRH Biosciences, USA), 1% antibiotic-antimycotic (15240-062, GIBCO, USA), and 15 mM HEPES (346-D1373, DOJINDO, Japan). The BPMECs were then seeded in 60-mm culture dishes (430166, Corning, USA) and cultivated under standard conditions (37°C, 5% CO_2). After reaching subconfluent, BPMECs were detached using trypsin-EDTA (25300-054, GIBCO, USA), and centrifuged 100×*g* for 2 min, then seeded onto 60-mm dish or collagen gel as described following. Cells of the sixth to ninth passage were used in all experiments.

4-2-2. *In Vitro* Network Formation Assay

Collagen gels were prepared as follows: 8 volumes of type I collagen solution (0.3%; KOKENCELLGEN I-AC, KOKEN, Japan) were mixed on ice with 1 volume of 10× Minimum Essential Medium (MEM; 61100-061, GIBCO, USA) and 1 volume of buffer solution (mixture of 0.08 N NaOH (192-02175, Wako Pure Chemicals Industries, Japan) containing 20 mM HEPES (346-01373, Wako Pure Chemical Industries, Japan)). The mixture was then poured into a

glass-base dish (3911-035, IWAKI, Japan) and allowed to gel at 37°C for 30 minutes.

Two types of growth factor distribution were used to make the models. In the gel-bFGF model, BPMECs were seeded onto 30 ng/ml bFGF (Recombinant Human Fibroblast Growth Factor-basic; 100-18B, Pepro Tech, UK) containing collagen gel, and then incubated with DMEM without bFGF. In the medium-bFGF model, BPMECs were seeded onto collagen gel without bFGF, and then incubated in DMEM with 30 ng/ml bFGF . In each model, the volume of gel and medium were both 0.875 ml, and 4×10^5 BPMECs were seeded per dish. The BPMECs were then incubated at 37°C in 5% CO_2. After the BPMECs reached confluence, they invaded the underlying gel and began forming the network.

4-2-3. ELISA for bFGF

To observe the time course change of growth factor distribution in both gel-bFGF and medium-bFGF models, we compared the difference between the bFGF concentration in the collagen gel and that in the medium of each model. Using ELISA, we measured directly (A) the bFGF concentration in the medium of each model without ECs at the time points of 12, 24, 48 and 72 hours and (B) that in 30 ng/ml bFGF medium without gels at the same time points as a control. (C) The bFGF concentration in the collagen gel of each model was calculated by subtracting the two concentrations: (C) = (B) – (A). We defined (C) / (A) as the concentration rate between the bFGF concentration in the collagen gel and that in the medium.

For analysis of bFGF distribution, we prepared the gel-bFGF model and medium-bFGF model without ECs, and 30 ng/ml bFGF DMEM (as a control) in a 24-well plate. After 12, 24, 48 and 72 hours, supernatants were collected and the concentration of bFGF in each medium was determined using a commercially available sandwich ELISA kit (Quantikine Kit, R&D systems, USA) following the manufacturer's guidelines. The concentrations of bFGF were measured using a microplate

reader set to 450 nm, the readings at 540 nm were subtracted from the readings at 450 nm. 3 samples were used for analysis respectively for each model at each time point.

4-2-4. Observation of Cell Proliferation and Migration

The proliferation and migration of BPMECs on the surface of collagen gel was observed by photographing BPMECs at 10-minute intervals using a phase-contrast microscope (ECLIPSE TE300, Nikon, Japan) equipped with a CCD camera (CoolSNAP HQ, Roper Scientific, NJ) and a time-lapse system (MetaMorph^{TM}-HDTL, Roper Scientific). For each model, 30 locations were randomly selected for observation, and the cell numbers were counted for all the 5 days of culture. The migration distance per 5 h from days 0 to 5 and the migration angle per 1 h on day 2 were calculated by tracking a single cell in the phase-contrast images. Migration angle was defined as the angle of EC migration direction with respect to that of the preceding hour. For each model, 30 cells of each type were randomly selected for analysis.

4-2-5. Observation of Network Sprouting

Sprouting of the 3-D networks was observed by photographing the BPMECs using a phase-contrast microscope (ECLIPSE TE300, Nikon, Japan) equipped with a CCD camera (AxioCam MRc5, Carl Zeiss, Germany). Phase-contrast images and bright-field images for both models were recorded at 3 and 5 days after BPMECs were seeded. In each model, 30 locations on the surface of the collagen gel were randomly selected for imaging. The number of locations that sprouted a network was counted from these images.

4-2-6. Observation of 3-D Network Morphology

The 3-D morphology of the networks was observed in detail by dyeing and then imaging the

3-D network models. After 3-D networks were formed, each sample was washed in PBS, then dyed with CellTracker Green BODIPY (C-2102, Molecular Probes, USA) at 25 mM concentration in DMEM and incubated for 45 minutes at 37°C, and finally imaged using a laser scanning confocal microscope with a 20× objective lens. The emission of BODIPY excited at a wavelength of 488 nm with a 25-mW argon ion laser was detected in the wavelength region longer than 515 nm. Images were recorded at 5-μm intervals in depth, starting from the confluent layer on the collagen surface. The acquired images were analyzed using a scion image analyzer (Scion, USA). In each model, about 30 networks were randomly selected for analysis, and the morphology of each of these networks was quantified by determining the total length of the network in each image. The network length distribution at 5-μm intervals in depth was normalized by the total cumulative length of each network in every tomogram. To compare the networks in the gel-bFGF model and those in the medium-bFGF model, the average normalized length of the gel-bFGF model was divided by that of the medium-bFGF model. The network centroid was calculated using the following formula

$$D_G = \Sigma D_i L_i / \Sigma L_i$$

where D_G is the observed depth of the centroid, D_i the observed depth of the network, and L_i the observed network length. The mean depth of the tomogram in which network most expanded was also calculated.

4-2-7. Statistical Analysis

Data are presented as mean ± S.E. Only for ELISA analysis, data are presented as mean ± S.D. Student's *t* test was used to test for differences.

4-3. Results

4-3-1. Observation of Model for Network Formation *in Vitro*

Fig. 4-1 shows an illustration of the network formation process based on observation results from this study. BPMECs (ECs) reached confluence on day 2, invaded the underlying gel on day 3, and formed a network. Fig. 4-2 shows the phase-contrast images of the ECs, revealing that in each model, the ECs formed 3-D networks in the collagen gel on day 5. In the gel-bFGF model (Fig. 4-2 (A)) and medium-bFGF model (Fig. 4-2 (B)), ECs reached confluence on the surface of the collagen gel 48 h after seeding and then invaded the underlying gel to form networks, whereas in the model without bFGF (Fig. 4-2 (C)), networks were hardly formed.

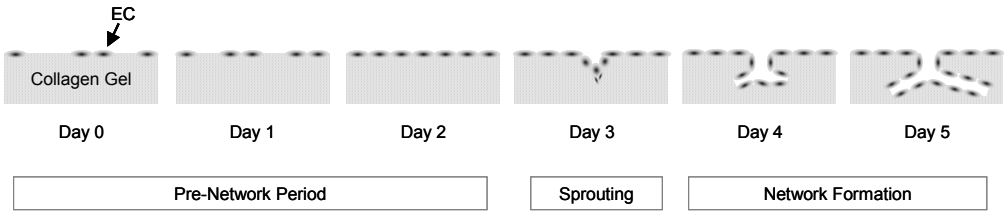

Fig. 4-1 Network formation process in the gel-bFGF model and medium-bFGF model. ECs reached confluence on the surface of collagen gel by day 2, then invaded the gel (after day 3), and finally formed networks (day 5).

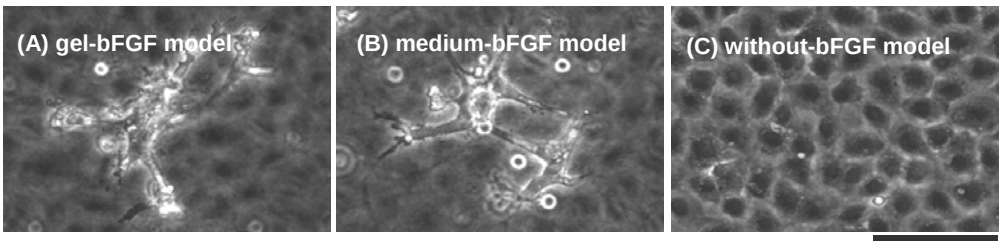

Fig. 4-2 Phase-contrast iImages of the models. Phase-contrast images of (A) gel-bFGF model and (B) medium-bFGF model. Both models showed network formation in the collagen gel. (C) Model without bFGF in both collagen gel and medium, showing almost no network formation. Bar scale: 100 μm.

4-3-2. Time Course Distribution of bFGF

To observe the time course change of growth factor distribution in both gel-bFGF model and medium-bFGF model, we measured the difference between the bFGF concentration in the collagen gel and that in the medium of each model (Fig. 4-3) using ELISA. The gel-bFGF model showed a high concentration rate in the beginning of the experiments which slightly decreased with time. On the other hand, the medium-bFGF model showed a low concentration rate at first which increased significantly with time. The concentration rate of the gel-bFGF model was approximately 4.4 times that of the medium-bFGF model at of 12 h, after which the difference between the two rates decreased, so that the rate of the gel-bFGF model was approximately 1.4 times to that of the medium bFGF model at 72 h. The gel-bFGF model has a significantly larger concentrate gradient than the medium-bFGF model at first, but this difference gradually disappears with time. This indicates that bFGF combines with collagen gel and does not diffuse quickly.

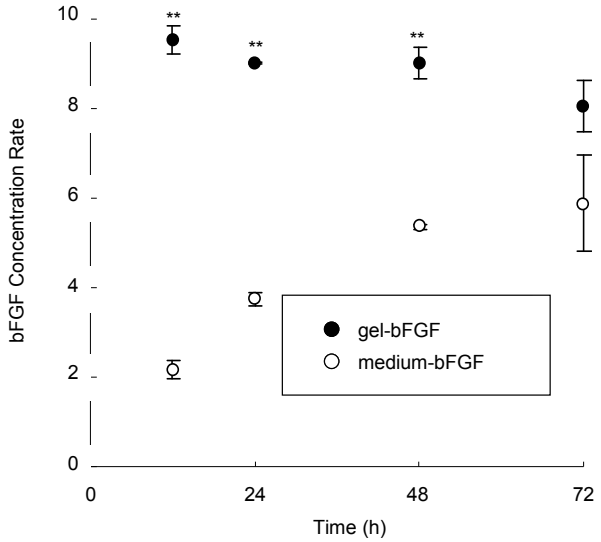

Fig. 4-3 Initial growth factor distribution in both gel-bFGF and medium-bFGF model. The bFGF concentration rate between the bFGF concentration in the collagen gel and that in the medium of each model were measured using ELISA to observe the time course change of growth factor distribution. Data are mean ± S.D. $^{**}P < 0.01$ vs. medium-bFGF model.

4-3-3. Effect of Initial Growth Factor Distribution on EC Migration and Proliferation of Pre-network Period

The measured migration distance of ECs of the gel-bFGF model during 5 h was longer than for the medium-bFGF model in the pre-network period (Fig. 4-4 (A)). The difference was particularly significant on day 2. The measured migration angles of ECs on day 2 (Fig. 4-4 (B)) revealed another difference. The migration angle for the gel-bFGF model was relatively small, indicating linear migration of the ECs and ECs migrated a long distance. On the other hand, the migration angle for the medium bFGF model was omnidirectional, indicating that migration occurred in various directions on the surface of the gel and then the ECs migrated over a small area. Between days 2-5, the migration distance of the gel-bFGF model gradually decreased, whereas that of the medium-bFGF model remained relatively constant. The migration distance for the gel-bFGF model on day 2 was significantly higher than that on day 5 ($P < 0.01$), whereas the migration distance for the medium-bFGF model remained small after day 1.

Fig. 4-5 shows the cell count on collagen gel in the two models during the 5 days of culture. There was hardly any difference between the cell numbers of each two models.

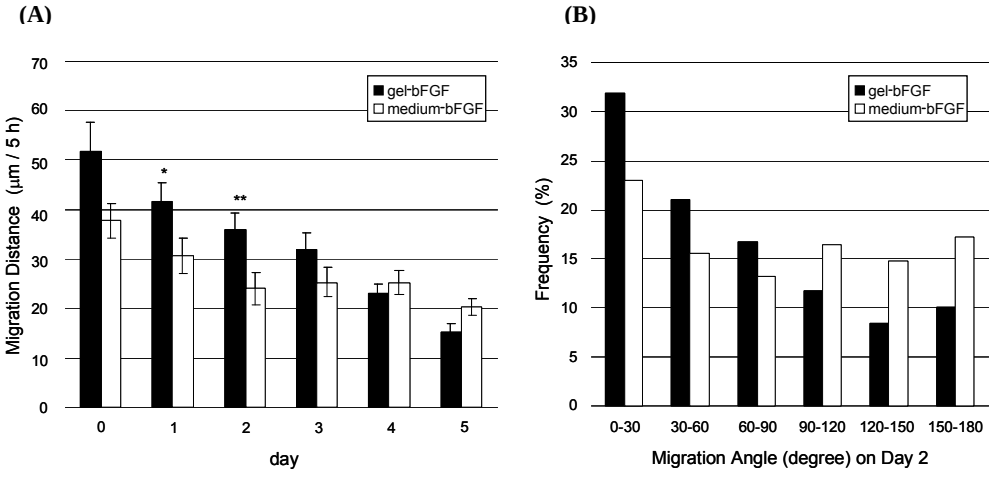

Fig. 4-4 Migration of ECs on the surface of collagen gel. (A) Migration distance per 5 h in the gel-bFGF model and medium-bFGF model measured daily up to day 5. Data are mean ± S.E. **P* < 0.05, ***P* < 0.01 vs. medium-bFGF model. (B) Migration angle of ECs measured on day 2. Migration angle of the gel-bFGF model was relatively small, whereas that of the medium-bFGF model was omnidirectional.

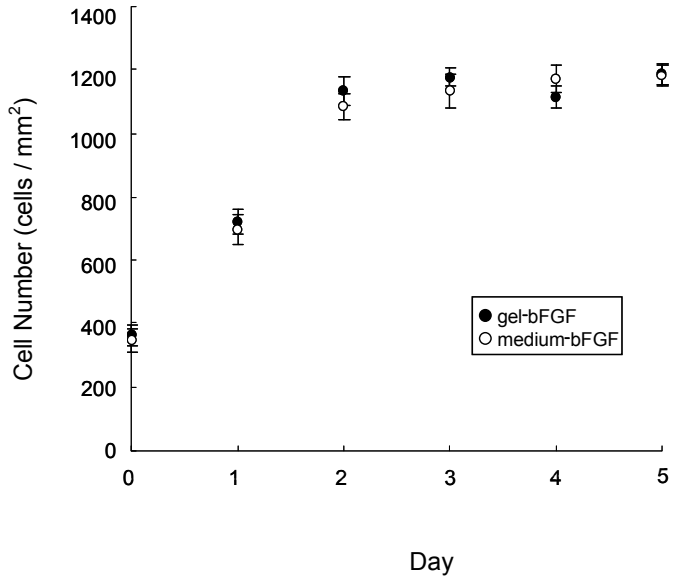

Fig. 4-5 Count of ECs Seeded on Collagen Gel up to Day 5. EC number on the surface of collagen gel was counted daily from seeding to day 5. Data are mean ± S.E.

4-3-4. Effect of initial growth factor distribution on network sprouting

Because of the significant difference in concentration rates between gel-bFGF model and medium-bFGF model during the first 48 h and initial growth factor distribution affects the migration of ECs, the effect of growth factor distribution on the early stage of network formation was also studied. ECs were seeded onto collagen gel on day 0, then reached confluence on day 2, and finally invaded the gel on day 3 (Fig. 4-1). The effect of growth factor distribution on network sprouting was clarified by counting the number of sprouting points visible on phase-contrast and bright-field images of both models obtained on days 3 and 5. For either day, the gel-bFGF model had significantly more sprouting points compared with the medium-bFGF model (Fig. 4-6), and the number in the medium-bFGF model increased from day 3 to day 5, whereas that in the gel-bFGF model remained relatively constant (Fig. 4-6).

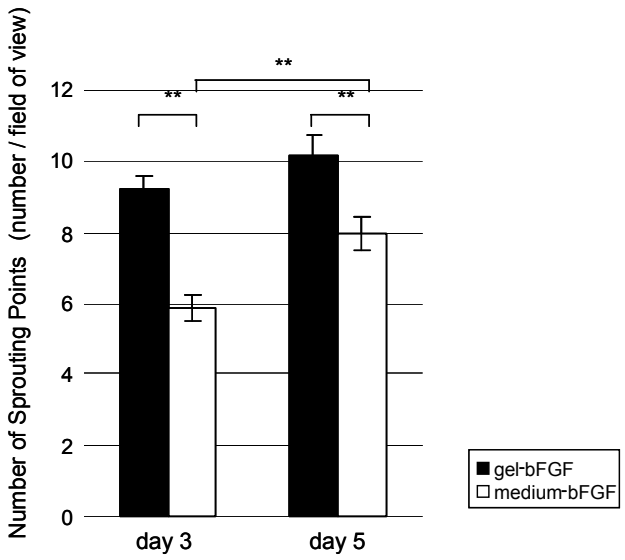

Fig. 4-6 Effect of growth factor distribution on early stage of network formation. Number of sprouting points on days 3 and 5 was counted from phase-contrast images. Data are mean ± S.E. $^{**}P < 0.01$.

4-3-5. Effect of Initial Growth Factor Distribution on Morphology of 3-D Networks

To determine if the formation mechanism of the network was influenced by the initial growth factor distribution, the 30 ng/ml gel-bFGF model and medium-bFGF model on day 5 were dyed with CellTracker, then images of the networks were recorded at 5-μm intervals in depth using confocal laser scanning microscopy, and finally the lengths of networks in each image were measured. Both models showed similar depth (~90 μm) and similar 2D total length measured from accumulated tomogram images (467.5 ± 55.2 μm for the gel-bFGF model, and 498.8 ± 82.0 μm for the medium-bFGF model: data are mean ± S.D.). Despite these similarities, the manner in which the networks extend differed. The network of the gel-bFGF model extended to a depth of ~20-50 μm in the collagen gel (Fig. 4-7 (A)), whereas that of the medium-bFGF model extended to a depth of only ~10 μm (Fig. 4-7 (B)). To evaluate the extension of the networks in the gel, the ratio of the average network length in the gel-bFGF model was compared to that of the medium-bFGF model (Fig. 4-7 (C)). The comparison revealed that at deeper positions, the networks of the gel-bFGF model extended wider than those of the medium-bFGF model.

To understand the effects of initial growth factor distribution on the network morphology in detail, we calculated the centroid and the maximum depth of the networks. Figure 8 shows the results. The centroid of the gel-bFGF model was deeper than that of the medium-bFGF model (Fig. 4-8 (A)). Similarly, the networks most expanded deeper in the gel-bFGF model than in the medium-bFGF model (Fig. 4-8 (B)). This indicates that the initial distribution of growth factor affects the morphology of the formed network and that the networks in the gel-bFGF model tend to extend deeper.

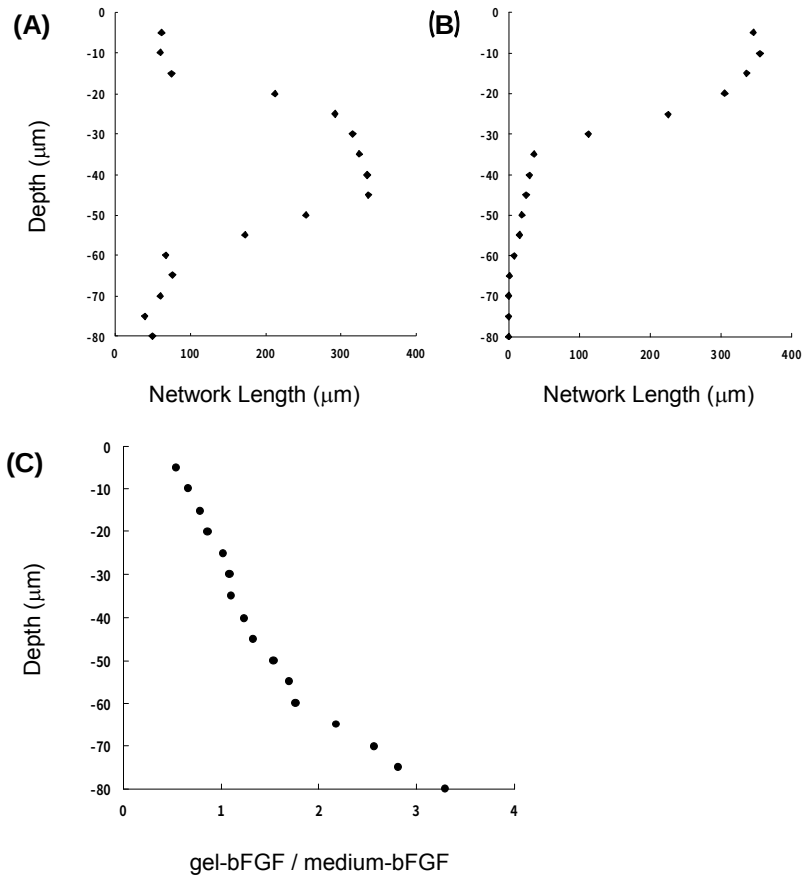

Fig. 4-7 Effect of initial growth factor distribution on network morphology. Each model on day 5 was dyed with CellTracker, and then imaged at 5-μm intervals in depth using confocal laser scanning microscopy. Typical network of gel-bFGF model (A) and medium-bFGF model (B). Networks in the gel-bFGF model extended deep into the collagen gel (A), whereas that of the medium-bFGF model extended only slightly beneath the collagen surface (B). (C) Network length measured from the CellTracker fluorescent image recorded at 5-μm intervals in depth, and calculated ratio of average network length in the gel-bFGF model to that in the medium-bFGF model. Networks in the gel-bFGF model tended to extend deeper, whereas those in the medium-bFGF model tended to extend only to a shallow position. Data are mean values.

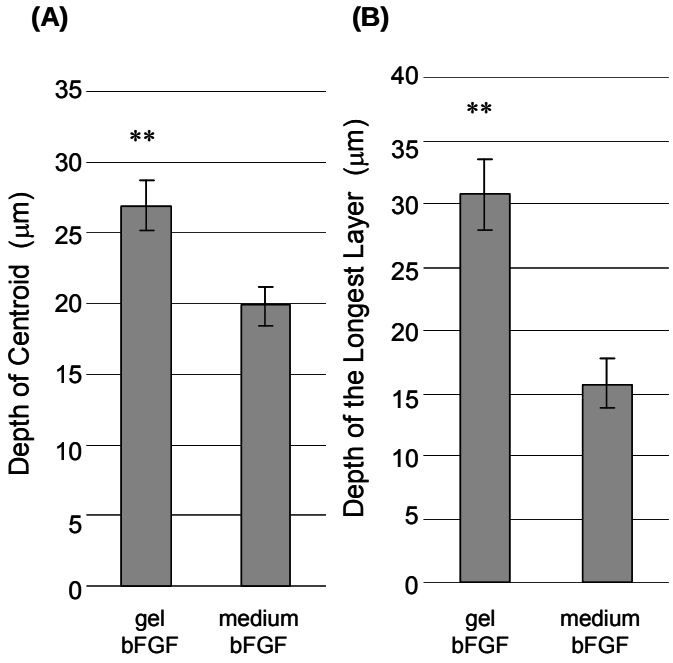

Fig. 4-8 Morphology of network ftructure. Centroid of networks (A) and tomogram in which network extends the longest distance (B) were used as morphological indexes. Data are mean ± S.E. $^{**}P < 0.01$ vs. medium-bFGF model

4-4. Discussion

The our results show that the morphology of microvessel networks depends on the initial distribution of the growth factor. Networks formed by the ECs differed in accordance with the concentration gradient conditions surrounding the ECs when they were seeded. The networks of the gel-bFGF model expanded mainly in a depth of 20-30 μm, and many reached a depth of 50-60 μm (Figs. 4-7 and 4-8). On the other hand, many networks in the medium-bFGF model expanded in a depth of only 10-20 μm, and only a few networks reached a depth of more than 50 μm. ELISA measurements indicate that a significantly large amount of bFGF is distributed in the collagen gel of gel-bFGF model compared to that of medium-bFGF model (Fig. 4-3). These results are consistent with previous studies in that the morphology of networks is influenced by the extracellular VEGF-A distribution *in vivo* (Pepper *et al*., 1995; Gerhardt *et al*., 2003). Kanematsu *et al*. reported the physiological relevance of interaction between bFGF and type I collagen (Kanematsu *et al*., 2004). In their study, after type I collagen solution mixed with bFGF solution in PBS was incubated for 1 h at 37°C, bFGF was incorporated into the collagen fibers (Kanematsu *et al*., 2004) as reported for heparin (Prestrelski *et al*., 1992). The bFGF complexed with collagen was protected from trypsin digestion (Kanematsu *et al*., 2004). This interaction could also occur in the gel-bFGF model used in our current study. 12 h after the beginning, the bFGF concentration in the collagen gel of the gel-bFGF model was approximately 9.5 times higher than in the culture medium, whereas in the medium-bFGF model, the bFGF concentration in the gel was approximately 2.2 times higher than in the culture medium. The bFGF in the gel of the gel-bFGF model decreased slowly; then the concentration rate was still over 8.0 times 3 days later. On the other hand, the bFGF in the gel of the medium-bFGF increased significantly and the bFGF concentration gradient between the gel and the medium was similar to that in the gel-bFGF model on day 3. These data indicate that bFGF combines with collagen gel and does not diffuse quickly. It seems that in the gel-bFGF model,

there is a high concentration of bFGF all over the gel. Since the bFGF is diffused from the surface, there is also probably a concentration gradient. The gel of the medium-bFGF model had both a low concentration and a low gradient, possibility because the gel surface absorbed most of the bFGF. If ECs in the gel-bFGF model detect a concentration gradient, they will become activated and migrate (Figs. 4-4 and 4-6). As a result, the networks in the gel-bFGF model will establish themselves in deeper positions (Figs. 4-7 and 4-8).

The difference between the pre-network period and the network formation period (Fig. 4-1) was compared for the two models. In the pre-network period, ECs migrated and proliferated on collagen gel. On day 2 (just before the beginning of sprouting), the measured migration distance of ECs per 5 h for the gel-bFGF model was significantly longer than that for the medium bFGF-model (Fig. 4-4 (A)). The migration angle of the ECs was relatively small in the gel-bFGF model, whereas in the medium-bFGF model, it was omnidirectional (Fig. 4-4 (B)). The resulting migration angle indicates that ECs in the gel-bFGF model migrated linearly over a long distance, whereas those in the medium-bFGF model migrated within a relatively small area. Previous studies show that EC migration is enhanced by bFGF (Ueda *et al*., 2004). Our results indicate that bFGF distribution is also a migration-regulating factor. The processes of EC migration, adhesion, and tube formation might depend on integrin activity (Ueda *et al*., 2004) and bFGF induces β1 integrin expression on microvascular ECs (Klein *et al*., 1993). The gradient of bFGF might affect integrin expression, and thus affect EC migration. In our study, EC proliferation on collagen gel was almost the same for both models (Fig. 4-3), indicating that bFGF distribution has little effect on the proliferation of ECs on collagen gel.

Based on our results, extracellular conditions of bFGF affect the number of sprouting points. The gel-bFGF model had a significantly larger number of sprouting points than did the medium bFGF-model (Fig. 4-6). bFGF causes significant changes in the expression of integrins in ECs

(Klein *et al*., 1993), migration ability of ECs, and onset of angiogenesis (Li et al., 2003). In our results, the migration distance for the gel-bFGF model on day 2 was significantly longer compared with that for the medium bFGF-model, but decreased with time (Fig. 4-4 (A)), and the number of sprouting points remained relatively constant (Fig. 4-6). On the other hand, in the medium-bFGF model, the migration distance was small but remained relatively constant after day 1 (Fig. 4-4 (A)) and the number of sprouting points increased between days 3 and 5 (Fig. 4-6). These results indicate that EC migration is closely related to the sprouting of network. Gerhardt *et al*. showed that the network tip-cell was guided toward a high concentration growth factor (Gerhardt *et al*., 2003). Active migration ability of ECs (Fig. 4-4 (A)) and/or sensing of bFGF distribution in the gel-bFGF model might result in many sprouting points.

Based on our results, network morphology was affected by bFGF distribution at the time the ECs were seeded. Ruhrberg *et al*. showed that heparin-binding VEGF-A establishes a steep concentration gradient in extracellular space (Ruhrberg *et al*., 2002), and Gerhardt *et al*. [(9)] showed that the concentration gradient is a regulation factor in network morphology (Gerhardt *et al*., 2003). Our results are consistent with these previous studies. ECs in the gel-bFGF model can detect a concentration gradient in the gel-bFGF model and invade and migrate actively (Figs. 4-4 and 4-6), then the networks therefore migrate and extend deeper (Figs. 4-7 and 4-8). Dynamic migration of ECs on the gel in the gel-bFGF model can also cause deeper migration of ECs. β1 integrin modulates epithelial cell migration and tubular morphogenesis in a type I collagen sandwich model (Coraux *et al*., 2000). Our previous study also suggested that network formation in collagen gel is associated with cell migration on the surface of the gel (Ueda *et al*., 2004). High motility of ECs at the onset of sprouting (Fig. 4-4) might result in migration of ECs deeper into the gel (Figs. 4-7 and 4-8). ECs then proliferate and extend their network, resulting in a network morphology that extends deeper into the gel. ECs on the gel in the medium-bFGF model, however, migrate within a

relatively small area (Fig. 4-4 (B)) and can invade beneath the collagen surface. Although the ECs would then proliferate and extend their network, the resulting network would remain shallow.

The results of this study are useful to regenerative medicine and tissue engineering, because the control of 3-D vessels is essential for the formation and maintenance of organ function. If the growth factor concentration of the center part of regenerated tissue would be kept in higher concentration compared to the surface of that, microvessel formation towards inside of the tissue could be induced, and then 3-D regenerated tissue would be kept in appropriate condition. Distribution of growth factors is, therefore, one of the critical factors to create 3-D regenerated tissue.

In conclusion, growth factor distribution at the time ECs are seeded affects the EC motility and thus affects the morphology of the EC network. This result can be applied to the arbitrary control of the formation of new microvessel networks.

References

Coraux C, Zahm JM, Puchelle E, Gaillard D. Beta(1)-integrins are involved in migration of human fetal tracheal epithelial cells and tubular morphogenesis. Am J Physiol Lung Cell Mol Physiol. 279: L224-L234, 2000.

Folkman J, Haudenschild C. Angiogenesis *in vitro*. Nature. 288: 551-556, 1980.

Gerhardt H, Golding M, Fruttiger M, Ruhrberg C, Lundkvist A, Abramsson A, Jeltsch M, Mitchell C, Alitalo K, Shima D, Betsholtz C. VEGF guides angiogenic sprouting utilizing endothelial tip cell filopodia. J Cell Biol. 161: 1163-1177, 2003.

Ingber DE, Folkman J. Mechanochemical switching between growth and differentiation during fibroblast growth factor-stimulated angiogenesis *in vitro*: role of extracellular matrix. J Cell Biol. 109: 317-330, 1989.

Kanematsu A, Marui A, Yamamoto S, Ozeki M, Hirano Y, Yamamoto M, Ogawa O, Komeda M, Tabata Y. Type I collagen can function as a reservoir of basic fibroblast growth factor. J Control Release. 99: 281-292, 2004.

Klein S, Giancotti FG, Presta M, Albelda SM, Buck CA, Rifkin DB. Basic fibroblast growth factor modulates integrin expression in microvascular endothelial cells. Mol Biol Cell. 4: 973-982, 1993.

Kubota Y, Kleinman HK, Martin GR, Lawley TJ. Role of laminin and basement membrane in the morphological differentiation of human endothelial cells into capillary-like structures. J Cell Biol. 107: 1589-1598, 1988.

Li J, Zhang YP, Kirsner RS. Angiogenesis in wound repair: angiogenic growth factors and the extracellular matrix. Microsc Res Tech. 60: 107-114, 2003.

Montesano R, Vassalli JD, Baird A, Guillemin R, Orci L. Basic fibroblast growth factor induces

angiogenesis *in vitro*. Proc Natl Acad Sci USA. 83: 7297-7301, 1986.

Pepper MS, Ferrara N, Orci L, Montesano R. Leukemia inhibitory factor (LIF) inhibits angiogenesis *in vitro*. J Cell Sci. 108: 73-83, 1995.

Prestrelski SJ, Fox GM, Arakawa T. Binding of heparin to basic fibroblast growth factor induces a conformational change. Arch Biochem Biophys. 293: 314-319, 1992.

Ruhrberg C, Gerhardt H, Golding M, Watson R, Ioannidou S, Fujisawa H, Betsholtz C, Shima DT. Spatially restricted patterning cues provided by heparin-binding VEGF-A control blood vessel branching morphogenesis. Genes Dev. 16: 2684-2698, 2002.

Shimizu T, Yamato M, Isoi Y, Akutsu T, Setomaru T, Abe K, Kikuchi A, Umezu M, Okano T. Fabrication of pulsatile cardiac tissue grafts using a novel 3-dimensional cell sheet manipulation technique and temperature-responsive cell culture surfaces. Circ Res. 90: e40, 2002.

Ueda A, Koga M, Ikeda M, Kudo S, Tanishita K. Effect of shear stress on microvessel network formation of endothelial cells with *in vitro* three-dimensional model. Am J Physiol Heart Circ Physiol. 287: H994-H1002, 2004.

Vailhé B, Vittet D, Feige JJ. *In vitro* models of vasculogenesis and angiogenesis. Lab Invest. 81: 439-452, 2001.

Chapter V

Effect of Hypoxia on Formation of Three-dimensional Microvessel Networks by Endothelial Cells *in Vitro*

5-1. Introduction

Angiogenesis, the formation of new microvessels by endothelial cells (ECs) migrating and proliferating from preexisting vessels, is essential for numerous physiological events, such as embryonic development, ovulation, and wound healing (Gerwins *et al*., 2000). Angiogenesis is also a critical factor in many pathological events, such as arteriosclerosis, diabetes, and tumor growth (Carmeliet *et al*., 2000). Because microvessel networks are essential for the formation and maintenance of organ functions, three-dimensional (3-D) control of network formation is also critical in regeneration medicine and tissue engineering. Regenerated 3-D tissue cannot maintain its physiological function in the absence of a 3-D microvessel network because diffusion alone can not supply sufficient nutrients and O_2 to the tissue. In the absence of vascularization, diffusion limits tissues to a thickness of less than ~100 μm (Shimizu *et al*., 2002); therefore, extensive 3-D microvessel networks of significant depth are required to supply O_2 and nutrients to cells comprising regenerated 3-D tissues.

To control microvessel network formation in regenerated tissue, we must first understand the effects of angiogenic factors, such as growth factors, shear stress, and hypoxia, on formation of the 3-D network. Several growth factors that induce vascular remodeling, and which are critical for new vessel formation, have been identified (Montesano *et al*., 1986; Pepper *et al*., 1995; Yang *et al*., 1998), including fibroblast growth factor (FGF) and vascular endothelial growth factor (VEGF)

(Folkman *et al*., 1992). The function and morphology of ECs are also regulated by hemodynamic stress (Ando *et al*., 1994; Fisher *et al*., 2001; Fukushima *et al*., 2001; Ueda *et al*., 2004) and shear stress is a significant stimulus for angiogenesis (Gloe *et al*., 2002; Ichioka *et al*., 1997; Ueda *et al*., 2004).

Since angiogenesis is one of the physiological responses to a low- O_2 environment (Vincent e *et al*., 2002), hypoxia is one of the major factors controlling network formation. In addition, solid tumors are commonly hypoxic (Fukumura *et al*., 2001), and O_2 concentration is an important determinant of tumor growth. Hence, the effect of hypoxia on angiogenesis has been studied extensively *in vivo* and *in vitro*. Angiogenesis-promoting factors, such as growth factors and their receptors, are induced by hypoxic conditions *in vivo* (Höper *et al*., 1995), and hypoxia also induces angiogenic factors *in vitro* (Yamagishi *et al*., 1999). Although hypoxia is also important for microvessel formation, its role in network formation is not yet well understood.

In this study, we examined the effects of hypoxia on 3-D network formation using an *in vitro* model system consisting of ECs cultured on collagen gel under controlled O_2 concentration. In this system, ECs were isolated from other factors affecting network formation, such as growth factors, so that we could pinpoint the effects of hypoxia itself on the extensiveness and depth of microvessel networks in the absence of other factors. Hypoxic (5% O_2) and normoxic conditions were achieved by adjusting the dissolved O_2 concentration in the culture medium. We also performed detailed, 3-D observations of network morphology using confocal laser-scanning microscopy.

5-2. Materials and Methods

5-2-1. Cell Culture

Cultured bovine pulmonary microvascular ECs (BPMECs) were purchased from Cell Systems (USA) and were used in all experiments. Cells were cultured in Dulbecco's modified Eagle's

medium (DMEM;, GIBCO, USA) supplemented with 10% fetal bovine serum (FBS; Cell Culture Technologies, Switzerland), 1% antibiotic-antimycotic (Invitrogen, USA), and 15 mM HEPES (DOJINDO, Japan). The BPMECs were seeded in 60-mm culture dishes (Corning, USA.) and cultivated under standard conditions (37°C, 5% CO_2). The passage number of the BPMECs used in our experiments ranged from 6 to 8.

5-2-2. *In Vitro* Model

Collagen gels were prepared as follows: eight volumes of Cellmatrix Type I-A solution (3 mg/ml; Nitta Gelatin, Japan) were mixed with one volume of 10 x Minimum Essential Medium (MEM; Invitrogen, USA) and one volume of buffer solution (20 mM HEPES, 0.08 N NaOH; both from Wako Pure Chemical Industries, Japan) on ice. Aliquots (0.5 ml) of the mixture were then poured into Cell Culture Inserts for 6-well plates (Becton Dickinson, USA) and allowed to gel at 37°C for 30 min. ECs were then seeded at 1 x 10^5 cells per insert and incubated at 37°C under 5% CO_2.

5-2-3. Application of Hypoxia

Cell Culture Inserts were transferred into the chamber of a hypoxia application apparatus (MK2000 Dynamic Co-culture System (Warabi *et al*., 2004), Yamato Scientific, Japan). DMEM was circulated through the apparatus with a sterile, continuous-flow loop (Fig. 5-1). The apparatus was kept at 37°C in an incubator, and the concentration of CO_2 in the incubator was maintained at 5%. The apparatus is designed to have a room of average 2 mm height above ECs and the flow volume is set on low level (3 ml/min) to eliminate the effect of shear stress. The dissolved O_2 concentration in the DMEM was controlled by bubbling of a gas mixture (5% CO_2 -95% N_2) through a porous tube. Bubbles were removed by a bubble trap, and the perfusate was circulated by a diaphragm pump in

the flow circuit. The total priming volume was greater than 10 ml for the entire circuit. For normoxic controls, ECs were incubated at 37°C under 5% CO_2 throughout the experiments.

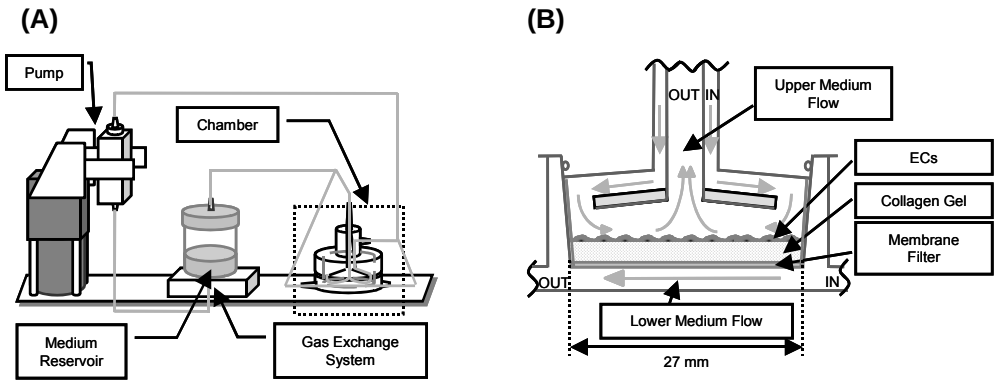

Fig. 5-1 Hypoxia application apparatus. (A) ECs were embedded in coullagen gel in chambers of the apparatus and grown under controlled O_2 concentration. (B) Close-up view of the inside of chamber.

5-2-4. Effect of Hypoxia on Network Formation

To examine the effect of hypoxia on network formation, ECs were seeded into the hypoxia application apparatus. The medium was changed 24 h after seeding, and the cells were cultured under hypoxic (5% O_2) or normoxic (21% O_2) conditions for 6 days. ECs cultured under 5% O_2 were exposed to normal room air for brief periods every other day, when the medium was replaced.

ECs were photographed at 24-h intervals using a phase-contrast microscope (ECLIPSE TE200, Nikon, Japan) equipped with a CCD camera (AxioCam MRc5, Carl Zeiss, Germany). Thirty fields were randomly recorded in this experiment, and the acquired images were analyzed using Scion Image software (Scion Corporation, USA). Both the total length and total number of networks were quantified, and these were normalized by the length and numbers on day 0.

5-2-5. Observation of 3-D Networks Using Confocal Laser-scanning Microscopy

Networks were visualized by staining the BPMEC nuclei with acridine orange (Invitrogen, USA), and the depth of the 3-D networks formed after 7 days of hypoxia or normoxia were observed. Samples were first washed in phosphate-buffered saline (PBS; Nissui Pharmaceutical, Japan) and then incubated with 10 μg/ml acridine orange for 15 min at 37°C. The samples were washed again in PBS, and images were recorded using an LSM5 Pascal confocal laser-scanning microscope (Carl Zeiss) with an excitation wavelength of 488 nm and detection in the region 515-530 nm. Images were recorded at 1.8-μm depth intervals. Thirty networks were randomly recorded in this experiment and the depth of the network was defined as the position of the deepest EC nucleus in the network.

To observe 3-D network structures in detail, the networks were also doubly stained with acridine orange (green; nuclei) and CellTracker Red CMTPX (red; cytoplasm; Invitrogen, USA).

The samples were first washed in PBS and then incubated with 10 μM CellTracker for 15 min at 37°C. After the samples were again washed in PBS, they were incubated with 10 μg/ml acridine orange for 15 min at 37°C. Samples were washed once more in PBS, and the 3-D network images were recorded using confocal laser-scanning microscopy with emission wavelengths of 488 and 543 nm. Images were recorded at 0.75-μm depth intervals. Network morphology was observed using Imaris software (Carl Zeiss).

5-2-6. Effect of Hypoxia on EC Secretions

To examine the effect of hypoxia on EC secretions, ECs were seeded into the hypoxia application apparatus, the medium was changed 24 h later, and the cells were then cultured for 2 days under hypoxic (5% O_2) or normoxic conditions. The hypoxic and normoxic EC-conditioned media were collected and transferred to fresh ECs already prepared on collagen gel inserts. The quantity of conditioned medium was approximately 10 ml. The fresh ECs were incubated in the hypoxic or normoxic EC-conditioned medium at 37°C under 5% CO_2, and they were photographed using phase-contrast microscopy at 24-h intervals after the addition of conditioned medium. Both the total length and total number of networks were quantified, and these were normalized by the length and numbers on day 0.

5-2-7. Effect of Hypoxia on Ability of ECs to Respond to Growth Factor

To examine the effect of hypoxia on the network formation status of ECs, we assessed the ability of the ECs to form networks in response to growth factors. ECs were seeded into the hypoxia application apparatus, the medium was changed 24 h after seeding, and the cells were cultured under hypoxic or normoxic conditions for 2 days. The medium was then replaced with DMEM containing 30 ng/ml Recombinant Human Fibroblast Growth Factor-basic (bFGF; Pepro

Tech, UK), and the ECs were incubated at 37°C under 5% CO_2. The ECs were photographed using a phase-contrast microscope 24 h after the addition of bFGF. Both the total length and total number of networks were quantified, and these were normalized by the length and numbers of normoxic conditions.

5-2-8. Effect of Hypoxia on mRNA Expression by ECs

Quantitative real-time polymerase chain reaction (QPCR) analysis was performed to identify mRNA transcription in the ECs. RNA was isolated from ECs 6-hour after culture under hypoxic or normoxic conditions using the RNeasy RNA isolation kit (Qiagen, Hilden, Germany). Reverse transcription was performed on 1 μg of total RNA using the oligo$(dT)_{20}$ primer and the SuperScript III reverse transcriptase (Invitrogen). The gene-specific primers used were designed using Primer3 software; most of primers were designed to amplify a region spanning the splice site of exon. The analysis was performed on HIF-1α, which plays an important role in ECs function under hypoxia condition. QPCR mixtures were composed of SYBR Green QPCR Master Mix (Stratagene, La Jolla, CA), 10 μM primer, 10 nM reference dye, and 1 μl cDNA in a total volume of 20 μl. The samples were incubated at 95°C for 5 min, followed by 45 cycles of 95°C for 5 sec, 65°C for 30 sec using the Mx3000P real-time PCR system (Stratagene). Amplification plots were analyzed using MxPro software (Stratagene).

We used a GeneChip Microarray (Affymetrix, USA) to examine the effects of hypoxia on mRNA expression by ECs. ECs were seeded at 2 x 10^5 cells per 60-mm dish, incubated for 24 h, and then moved into an incubator under 5% O_2 or normoxic conditions, where they were conditioned by incubation for 48 h. Total RNA was prepared from the conditioned cells using the Qiagen RNeasy protocol and reagents, and scanned against GeneChip bovine arrays with a GeneChip Scanner (Affymetrix). The data were exported to Excel (Microsoft, USA) and analyzed. The scanned data

for hypoxia- and normoxia-conditioned cells were normalized to data obtained from the AFFIX gene.

5-2-9. Statistical Analysis

Data are presented as the mean ± S.E. The Student's t test was used to test for differences.

5-3. Results

5-3-1. Hypoxia-induced Network Formation *in Vitro*

ECs cultured under 5% O_2 for 6 days formed networks in the collagen gel (Fig. 5-2). In both the hypoxia and normoxia model samples, the ECs reached confluency on day 2 or 3. On day 3, the hypoxic ECs began to penetrate the underlying collagen gel, and they formed a network by day 6, whereas the normoxic ECs barely penetrated the gel by day 6. On day 6, the total length and total number of networks formed by the hypoxic ECs were approximately 10- and 7-fold greater than those of the networks formed by the normoxic ECs, respectively (Fig. 5-3).

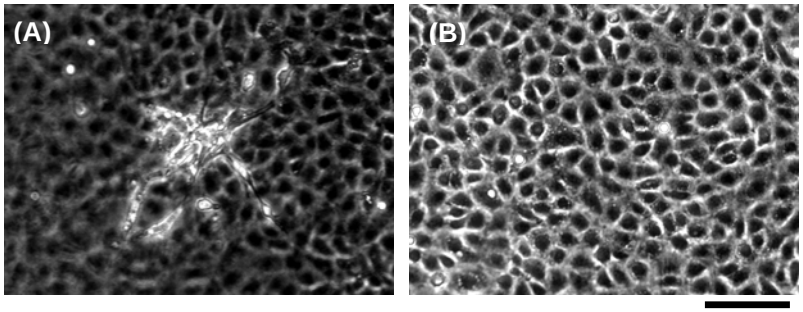

Fig. 5-2 Network formation by ECs in collagen gel. (A) On day 6 of growth under hypoxia, ECs invaded the underlying collagen gel and formed networks. (B) ECs grown under normoxia exhibited very little tendency to form networks. Bar scale: 100 μm.

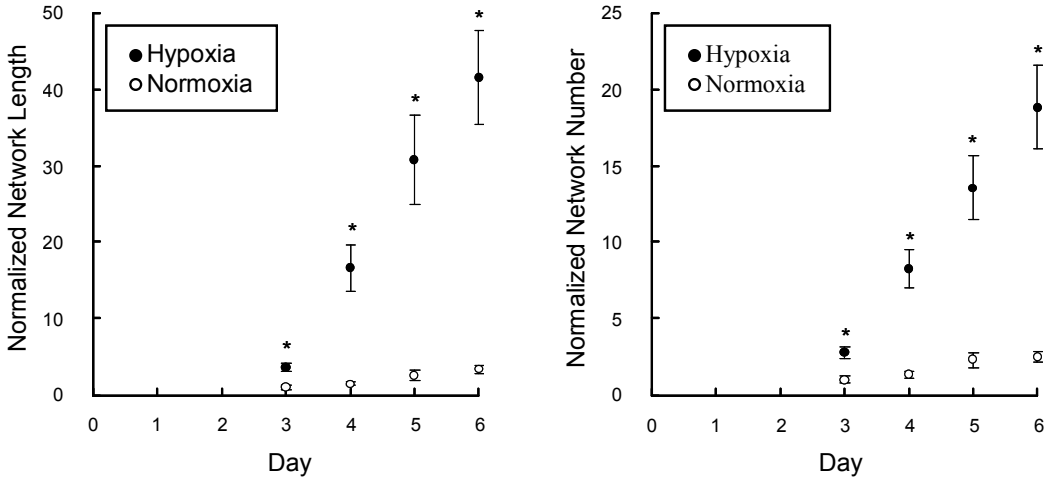

Fig. 5-3 Effect of hypoxia on network formation. Total network length (A) and total network number (B) are indicated. Data shown represent means ± S.E; n = 15. *P < 0.001 vs. normoxia.

5-3-2. Observation of 3-D Network Morphology

We observed the 3-D network morphology in detail using confocal laser-scanning microscopy. ECs were dyed with acridine orange after 7 days of incubation under hypoxic or normoxic conditions. Under hypoxia, networks not only spread more widely, but they also penetrated more deeply into the underlying collagen gel (Fig. 5-4 (A)). These cells organized into branching, capillary-like structures and formed an extensive network under the monolayer surface (Fig. 5-4 (C)). In contrast, the networks formed under normoxia penetrated only slightly into the gel (Figs. 5-4 (B), (D)). The nuclei of the hypoxic networks were found at a significantly greater maximum depth than those of the normoxic networks (Fig. 4-5). Under hypoxia, the tips of some networks penetrated to a depth greater than 75 μm, and 60% of the tips penetrated to a depth greater than 25 μm. In contrast, 90% of the normoxic network tips penetrated to a depth of less than 25 μm.

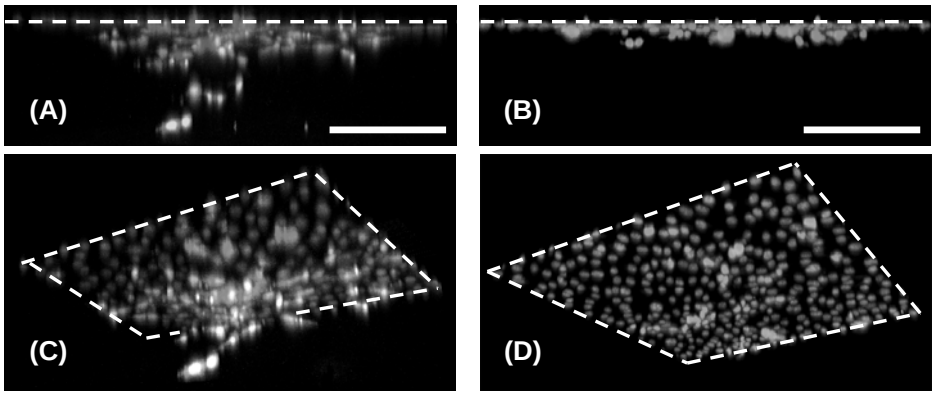

Fig. 5-4 The 3-D Structures of Networks Grown under Hypoxia or Normoxia. The 3-D structures of networks grown under hypoxia or normoxia were observed using confocal laser-scanning microscopy. (A, C) Networks formed under hypoxia penetrated deeply into the underlying collagen gel and formed continuous, tube-like structures. (B, D) Networks formed under normoxia were very shallow. Broken lines indicate the confluent EC monolayer on the collagen gel. Bar scale in (A) and (B): 100 μm.

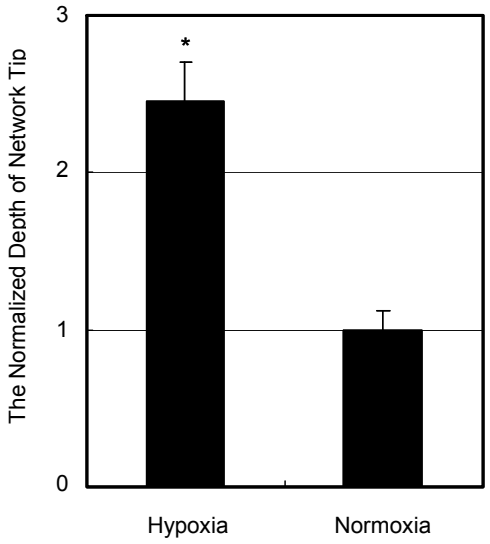

Fig. 5-5 Effect of hypoxia on depth of network tips. The normalized maximum depths of nuclei in the EC networks are indicated. Data shown represent means ± S.E; n = 30. *P < 0.001 vs. normoxia.

5-3-3. Effect of Hypoxia on EC Secretions

We also examined the effect of hypoxia- and normoxia-conditioned media on network formation by ECs. Conditioned media from ECs cultured for 2 days under hypoxic or normoxic conditions were loaded onto ECs on collagen gels. In both cases, the ECs began to penetrate into the gel on day 2, and then formed networks. After 4 days, the total length of the network induced by the hypoxia-conditioned medium was approximately twice that of the network induced by the normoxia-conditioned medium (Fig. 5-6).

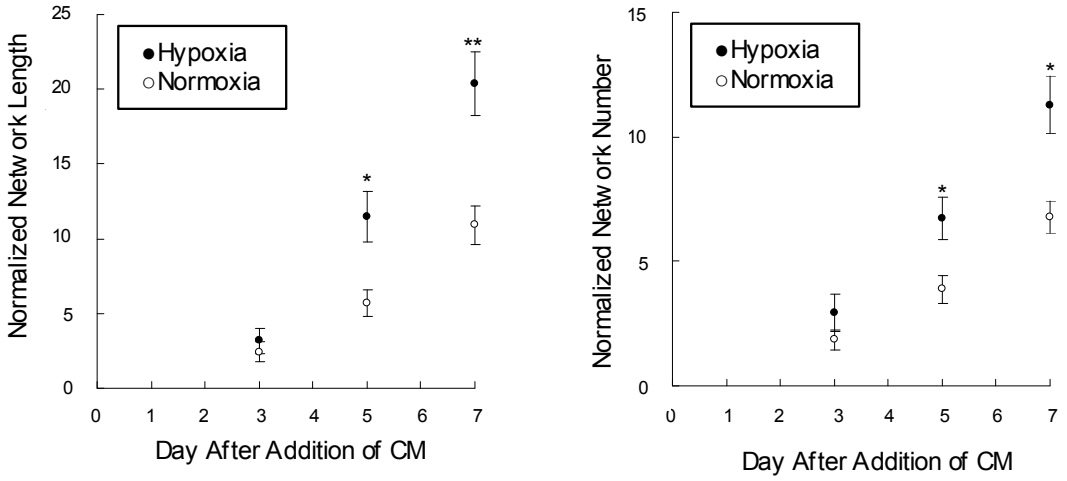

Fig. 5-6 Effect of hypoxia on EC secretions. Media were conditioned by culturing of ECs for 2 days under hypoxia or normoxia (control) and then loaded onto collagen gel-mounted ECs. The total length (A) and total number (B) of networks that formed after addition of the conditioned media (CM) are indicated. Data shown represent means ± S.E; n = 40-50. *P < 0.01, **P < 0.001 vs. normoxia.

5-3-4. Effect of Hypoxia on Sensitivity of ECs to the Growth Factor bFGF

To determine whether hypoxia promotes network formation by increasing the sensitivity of ECs to growth factors, we examined the ability of ECs to form networks in response to bFGF, an archetypal network formation factor. After ECs were incubated under hypoxic or normoxic conditions for 2 days, the medium was replaced with medium containing 30 ng/ml bFGF. Twenty-four hours later, the ECs had penetrated the underlying gel and formed networks. Both the total length and the total number of networks formed by the hypoxia-conditioned ECs were significantly greater than those formed by the normoxia-conditioned ECs (Fig. 5-7).

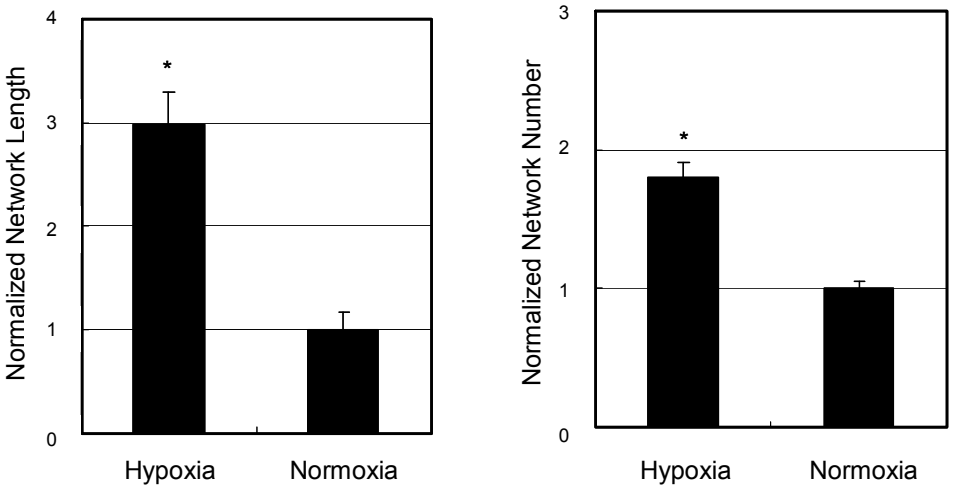

Fig. 5-7 Effect of hypoxia on sensitivity of ECs to bFGF. After ECs were cultured under hypoxic or normoxic conditions for 2 days, the medium was replaced with bFGF-containing medium. The total length (A) and total number (B) of networks present 24 h after the addition of bFGF are indicated. Data shown represent means ± S.E; n = 30. *P < 0.001 vs. normoxia.

5-3-5. Effect of Hypoxia on mRNA Expression by ECs

We examined the expression of HIF-1α mRNA using QPCR after six-hour culture under hypoxia or normoxia condition. The level of HIF-1α mRNA in hypoxia-conditioned ECs expression is ~55% higher than that under normoxia-conditioned ECs. This result indicates that HIF-1α mRNA is induced by hypoxia in early time of this experiment.

In addition, to determine how hypoxia affects mRNA expression by ECs, we used a GeneChip Microarray. The mRNA expression levels for approximately 30 genes were at least about twice as high in hypoxia-conditioned ECs than in normoxia-conditioned ECs. In contrast, mRNA expression levels for only 2 genes were at least twice as high in normoxia-conditioned ECs than in hypoxia-conditioned ECs. Some of the proteins whose genes were expressed at substantially different levels under hypoxia vs. normoxia were known angiogenic factors, including activin receptor, VLDL receptor, ICAM3, and chemokine ligand 5, suggesting that these factors are involved in network induction in our model system.

Hypoxia- and normoxia-conditioned ECs also expressed different levels of members of the well-known angiogenic VEGF and FGF families. Under hypoxic conditions, levels of VEGF, VEGF-B, VEGF-C, and acidic FGF (aFGF) increased by 54, 13, 18, and 30%, respectively, compared to normoxic conditions.

5-4. Discussion

Our results indicate that hypoxia (5% O_2) induces penetration of ECs into the underlying collagen gel, where they form 3-D, capillary-like networks with depth and breadth, even in the absence of external factors (Figs. 5-2 and 5-3). These results have considerable potential significance, given that penetration of 3-D networks to greater depths is a critical goal in tissue engineering, and that deep and extensive vessel networks are required to supply O_2 and nutrients to

regenerated tissue. We also found that networks formed under hypoxic conditions penetrate more deeply than those formed under normoxic conditions (Figs. 5-4 and 5-5), forming continuous, tubular structures at greater depth. Several steps of network formation may be affected by hypoxia, including EC proliferation and migration, sprouting into the collagen gel, and network formation in the gel.

Our results are similar to the results of previous studies performed *in vivo* and *in vitro*. Höper *et al*. found that hypoxia (10% O_2) induced enlargement of the blood vessel area in chick embryos (Höper *et al*., 1995), and Yamagishi *et al*. found that hypoxia (5% O_2) significantly increased the length of two-dimensional, capillary-like structures formed by ECs on Matrigel (Yamagishi *et al*., 1999), which includes several kinds of growth factors. Unlike these studies, however, our study is the first to demonstrate that hypoxia promotes network formation by ECs even in the absence of external growth factors or other kinds of cells. Thus, hypoxia must cause ECs to either increase their secretion of network-inducing factors, such as growth factors, or to become more sensitive to such factors, or both.

In our model system, larger networks were formed by hypoxia-conditioned media than by normoxia-conditioned media (Fig. 5-6), indicating that increased secretion of network-inducing factors by ECs may be a mechanism by which hypoxia induces network formation. Previous studies have shown that hypoxia induces expression of VEGF (Fukumura *et al*., 2001; Shweiki *et al*.,1992; Ladoux *et al*., 1993; Shweiki *et al*., 1995; Ikeda *et al*., 1995; Tuder *et al*., 1995), and Bos *et al*. have shown that HIF-1α is associated with angiogenesis and expression of bFGF and PDGF (Bos *et al*., 2005). We previously showed that bFGF induces formation of 3-D networks by ECs in collagen gel (Ueda *et al*., 2004), and other studies have shown that many kinds of growth factors can promote network formation (Montesano *et al*., 1985; Montesano *et al*., 1986; Pepper *et al*., 1995). These observations are consistent with increased secretion of 3-D network-inducing factors by ECs

under hypoxia.

Another possible reason for increased network formation in response to hypoxia is that hypoxia induces a change in the ability of ECs to respond to growth factors by forming networks. To examine this issue, ECs were subjected to hypoxic or normoxic conditions for 2 days, and then bFGF was added to the medium. We found that the total length and number of networks formed by ECs under hypoxia were significantly greater than those formed by ECs under normoxia (Fig. 5-7) in response to the same concentration of growth factors. Previously, Tuder *et al*. found that *ex vivo* perfusion of isolated lungs under hypoxic conditions (0% O_2) caused an increase in levels of mRNA for the VEGF receptors KDR/Flk and Flt (Tuder *et al*., 1995), and Akimoto *et al*. found that mouse embryonic aortic cells cultured under 5% O_2 expressed increased amounts of Flk-1 and FGFR1, and that they were more responsive to VEGF and bFGF than were those exposed to room air (Akimoto *et al*., 2003; Akimoto *et al*., 2002). Furthermore, Waltenberger *et al*. found that the VEGF receptor KDR was up-regulated in human umbilical vein endothelial cells in response to hypoxia (2% O_2) (Waltenberger *et al*., 1996). Taken together with our data, these results suggest that ECs grown under hypoxic conditions have an increased ability to form networks in response to growth factors.

We performed QPCR and GeneChip microarray experiments to identify the EC genes affected by hypoxia. Using QPCR, we indicated the expression of HIF-1α mRNA is induced by hypoxia condition after 6 hours. HIF-1α is known a factor which plays an important role in ECs function under hypoxia condition (Calvani *et al*., 2006). Hypoxia increases ECs responsiviness to bFGF and this is mediated by HIF-1α dependent regulation of enzymes (Li *et al*., 2002), and HIF-1α is required for bFGF dependent EC cord formation (Calvani *et al*., 2006). In addition, for approximately 30 genes, mRNA expression levels were at least two times higher in hypoxia-conditioned ECs than in normoxia-conditioned ECs. In contrast, only 2 genes exhibited mRNA expression levels that were two or more times higher in normoxia-conditioned ECs than in

hypoxia-conditioned ECs. Some of the genes up-regulated by hypoxia were activin receptor, VLDL receptor, and ICAM3, which are known angiogenesis-promoting factors. Activin A stimulates angiogenesis by increasing VEGF levels (Poulaki *et al*., 2004), VLDL receptor is involved in angiogenesis (Takahashi *et al*., 2004) and high levels of ICAM-3 expression is founded on proliferating vessels (Verkarre *et al*., 1999). Chemokine (C-C motif) ligand 5, which enhances cell migration (Chabot *et al*., 2006) is also upregulated. Results from our previous study suggest that network formation in collagen gel is associated with cell migration (Ueda *et al*., 2004). Members of the VEGF and FGF angiogenic families were also upregulated under hypoxic conditions; these factors are known to affect the entire process of angiogenesis, including EC migration and proliferation and lumen formation (Montesano *et al*., 1986; Distler *et al*., 2003). Although many previous *in vitro* studies have identified individual growth factors or receptors that are up-regulated by hypoxia (Akimoto *et al*., 2003; Akimoto *et al*., 2002; Waltenberger *et al*., 1996), our experiments here identify that hypoxia activates HIF-1α expression, and many genes are also up-regulated. Thus, hypoxia induces HIF-1α-mediated expression of many genes that may stimulate several steps in network formation, leading to an extensive and deeply penetrating network.

Using a *in vitro* EC and collagen model, Semino *et al*. showed that two coupled processes drive capillary morphogenesis: active proliferation of ECs in the collagen gel monolayer, and migration of the extending sprout (Semino *et al*., 2006). They also showed that these processes are controlled by two different pathways. The VEGF pathway stimulates cell proliferation, and the EGF pathway acts to stimulate migration into the growing capillary structure. In our model system, hypoxia caused ECs to secrete network-inducing factor(s), increased the responsiveness of ECs to growth factors, and increased expression of many angiogenesis-related genes. We speculate that induction of angiogenesis-related genes by hypoxia leads to enhanced secretion of network formation factors by ECs and also increases the sensitivity of ECs to such factors, resulting in increased formation of 3-D,

microvessel networks.

References

Akimoto T, Hammerman MR. Fibroblast growth factor 2 promotes microvessel formation from mouse embryonic aorta. Am J Physiol Cell Physiol. 284: C371-C377, 2003.

Akimoto T, Liapis H, Hammerman MR. Microvessel formation from mouse embryonic aortic explants is oxygen and VEGF dependent. Am J Physiol Regul Integr Comp Physiol. 283: R487-R495, 2002.

Ando J, Tsuboi H, Korenaga R, Takada Y, Toyama-Sorimachi N, Miyasaka M, Kamiya A. Shear stress inhibits adhesion of cultured mouse endothelial cells to lymphocytes by downregulating VCAM-1 expression. Am J Physiol Cell Physiol. 267: C679-C687, 1994.

Bos R, van Diest PJ, de Jong JS, van der Groep P, van der Valk P, van der Wall E. Hypoxia-inducible factor-1alpha is associated with angiogenesis, and expression of bFGF, PDGF-BB, and EGFR in invasive breast cancer. Histopathology. 46: 31-36, 2005.

Calvani M, Rapisarda A, Uranchimeg B, Shoemaker RH, Melillo G. Hypoxic induction of an HIF-1alpha-dependent bFGF autocrine loop drives angiogenesis in human endothelial cells. Blood. 107: 2705-2712, 2006.

Carmeliet P, Jain RK. Angiogenesis in cancer and other diseases. Nature. 407: 249-257, 2000.

Chabot V, Reverdiau P, Iochmann S, Rico A, Senecal D, Goupille C, Sizaret PY, Sensebe L. CCL5-enhanced human immature dendritic cell migration through the basement membrane *in vitro* depends on matrix metalloproteinase-9. J Leukoc Biol. 79: 767-778, 2006.

Distler JH, Hirth A, Kurowska-Stolarska M, Gay RE, Gay S, Distler O. Angiogenic and angiostatic factors in the molecular control of angiogenesis. Q J Nucl Med. 47: 149-161, 2003.

Fisher AB, Chien S, Barakat AI, Nerem RM. Endothelial cellular response to altered shear stress. Am J Physiol Lung Cell Mol Physiol. 281: L529-L533, 2001.

Folkman J, Shing Y. Angiogenesis. J Biol Chem. 267: 10931-10934, 1992.

Fukumura D, Xu L, Chen Y, Gohongi T, Seed B, Jain RK. Hypoxia and acidosis independently up-regulate vascular endothelial growth factor transcription in brain tumors *in vivo*. Cancer Res. 61: 6020-6024, 2001.

Fukushima S, Nagatsu A, Kaibara M, Oka K, Tanishita K. Measurement of surface topography of endothelial cell and wall shear stress distribution on the cell. JSME Int J C-Mech Sy. 44: 972-981, 2001.

Gerwins P, Sköldenberg E, Claesson-Welsh L.. Function of fibroblast growth factors and vascular endothelial growth factors and their receptors in angiogenesis. Crit Rev Oncol Hematol. 34: 185-194, 2000.

Gloe T, Sohn HY, Meininger GA, Pohl U. Shear stress-induced release of basic fibroblast growth factor from endothelial cells is mediated by matrix interaction via integrin avb3. J Biol Chem 277: 23453-23458, 2002.

Höper J, Jahn H. Influence of environmental oxygen concentration on growth and vascular density of the area vasculosa in chick embryos. Int J Microcirc Clin Exp. 15: 186-192, 1995.

Ichioka S, Shibata M, Kosaki K, Sato Y, Harii K, Kamiya A. Effects of shear stress on wound-healing angiogenesis in the rabbit ear chamber. J Surg Res. 72: 29-35, 1997.

Ikeda E, Achen MG, Breier G, Risau W. Hypoxia-induced transcriptional activation and increased mRNA stability of vascular endothelial growth factor in C6 glioma cells. J Biol Chem. 270: 19761-19766, 1995.

Ladoux A, Frelin C. Hypoxia is a strong inducer of vascular endothelial growth factor mRNA expression in the heart. Biochem Biophys Res Commun. 195: 1005-1010, 1993.

Li J, Shworak NW, Simons M. Increased responsiveness of hypoxic endothelial cells to FGF2 is mediated by HIF-1a-dependent regulation of enzymes involved in synthesis of heparan sulfate

FGF2-binding sites. J Cell Sci. 115: 1951-1959, 2002.

Montesano R, Orci L. Tumor-promoting phorbol esters induce angiogenesis *in vitro*. Cell. 42: 469-477, 1985.

Montesano R, Vassalli JD, Baird A, Guillemin R, Orci L. Basic fibroblast growth factor induces angiogenesis *in vitro*. Proc Natl Acad Sci USA. 83: 7297-7301, 1986.

Pepper MS, Ferrara N, Orci L, Montesano R. Leukemia inhibitory factor (LIF) inhibits angiogenesis *in vitro*. J Cell Sci. 108: 73-83, 1995.

Poulaki V, Mitsiades N, Kruse FE, Radetzky S, Iliaki E, Kirchhof B, Joussen AM. Activin a in the regulation of corneal neovascularization and vascular endothelial growth factor expression. Am J Pathol. 164: 1293-1302, 2004.

Semino CE, Kamm RD, Lauffenburger DA. Autocrine EGF receptor activation mediates endothelial cell migration and vascular morphogenesis induced by VEGF under interstitial flow. Exp Cell Res. 312: 289-298, 2006.

Shimizu T, Yamato M, Isoi Y, Akutsu T, Setomaru T, Abe K, Kikuchi A, Umezu M, Okano T. Fabrication of pulsatile cardiac tissue grafts using a novel 3-dimensional cell sheet manipulation technique and temperature-responsive cell culture surfaces. Circ Res. 90: e40, 2002.

Shweiki D, Itin A, Soffer D, Keshet E. Vascular endothelial growth factor induced by hypoxia may mediate hypoxia-initiated angiogenesis. Nature. 359: 843-845, 1992.

Shweiki D, Neeman M, Itin A, Keshet E. Induction of vascular endothelial growth factor expression by hypoxia and by glucose deficiency in multicell spheroids: implications for tumor angiogenesis. Proc Natl Acad Sci U S A. 92: 768-772, 1995.

Takahashi S, Sakai J, Fujino T, Hattori H, Zenimaru Y, Suzuki J, Miyamori I, Yamamoto TT. The very low-density lipoprotein (VLDL) receptor: characterization and functions as a peripheral

lipoprotein receptor. J Atheroscler Thromb. 11: 200-208, 2004.

Tuder RM, Flook BE, Voelkel NF. Increased gene expression for VEGF and the VEGF receptors KDR/Flk and Flt in lungs exposed to acute or to chronic hypoxia. Modulation of gene expression by nitric oxide. J Clin Invest. 95: 1798-1807, 1995.

Ueda A, Koga M, Ikeda M, Kudo S, Tanishita K. Effect of shear stress on microvessel network formation of endothelial cells with *in vitro* three-dimensional model. Am J Physiol Heart Circ Physiol. 287: H994-H1002, 2004.

Ueda A, Shimomura M, Ikeda M, Yamaguchi R, Tanishita K. Effect of glycocalyx on shear-dependent albumin uptake in endothelial cells. Am J Physiol Heart Circ Physiol. 287: H2287-H2294, 2004.

Verkarre V, Patey-Mariaud de Serre N, Vazeux R, Teillac-Hamel D, Chretien-Marquet B, Le Bihan C, Leborgne M, Fraitag S, Brousse N. ICAM-3 and E-selectin endothelial cell expression differentiate two phases of angiogenesis in infantile hemangiomas. J Cutan Pathol. 26: 17-24, 1999.

Vincent KA, Feron O, Kelly RA. Harnessing the response to tissue hypoxia: HIF-1 alpha and therapeutic angiogenesis. Trends Cardiovasc Med. 12: 362-367, 2002.

Waltenberger J, Mayr U, Pentz S, Hombach V. Functional upregulation of the vascular endothelial growth factor receptor KDR by hypoxia. Circulation. 94: 1647-1654, 1996.

Warabi E, Wada Y, Kajiwara H, Kobayashi M, Koshiba N, Hisada T, Shibata M, Ando J, Tsuchiya M, Kodama T, Noguchi N. Effect on endothelial cell gene expression of shear stress, oxygen concentration, and low-density lipoprotein as studied by a novel flow cell culture system. Free Radic Biol Med. 37: 682-694, 2004.

Yamagishi S, Kawakami T, Fujimori H, Yonekura H, Tanaka N, Yamamoto Y, Urayama H, Watanabe Y, Yamamoto H. Insulin stimulates the growth and tube formation of human microvascular

endothelial cells through autocrine vascular endothelial growth factor. Microvasc Res. 57: 329-339, 1999.

Yang HT, Ogilvie RW, Terjung RL.. Exercise training enhances basic fibroblast growth factor-induced collateral blood flow. Am J Physiol Heart Circ Physiol. 274: H2053-H2061, 1998.

Chapter VI

Concluding Remarks

6-1. Summary

This thesis deals with ECs microvessel formation. The control of new microvessel formation is a matter of importance for cure of disease or tissue engineering (regenerative medicine). Pathological angiogenesis is occurred in a lesion, such as cancer, arteriosclerosis, and diabetic retinopathy. The microvessel formation is closely linked to progress of these diseases. Control of microvessel network formation is also key issue in tissue engineering because vessels are essential for the formation and maintenance of organ functions. Regenerated 3-D tissue cannot maintain its physiological function in the absence of a 3-D microvessel network because diffusion alone can not supply sufficient nutrients and O_2 to the tissue in the absence of vascularization. Extensive 3-D microvessel networks of significant depth are, therefore, required to supply O_2 and nutrients to cells comprising regenerated 3-D tissues.

ECs of vessel wall are subjected to hemodynamically shear stress, therefore it is important to examine the effects of shear stress on ECs functions. In Chapter II, shear stress influences on albumin uptake due to change the ECs surface structure. The albumin uptake into ECs at a shear stress of 1.0 Pa increased by 16% and that at 3.0 Pa decreased by 27%, compared to the uptake in cells under static conditions. Shear stress affects the thickness of cell surface glycocalyx, and then influences the albumin uptake in ECs. Chapter III shows that shear stress promoted the growth of 3-D network formation *in vitro*. The enhancement became detectable 10 hours after the initiation of shear stress. After 48 hours, the growth rate of a network under shear stress conditions was

approximately 2 times faster than that of a network under static conditions. Furthermore, shear stress applied to ECs on the surface of collagen gel influenced the process of network formation in the gel. The endpoints of the network branches were extended, and the networks were significantly expanded due to repeated bifurcation and elongation.

The control of morphology of formed networks is also important issue to introduce microvessels deep into tissue. Chapter IV shows the growth factor distribution, at the time ECs are seeded, affects the EC motility and thus affects the morphology of the EC network. This result can be applied to the arbitrary control of the formation of new microvessel networks.

Since angiogenesis is one of the physiological responses to a low-O_2 environment, hypoxia is one of the major factors controlling network formation. In chapter V, the effects of hypoxia on 3-D network formation are examined using an *in vitro* model system consisting of ECs cultured on collagen gel under controlled O_2 concentration. Hypoxia caused ECs to secrete network-inducing factor(s), increased the responsiveness of ECs to growth factors, and increased expression of many angiogenesis-related genes. Induction of angiogenesis-related genes by hypoxia probably leads to enhanced secretion of network formation factors by ECs and also increases the sensitivity of ECs to such factors, resulting in increased formation of 3-D microvessel networks.

To control microvessel network formation in regenerated tissue, this thesis shows the effects of angiogenic factors, such as growth factors, shear stress, and hypoxia, on formation of the 3-D network as above.

6-2. Perspectives

This study reveals several factors, which could control 3-D microvessel network formation. Shear stress changes the microstructure of ECs, including glycocalyx (Chapter II), and microvessel formation is also affected by the stress (Chapter III). In addition, hypoxia induces microvessel

formation through alteration of growth factors secretion and sensitivity for these factors (Chapter V), and the distribution of growth factors have effect on 3-D network morphology (Chapter IV).

Vascularizaion is vital factor for regeneration of 3-D tissue, and studies for 3-D microvessel formation *in vitro* are becoming increasingly important as a key factor for tissue engineering. Diffusion of nutrients and O_2 limits tissues to a thickness of less than ~100 μm in the absence of vascularization (Shimizu *et al*., 2002), and development of tissues *in vitro* with dimensions larger than 100 to 150 μm requires the presence of functional vascular network (Vera *et al*., 2009). Considering the implantation of regenerative tissue, long-term function of 3-D tissue constructs depends on adequate vascularization after implantation (Laschke *et al*., 2006), and further studies for microvessel formation in 3-D models may provide approaches to this problem (Yamada *et al*., 2007).

The results of present study, mechanical stress and physiological changes in environment could play a important role in the promotion and morphological control of microvessel network, have significance for linking gene and cell level factors with tissue engineered approach for organ regeneration.

New hurdle, on the other hand, simultaneously arises for regenerative medicine. While the depth of the network tips in this study is only 100-200 μm, wider and deeper networks would be required for realization the regenerative medicine. In addition, some network inducible factors, such as shear stress and hypoxia, could be disorder of proliferation and function of organ cells, to be regenerated.

Efforts for the organ regeneration, including optimization of mechanical stress stimulation, growth factor supply and co-culture system, are on the way. Using bioreactor, capillaries are induces by interstitial fluid flow with VEGF stimulation (Semino *et al*., 2006), and intensity of fluid flow could modules capillary morphogenesis (Vera *et al*., 2009). Levenberg *et al*. showed that prevascularization of implants improves implant vascularization and survival, using co-culture

system, which includes ECs, skeletal myoblast cells and embryonic fibroblasts (Levenberg *et al*., 2005). In the approach to regenerate 3-D tissue, 3-D culture method was developed by stacking up the 2D tissues of small hepatocytes (Sudo *et al*., 2005).

Among the several potential factors, I think that mechanical stress could be practical procedure due to ease of control. In addition, co-culture systems not only bring environment closer to *in vivo* organs, it is also important for network formations from a viewpoint of secretion and distribution of growth factors.

Progression toward organ regeneration would be realized thorough integration of many factors, such as growth factors, mechanical stresses, and co-culture systems. Living organ is totally optimized system, which consists of various elements, and, therefore, we need to discover an appropriate integration condition. Although micro information for these elements, including genes data, is revealed rapidly, the more investigation is required for the environment around and interactions between the elements. The information which makes a connection between micro and macro information would be vital, and I believe the results of this thesis has significant implications toward the realization of 3-D organ regeneration.

References

Laschke MW, Harder Y, Amon M, Martin I, Farhadi J, Ring A, Torio-Padron N, Schramm R, Rücker M, Junker D, Häufel JM, Carvalho C, Heberer M, Germann G, Vollmar B, Menger MD. Angiogenesis in tissue engineering: breathing life into constructed tissue substitutes. Tissue Eng. 12: 2093-2104, 2006.

Levenberg S, Rouwkema J, Macdonald M, Garfein ES, Kohane DS, Darland DC, Marini R, van Blitterswijk CA, Mulligan RC, D'Amore PA, Langer R. Engineering vascularized skeletal muscle tissue. Nat Biotechnol. 23: 879-84, 2005.

Semino CE, Kamm RD, Lauffenburger DA. Autocrine EGF receptor activation mediates endothelial cell migration and vascular morphogenesis induced by VEGF under interstitial flow. Exp Cell Res. 312: 289-298, 2006.

Shimizu T, Yamato M, Isoi Y, Akutsu T, Setomaru T, Abe K, Kikuchi A, Umezu M, Okano T. Fabrication of pulsatile cardiac tissue grafts using a novel 3-dimensional cell sheet manipulation technique and temperature-responsive cell culture surfaces. Circ Res. 90: e40, 2002.

Sudo R, Mitaka T, Ikeda M, Tanishita K. Reconstruction of 3D stacked-up structures by rat small hepatocytes on microporous membranes. FASEB J. 19: 1695-1697, 2005.

Vera RH, Genové E, Alvarez L, Borrós S, Kamm R, Lauffenburger D, Semino CE. Interstitial Fluid Flow Intensity Modulates Endothelial Sprouting in Restricted Src-Activated Cell Clusters During Capillary Morphogenesis. Tissue Eng Part A. 15: 175-185, 2009.

Yamada KM, Cukierman E. Modeling tissue morphogenesis and cancer in 3D. Cell. 130: 601-610, 2007.

Bibliography

Journal Articles

1. Akinori Ueda, Masaki Koga, Mariko Ikeda, Susumu Kudo, and Kazuo Tanishita**.** Effect of Shear Stress on Microvessel Network Formation of Endothelial Cells with *in Vitro* Three-dimensional Model. *American Journal of Physiology. Heart and Circulatory Physiology.* 283 (3): H994-H1002, 2004.
2. Akinori Ueda, Manabu Shimomura, Mariko Ikeda, Ryuhei Yamaguchi, and Kazuo Tanishita. Effect of Glycocalyx on Shear-dependent Albumin Uptake in Endothelial Cells. *American Journal of Physiology. Heart and Circulatory Physiology.* 287 (5): H2287-H2294, 2004.
3. Akinori Ueda, Ryo Sudo, Mariko Ikeda, Susumu Kudo, and Kazuo Tanishita. Initial bFGF Distribution Affects the Depth of Three-dimensional Microvessel Networks *in Vitro*. *Journal of Biomechanical Science and Engineering.* 1 (1): 136-146, 2006.
4. Akinori Ueda, Ryo Sudo, Mariko Ikeda, Ken-ichi Kokubo, Susumu Kudo, Hirosuke Kobayashi, Kazuo Tanishita. Effect of Hypoxia on Formation of Three-dimensional Microvessel Networks by Endothelial Cells *in Vitro*. *Journal of Biomechanical Science and Engineering.* 3 (2): 299-310, 2008.

Other Publications

1. 植田晃然，古賀理基，池田満里子，工藤奨，谷下一夫．*In Vitro* モデルを用いた血管新生に関する研究．慶應義塾大学日吉紀要 自然科学，37：1-13，2005．
2. Kazuo Tanishita, Manabu Shimomura, Akinori Ueda, Mariko Ikeda, and Susumu Kudo. Shear Dependent Albumin Uptake In Cultured Endothelial Cells. In: *Biomechanics at Micro- and Nanoscale Levels Volume 1*, edited by Hiroshi Wada: World Scientific Publishing Co. Pte. Ltd.:

26-41, 2005.

Proceedings (International)

1. Akinori Ueda, Masaki Koga, Mariko Ikeda, Susumu Kudo, and Kazuo Tanishita. Mechanical Modification of Endothelial Cell Organization. *The First International Congress on Bio-Nanointerface*. Tokyo, Japan, May 2003.
2. Akinori Ueda, Masaki Koga, Mariko Ikeda, Susumu Kudo, and Kazuo Tanishita. The Effect of Shear Stress on Micro-vessel Network Formation of Endothelial Cells. *ASME Summer Bioengineering Conference*. Florida, USA, June 2003.
3. Akinori Ueda, Masaki Koga, Mariko Ikeda, Susumu Kudo, and Kazuo Tanishita. Mechanical Modification of Endothelial Cell Organization. *The International Symposium on Arteriosclerotic Vascular Disease*. Miyagi, Japan, October 2003.
4. Akinori Ueda, Masaki Koga, Mariko Ikeda, Susumu Kudo, and Kazuo Tanishita. Shear stress induces the formation of three-dimensional angiognesis network. *International Symposium of 21st Century COE Program "Understanding and Control of Life's Function via System Biology."* Kanagawa, Japan, November 2003.
5. Akinori Ueda, Masaki Koga, Mariko Ikeda, Susumu Kudo, and Kazuo Tanishita. Effect of Shear Stress on the Formation of Three-Dimensional Angiogenesis Network. *Asian Pacific Conference on Biomechanics*. Osaka, Japan, March 2004.
6. Akinori Ueda, Ikuko Yoneyama, Mariko Ikeda, Hiroko Kajiwara, Masatoshi Tsuchiya, Susumu Kudo, and Kazuo Tanishita. Effect of hypoxia on micro-vessel fomation *in vitro*. *ASME Summer Bioengineering Conference*. Colorado, USA, June 2005.
7. Yoshiyuki Ozaki, Masaki Koga, Akinori Ueda, Ryo Sudo, Mariko Ikeda, Kimiko Yamamoto, Joji Ando and Kazuo Tanishita. Contribution of Endothelial Progenitor Cells on

Microvessel-like Network Formation *in vitro*. *Asian Pacific Conference on Biomechanics*. Taipei, Taiwan, November 2005.

Proceedings (Japanese)

1. 下村学，植田晃然，池田満里子，谷下一夫．血管内皮細胞におけるせん断応力依存アルブミン取込み変化に対する糖衣の影響. 第 13 回バイオエンジニアリング学術講演会. 仙台，2001 年 1 月.
2. 下村学，植田晃然，池田満里子，谷下一夫．血管内皮細胞におけるせん断応力依存アルブミン取り込み変化に対する糖衣の影響. 第 40 回日本エム・イー学会大会. 名古屋, 2001 年 5 月.
3. 植田晃然，古賀理基，池田満里子，谷下一夫．毛細血管ネットワーク形成に及ぼすせん断応力の影響．第 15 回バイオエンジニアリング学術講演会．大阪，2003 年 1 月.
4. 植田晃然，古賀理基，池田満里子，工藤奨，谷下一夫．毛細血管ネットワーク形成に及ぼすせん断応力の影響．平成 14 年度文部科学省学術フロンティア推進事業採択 生体医工学研究センター公開シンポジウム．東京，2003 年 3 月.
5. 植田晃然，古賀理基，池田満里子，工藤奨，谷下一夫．せん断応力が内皮細胞の毛細血管 3 次元ネットワーク構築へ及ぼす影響．第 42 回日本エム・イー学会大会．札幌，2003 年 6 月.
6. 古賀理基，植田晃然，工藤奨，池田満里子，谷下一夫．せん断応力による毛細血管網形成の促進．第 12 回日本バイオイメージング学会学術集会．横浜，2003 年 10 月.
7. 植田晃然，古賀理基，池田満里子，工藤奨，谷下一夫．せん断応力による 3 次元毛細血管ネットワーク形成の促進．第 24 回日本炎症・再生医学会．京都，2003 年 11 月.
8. 植田晃然，池田満里子，工藤奨，谷下一夫．内皮細胞播種時の bFGF の分布が毛細血管ネットワーク形態に及ぼす影響．第 17 回バイオエンジニアリング講演会．名古屋，

2005 年 1 月.

9. 山村菜穂子，植田晃然，須藤亮，池田満里子，谷下一夫．細胞外基質の弾性が毛細血管ネットワーク形成に与える影響．第 17 回バイオエンジニアリング講演会．名古屋，2005 年 1 月.
10. 古賀理基，尾崎亮之，植田晃然，須藤亮，池田満里子，谷下一夫．*in vitro* 毛細血管ネットワーク形成における内皮前駆細胞の寄与. 第 17 回バイオエンジニアリング講演会．名古屋，2005 年 1 月.
11. 植田晃然，米山育子，池田満里子，梶原寛子，土屋正年，工藤奨，谷下一夫．培養液中の溶存酸素濃度の低下が内皮細胞の毛細血管ネットワーク形成能に及ぼす影響．第 4 回日本再生医療学会総会．大阪，2005 年 3 月.
12. 植田晃然，谷下一夫．内皮細胞の周辺環境が血管ネットワーク形成に及ぼす影響．第 104 回バイオメカニクス研究会．東京，2005 年 3 月.
13. 植田晃然，谷下一夫．生命化へ向けた血管ネットワーク形成の制御．21 世紀 COE8 大学拠点合同シンポジウム．東京，2005 年 3 月.
14. 植田晃然，山村菜穂子，古賀理基，池田満里子，工藤奨，谷下一夫．内皮細胞周辺の力学的特性が毛細血管ネットワーク形成に及ぼす影響．第 44 回生体医工学会大会．つくば，2005 年 4 月.
15. 尾崎亮之，古賀理基，植田晃然，須藤亮，池田満里子，山本希美子，安藤譲二，谷下一夫．内皮前駆細胞による *in vitro* 毛細血管様ネットワーク形成促進への影響．第 16 回バイオフロンティア講演会．草津，2005 年 11 月
16. 米山育子，植田晃然，梶原寛子，土屋正年，池田満里子，谷下一夫．低酸素状態における内皮細胞の血管ネットワーク形成促進. 第 16 回バイオフロンティア講演会. 草津，2005 年 11 月
17. 植田晃然，米山育子，須藤亮，池田満里子，小久保謙一，工藤奨，小林弘祐，谷下一

夫．低酸素による生体外 3 次元血管様ネットワーク構造の誘導．第 18 回バイオエンジニアリング講演会．新潟，2006 年 1 月．

18. 植田晃然，米山育子，須藤亮，池田満里子，小久保謙一，工藤奨，小林弘祐，谷下一夫．低酸素による 3 次元血管様ネットワーク形成．第 45 回生体医工学会大会．福岡，2006 年 5 月．

Acknowledgments

My research activities for this thesis were conducted at School of Fundamental Science and Technology, Keio University, under the coaching of Prof. Kazuo Tanishita. I would like to make an address of thanks to his appropriate guidance. The encounter with him is the initiation of life as a researcher, and I learned and absorbed a lot about research activities.

I would like to express an acknowledgment to Prof. Kazuo Umezawa, Prof. Tetsuya Suzuki, and Prof. Keiji Fujimoto for kind review for this thesis.

I appreciate Prof. Hirosuke Kobayashi and Assistant Prof. Ken-ichi Kokubo of Kitasato University for their support and advices for gene analysis. I am also pleased to extend my gratitude to Prof. Mariko Ikeda for her advices, especially from a viewpoint of biology. I express my appreciation to Associate Prof. Susumu Kudo of Shibaura Institute of Technology, and Research Associate Shuichiro Fukushima of Osaka University for valuable discussions for my research.

I also thank the members of Tanishita Lab. for their support. They made my laboratory life fulfilling in the conduct of my academic and personal affair. In particular, I feel grateful to Dr. Ryo Sudo for many useful advices.

Finally, I wish to add my warmest appreciation to my family for their full support and understanding.

March 2009

Akinori Ueda